Development of Nanoparticulate Drug Delivery Systems for Cytostatic Application in PIPAC

Dissertation
zur Erlangung des Grades
des Doktors der Naturwissenschaften
der Naturwissenschaftlich-Technischen Fakultät
der Universität des Saarlandes

von

Alexandra Johanna Zander

Saarbrücken
2021

Tag des Kolloquiums:	10. Dezember 2021
Dekan:	Prof. Dr. rer. nat. Jörn Walter
Berichterstatter:	Prof. Dr. rer. nat. Marc Schneider
	Prof. Dr. rer. nat. Claus-Michael Lehr
Vorsitz:	Prof. Dr. rer. nat. Christian Ducho
Akad. Mitarbeiter:	PD Dr. rer. nat. Matthias Engel

Für meine Familie

Table of Content

Abbreviations

ACE	Acetone
ACN	Acetonitrile
AIDS	Acquired immunodeficiency syndrome
APF	Artificial peritoneal fluid
AUC	Area under-the-curve
BSA	Bovine serum albumin
BT	Bench top
CAWS	Closed aerosol waste system
CL-BSA	Crosslinked bovine serum albumin
CLSM	Confocal laser scanning microscope
CRS	Cytoreductive surgery
CS	Chitosan-HCl
CUR	Curcumin
DL	Drug loading
DLS	Dynamic light scattering
DS	Degree of substitution
EC (EC 4 or 10)	Ethyl cellulose (Ethocel™ Standard 4 or 10)
ECM	Extracellular matrix
EE	Encapsulation efficiency
eIBUB	Enhanced inverted bovine urinary bladder
EMT	Epithelial-mesenchymal transition
ePIPAC	Electrostatic pressurized intraperitoneal aerosol chemotherapy
EPR	Enhanced permeation and retention
EtOAc	Ethyl acetate
EtOH	Ethanol
FD	Freeze-dried
FITC-BSA	Fluorescein isothiocyanate conjugated bovine serum albumin
Glc	Glucose
GRAS	Generally recognized as safe
HBSS	Hanks Balanced Salt Solution
HER2	Human epidermal growth factor receptor 2
HIPEC	Hyperthermic intraperitoneal chemotherapy
HPLC	High-performance liquid chromatography
IFP	Intestinal fluid pressure
IVIVC/R	*In vitro-in vivo* correlation/relation
IP	Intraperitoneal
IPC	Intraperitoneal chemotherapy
iPrOH	Isopropyl alcohol
ISO	International Organization for Standardization
LoD	Limit of detection
LoQ	Limit of quantification
LS	Lymphatic stomata
MeOH	Methanol
MMT	Mesothelial-mesenchymal transition
MPS	Mononuclear phagocyte system
MTT	3-(4,5-dimethythiazol-2-yl)-2,5-diphenyl tetrazolium bromide
MWCO	Molecular weight cut off

nab™	nanoparticle albumin-bound
NP	Nanoparticles
NPr	Nanoprecipitation technique
P-gp	P-glycoprotein
PCI	Peritoneal cancer index
PCS	Photon correlation spectroscopy
PDI	Polydispersity index
PEC	Low methylated pectin
PILAC	Pressurized intraluminal aerosol chemotherapy
PIPAC	Pressurized intraperitoneal aerosol chemotherapy
PITAC	Pressurized intrathoracic aerosol chemotherapy
PIVAC	Pressurized intravesical aerosol chemotherapy
PLGA	Poly(lactic-*co*-glycolic acid)
PM	Peritoneal metastasis
PS	Polysorbate
PTX	Paclitaxel
PVA	Polyvinyl alcohol
RCF	Relative centrifugal forces
S	Slope of calibration curve
SAN	Semi-automated nanoprecipitation
SDR	Spinning disc reactor
SDS	Spinning disc system
SE	Single emulsion solvent evaporation technique
SEM	Scanning electron microscopy
SLS	Sodium lauryl sulfate
TAM	Tumor-associated macrophages
THF	Tetrahydrofuran
Tre	Trehalose
UHPLC-MS	Ultrahigh-performance liquid chromatography coupled to orbitrap mass spectrometry
UKT	Universitätsklinikum Tübingen
VEGF	Vascular endothelial growth factor
ZP	ζ-potential
$\boldsymbol{\lambda_{em}}$	Emission wavelength
$\boldsymbol{\lambda_{ex}}$	Excitation wavelength
$\boldsymbol{\sigma}$	Standard deviation of blank samples

Summary

Local treatment of peritoneal malignancies has been gaining importance for years. The development of intraperitoneal drug delivery strategies aims towards optimal local efficacy while minimizing systemic side effects. By combining the minimally invasive pressurized intraperitoneal aerosol chemotherapy (PIPAC), which was introduced a few years ago for palliative treatment, with nanoparticulate drug delivery systems, which have the potential to increase peritoneal retention, a prolonged effect in the tumor tissue is expected.

In this work, paclitaxel-loaded polymeric nanoparticles (NP) of poly(lactic-*co*-glycolic acid) (PLGA) and ethyl cellulose were developed. By surface modification of PLGA NP with chitosan, a desired prolonged drug release could be achieved. With a release rate of just over 40 % in 10 d, the release *in vitro* could be reduced by more than 50 % compared to unmodified NP. It has been demonstrated that PLGA NP can be nebulized in the angioinjector nebulizer system used in the PIPAC procedure and can also reach therapy-relevant penetration depth in an *ex vivo* model. Furthermore, the development of a continuous evaporation-triggered nanoprecipitation method operating on a spinning disc system offers a promising approach for future commercial production of PLGA NP-based drug delivery systems.

In conclusion, this work provides promising approaches for the further development of a marketable nanoparticulate formulation, and thus, to improve the treatment of peritoneal malignancies.

Zusammenfassung

Die intraperitoneale Applikation von Zytostatika zur Behandlung der Peritonealkarzinose gewinnt aufgrund optimaler lokaler Wirksamkeit bei gleichzeitiger Minimierung der systemischen Nebenwirkungen seit Jahren an Bedeutung. Durch die Kombination der neu entwickelten, minimalinvasiven intraperitonealen Druck-Aerosol-Chemotherapie (engl. PIPAC) mit nanopartikulären Wirkstoffträgern, die potenziell eine erhöhte peritoneale Retention ermöglichen, wird eine verlängerte Wirkdauer im Tumorgewebe angestrebt.

In dieser Arbeit wurden mit Paclitaxel beladene polymere Nanopartikel aus Poly(milch-*co*-glykolsäure) (PLGA) und Ethylcellulose entwickelt. Durch Oberflächenmodifikation der PLGA basierten Nanopartikel mit Chitosan konnte eine verlängerte Wirkstofffreisetzung *in vitro* erreicht werden. Mit einer Freisetzungsrate von knapp über 40 % in 10 Tagen wurde die Freisetzung mit Hilfe des Chitosans um mehr als 50 % im Vergleich zu Nanopartikel mit nicht modifizierter Oberfläche reduziert. Experimente mit PLGA Nanopartikel bestätigten sowohl ihre Aerosolisierbarkeit im PIPAC Vernebelungsverfahren als auch therapierelevante Eindringtiefen in einem *ex vivo* Modell. Darüber hinaus wurde eine kontinuierliche evaporations-getriggerte Nanopräzipitationsmethode auf der Basis eines Spinning-Disc-Systems entwickelt, welche die Grundlage einer zukünftigen kommerziellen Produktion von PLGA Nanopartikel-basierten Arzneimitteln darstellen kann.

Die hier dargelegten Erkenntnisse bieten einen vielversprechenden Ansatz für die weitere Entwicklung einer marktfähigen nanopartikulären Formulierung und damit zur Verbesserung der Behandlung peritonealer Malignome.

1. Introduction

Peritoneal malignancies (PM) are mostly manifested as advanced tumor diseases within the abdominal cavity and are considered as the terminal stage of diverse visceral and gynecological cancers. A generally poor prognosis, accompanied by a median survival of only few months depending on burden and origin of metastasis, diagnosis declared the disease incurable in the past. Therefore, only a palliative treatment strategy was prioritized. Introduction of a multimodal treatment concept by the pioneers Sugarbaker and Spratt for resectable PM significantly improved survival and even enabled curative treatment [1, 2, 3]. However, for a variety of patients only palliative therapy approaches remain available for reasons of unresectable peritoneal metastases. In this context, pressurized intraperitoneal aerosolized chemotherapy (PIPAC) is a substantial improvement after intensive research, comprising a novel application procedure for cytostatic drugs, developed by the research group of Reymond (University hospital of Tübingen) [4]. PIPAC is a well-tolerated, minimally invasive, local application method, which is currently used in clinical studies, especially for palliative therapy. Nevertheless, the current application of cytostatic solutions in PIPAC offers only a limited duration of action in tumor tissue [5]. A sustained effect of the applied cytostatic drug might prolong additional application intervals of PIPAC, and thus, reduce the number of surgical interventions and hospitalizations, and increase patient's quality of life. This might be achieved by a nanoparticulate formulation with modified drug release. The use of nanoparticles (NP) as drug delivery systems was targeted by researchers worldwide for decades, however, the number of products available on the market is quite limited. Sufficient loading properties, suitable release behavior, as well as large-scale industrial production of NP still challenge development and production of an appliable product. This thesis aimed to develop a nanoparticulate formulation with modified drug release for PIPAC application. For this, various cytostatic-loaded, polymeric NP were fabricated, and additionally coated, aiming for a prolonged release of the active substance. Apart from the release behavior, the development particularly addressed sprayability of particles at high pressure (up to 21 bar) and a sufficient penetration into tumor tissue within the PIPAC application technique. With respect to a potential industrial production of a nanoparticulate formulation, a continuous process was developed, which might enable large-scale production for a marketable product.

The following chapters are intended to provide scientific background to the research project in detail.

1.1 Peritoneal malignancies

1.1.1 Peritoneum

Most visceral organs of the abdomen, including stomach, liver, and intestine, are located within the peritoneal cavity. In case of females, it additionally incorporates gynecological organs (e.g., ovaries and uterus), and thus, is opened to the outer genitals, whereas in men, the peritoneal cavity

is a closed environment. With a surface of approx. 2 m^2, the peritoneum is the largest serous membrane of the human body. It is distinguished between a parietal peritoneum (approx. 30 %), covering the cavity from the outside, and a visceral peritoneum (approx. 70 %), entrapping the single intraabdominal organs. A thin film of peritoneal fluid allows movement of the intraperitoneal organs, which are covered by the serosa, a single layer of mesothelial cells. A basement membrane connects the serosa to submesothelial layers, which include blood and lymph vessels, as well as nerves. These are particularly prominent within the visceral peritoneum for supply of the abdominal organs. Furthermore, the peritoneum performs immunological functions via lymphatic stomata (LS), openings in the basement membrane that are connected to the lymphatic system below. The LS ensure clearance of bacteria, tumor cells, ascites, and other particles. They are not distributed homogeneously but are mainly located on omentum majus, appendices epiploicae of the colon, and within the Douglas cavity. So called "milky spots", which are located next to LS, comprise reservoirs of macrophages and lymphocytes for humoral and cellular immune response and blood vessels for liquid exchange [6].

1.1.2 Disease

Germline or somatic mutations lead to alterations in cell cycle regulation and cell differentiation, and thus, might result in the development of neoplasms with proliferative properties. By detachment of tumor cells from the cell association and dissemination, the metastasis process begins. In addition to hematogenous and lymphogenous dissemination, local regional transport (*per continuitatem*) and intraperitoneal seeding by ascites or surgical interventions are possible. This is followed by adhesion to the peritoneal surface and invasion of the mesothelium either translymphatic (frequently; via LS) or transperitoneal (rarely; via damaged mesothelium). Subsequently, in neoangiogenesis, tumor cells express vascular endothelial growth factor (VEGF) for nutrition and cancer growth. In addition, VEGF initiates increased vascular permeation and extravasation of plasma and plasma proteins, thus, altering oncotic pressure and promoting ascites formation in this manner. Recruitment of cancer-associated fibroblasts, which additionally secrete epidermal growth factors, enhance tumor and ascites growth [7].

The infestation of the peritoneal cavity with tumor cells can be classified into primary and secondary peritoneal tumors. Among these, the overwhelming majority are secondary, metastatic malignancies, which are mainly from gastrointestinal or gynecological origins, while primary malignancies originating from the peritoneum itself like mesothelioma are rare. At initial diagnosis, PM is already present in numerous malignancies, most notably ovarian cancer (80 %), colorectal carcinomas (10 %), gastric carcinomas (30 %), and pancreatic carcinomas (5 - 10 %) [8]. This results in approx. 250k (ovarian), 200k (colorectal), 330k (gastric) and 40k (pancreatic) cases of PM, considering the worldwide incidence values of 2020, shown in Figure 1.1 [9]. In early stage, the clinical symptoms are rather unspecific, such as fatigue, abdominal pain, and distension. Later, in advanced stage, malign ascites and intestinal obstruction occur. Overall survival varies depending on primary cancer type and extent or stage of tumor progression during diagnosis. A study by Chu *et al.* from 1989, observed median overall survivals of 0.7 to 12 months for diverse

nongynecological malignancies without chemotherapy or surgical cytoreduction [10].

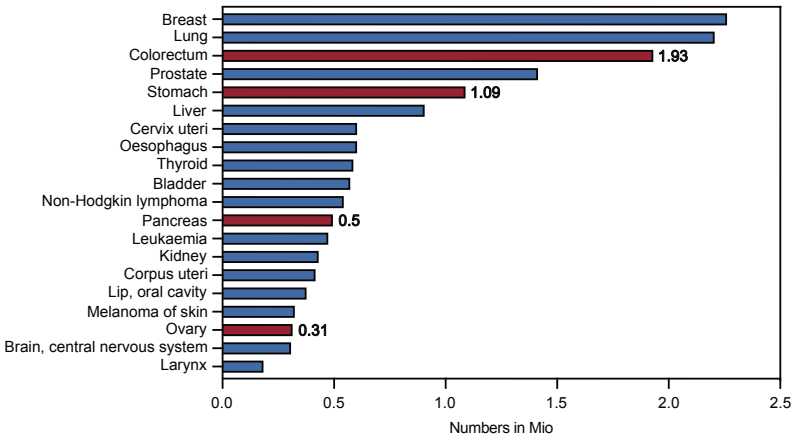

Figure 1.1: Cancer incidences worldwide in 2020.

Red bars highlight the mentioned cancer types in this section. Adapted from the International Agency for Research on Cancer [9].

1.1.3 Therapy

Until the 1980s/90s, therapy of peritoneal metastases was limited to systemic application (intravenous) of cytostatic drugs, acute surgical treatment of life-threatening complications, and supportive measures with palliative aim. Poor vascularization of tumors required high doses of intravenous chemotherapy to achieve required drug concentrations at the target region. Consequently, enormous systemic toxicity restricted therapy success and patients' quality of life [11]. Due to a better understanding of peritoneal malignancies, differentiating a local infiltration from a general cancer disease in terminal stage, the use of hyperthermic intraperitoneal chemotherapy (HIPEC) by Spratt *et al*. beginning in the 1980s and cytoreductive surgery (CRS) developed by Sugarbaker in 1995 allowed the latter to set a multimodal therapeutic concept for curative intention [2, 3]. With CRS, all macroscopically visible areas of the peritoneum affected by cancer sites are removed by visceral and parietal peritonectomy and, depending on diagnosis, partial or total organs are resected. Then, installing several inlet and outlet drains within a closed or opened HIPEC procedure, a cytostatic saline- or dextrose-based solution of several liters is heated to 41 - 43 °C and flushed through the peritoneum for 30 - 90 min for total microscopic removal of tumor cell remnants [12]. HIPEC was intended to combine the advantages of hyperthermia, with its direct cytotoxic effect, the synergistic increase of drug toxicity and higher penetration levels of the drug, and local-regional application, achieving higher tissue concentrations compared to systemic application. Consequently, systemic toxicity was markedly reduced as drug levels in systemic circulation were kept low [13, 14, 15]. In addition, combinations with early postoperative intraperitoneal chemotherapy (EPIC) and neoadjuvant intraperitoneal and systemic chemotherapy (NIPS) emerged [16]. Over the past 20 years the use of multimodal therapy comprising combinations of intravenous chemotherapy, HIPEC and CRS has become standard therapy with potentially curative approach [17]. Due to very long surgeries, as well as increased morbidity and mortality of therapy, expertise within a specialized center is required [18].

For optimal therapy, accurate identification of cancer and its extent are obligatory. For histological differentiation of cancer origin, various markers such as calretinin and different cytokeratin types are available for immunohistochemical staining. Laparoscopy is the gold standard of diagnosis. Here, distribution pattern and size of metastases are assessed minimally invasively within a CO_2-filled peritoneum, also known as pneumo- or capnoperitoneum [19]. Furthermore, depending on cancer origin, computed tomography (CT) and sonography are recommended as standard procedures for tumor staging. Using the peritoneal carcinoma index (PCI) score (values between 0 - 39), which includes infestation and size of peritoneal metastasis within the 13 regions as illustrated in Figure 1-2, a possible postoperative tumor-free prognosis can be estimated, and therapy can be initiated accordingly [20].

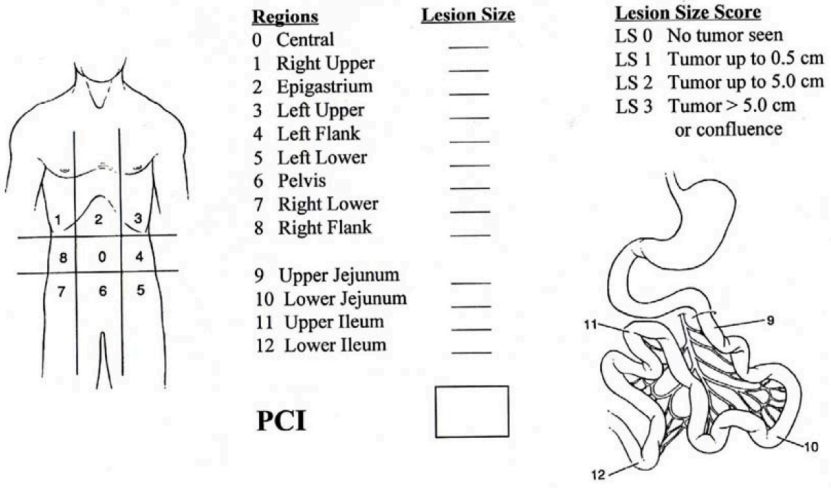

Figure 1.2: Peritoneal cancer index (PCI) according to Sugarbaker.

For each region, the largest tumour lesion is evaluated according to its size with a score of 0 - 3, and the scores of all regions are summed subsequently. Reprinted with permission [20]. Copyright © 1996, Kluwer Academic Publishers, Boston.

Cancer type and PCI determine optimal therapy regimes ranging from curative CRS-HIPEC combination to palliative intravenous chemotherapy. For colorectal cancer, a current S3 guidline recommends multimodality therapy in the presence of peritoneal metastasis only at PCI of less than 20. In addition, no extra-abdominal metastases may be diagnosed and there must be a possibility of complete microscopic resection of all tumor manifestations [21]. According to some literature, a PCI higher than 15 implies relative contraindication for CRS-HIPEC [22]. For gastric cancer with isolated peritoneal metastasis, the multimodal therapy is highly recommended at PCI below 6, but not in the presence of chemotherapy-refractory malignant ascites [23]. In contrast, CRS-HIPEC is not recommended for treatment of peritoneal metastases of ovarian origin according to current guidelines [24].

Until recently, multimodality therapy with CRS-HIPEC was common standard procedure in the management of peritoneal metastases of epithelial appendiceal tumors, colorectal carcinomas and peritoneal mesotheliomas [25, 26, 27]. However, results of most recent studies refuted a benefit in overall survival from HIPEC application for different cancer types, such as advanced colorectal and ovarian cancer [28, 29]. Thus, use of HIPEC is currently further evaluated. Irrespective of

this, benefit and risk of the multimodal therapy should be well considered due to invasive, radical and aggressive CRS procedure, and thus, pronounced postoperative morbidity, which varies between 14 and 70 % [30]. For this reason and due to limitations, e.g., cancer type, PCI score and resectability, curative but radical therapy is available only to a minority of oncologic patients with PM, whereas for the majority only palliative regimens exist. However, relevant progress and improvements also emerged for the latter in recent years.

1.1.4 Pressurized intraperitoneal aerosol chemotherapy (PIPAC)

The research group of Prof. Marc Reymond at University Hospital Tübingen developed a novel method of intraperitoneally applied chemotherapy for palliative treatment, called Pressurized IntraPeritoneal Aerosol Chemotherapy (PIPAC). The concept is based on aerosolized application of an active substance into a pressurized capnoperitoneum (12 - 15 mmHg, 37 °C). After laparoscopic tumor staging and ascites paracentesis, local peritonectomy is performed if necessary, and the peritoneum is checked for leakage. Depending on the active ingredient, 50 or 150 ml isotonic cytostatic solution is applied to the capnoperitoneum with pressures of up to 21 bar via a contrast medium injector, which is also used for angiography, and a customized nebulizer (Capnopen®). In addition to the balloon trocar of the nebulizer, a second laparoscopic trocar is inserted for a camera to monitor the application (Figure 1.3). Maintaining the conditions for 30 min, the excess solution is removed via a closed extraction system. The PIPAC procedure is usually repeated in cycles of 6 - 8 weeks. In case of high-grade or complete histologic remission, the application-free period may be extended up to 12 weeks [31].

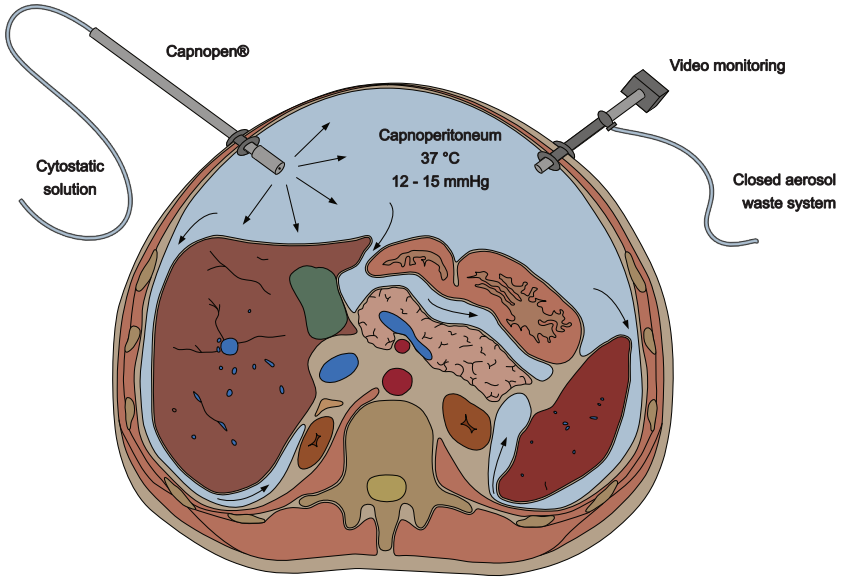

Figure 1.3: Schematic overview on PIPAC application within peritoneal cavity.

Repainted and modified from Solass *et al.* [4].

In 2011, Solass *et al.* reported a first application in humans [4]. Previous pharmacokinetic limitations regarding depth of penetration into tumor tissue and accessibility of treated tissue area are increased by the applied pressure within the peritoneal cavity and aerosolized formulation

[32, 33, 34]. In addition, advantages of local application already mentioned for HIPEC also apply for PIPAC. High effective drug levels are achieved in tumor tissue, while cumulative toxicity and side effects are minimal due to low systemic chemotherapeutic burden [35].

In a retrospective cohort study, Hübner and coworkers concluded that PIPAC does not affect the quality of life [36]. A median overall survival of 8.4 - 19.5 months depending on cancer origin and treatment combinations, is encouraging [31]. The clinical evidence for PIPAC is based on several phase I and II studies [37, 38, 39, 40]. Currently, phase III studies are conducted in anticipation of widespread clinical application of the PIPAC technique [41, 42]. PIPAC is used palliatively as second- or third-line treatment in progression of isolated peritoneal metastases of diverse origin despite systemic chemotherapy [43, 44, 45, 46]. In this context, the S3 guideline for gastric cancer recommends and supports the use of PIPAC in clinical trials for advanced tumor stage [23]. However, future PIPAC applications might additionally include bidirectional palliative therapy together with systemic drug application, and neoadjuvant treatment within the multimodal CRS-HIPEC approach to reduce the extend of CRS or even to allow curative therapy [37, 47, 48, 49]. Based on the increasing number of publications and countries where PIPAC is implemented, a worldwide expansion of PIPAC application becomes apparent [50]. The principle of PIPAC is already adapted to applications in other body cavities and hollow organs, such as pleural cavity (PITAC), esophagus (PILAC) and urinary bladder (PIVAC) [51].

A recent development of PIPAC administration includes additional electrostatic precipitation (ePIPAC) for further enhancement of homogenous distribution of the applied drug [52]. For this technique, an additional brush electrode is inserted laparoscopically into the capnoperitoneum and negatively charges the aerosol droplets via an electron current. A counter-electrode attached to the skin of the abdomen imparts a weakly positive charge to the peritoneal tissue. The electrostatic attraction between negatively charged aerosol droplets and positively charged tissue surface leads to electro precipitation within seconds, i.e., absorption of the aerosol droplets into the target tissue. Kakchekeeva *et al.* demonstrated its technical feasibility and reported tenfold higher tissue uptakes compared to PIPAC using an *in vivo* porcine model [53]. Reymond and coworkers successfully performed the first application of ePIPAC in humans in the same year [54]. In 2019, phase II studies of de Hingh *et al.* as well as Sgarbura *et al.* launched regarding safety and efficacy of ePIPAC, and first results reported by Taibi *et al.* confirmed ePIPAC being a safe and well-tolerated treatment option, which even allows a reduction of the application time to a median of 12 min [55, 56].

Despite the promising results of PIPAC technique so far, further optimization is still required. At present, cytostatic drugs are applied in form of solutions. This results in short residence time and thus, a short duration of action of the cytostatic drug within the tumor tissue [5]. Therefore, a cytostatic formulation is needed with prolonged action in the affected tumor tissue. At the same time this would extend the application cycle of repeated PIPAC administration.

1.2 Drug delivery to peritoneal malignancies

Tumor tissue is known to vary from normal, healthy tissue. In this regard, mutations of functional genes, epigenetic changes, and limited penetration can cause drug resistance [57]. In the following, alterations in tumor microenvironment, and the associated tissue penetration, cell uptake, and peritoneal clearance of drugs will be presented.

1.2.1 Altered microenvironment in tumor tissue

Formation of malignancies affects the extracellular matrix (ECM) in terms of its extent and composition, known as epithelial-mesenchymal transition (EMT) and mesothelial-mesenchymal transition (MMT) [58]. Herein, increased fibroblast activity, restricted or absent lymphatic vessels and abnormal vascularization occur [59, 60]. This abnormal vascularization is associated with a heterogeneous distribution of blood vessels. On the one hand this distribution results in tumor tissue regions with dilatation and excessive branching of vessels. VEGF induced fenestration of tumor blood vessels causes hyperpermeability of plasma proteins and other macromolecules to the surrounding tumor tissue [61]. On the other hand, in other tumor regions compression and temporary occlusion of blood vessels, and blind vascular endings result in a reduction of blood flow. This causes a decrease in supplementation of nutrients and oxygen, and removal of metabolites (clearance) in areas with distances from blood vessels of 100 µm and more [57, 62, 63]. In these hypoxic regions, cellular metabolism is based on glycolysis leading to acidic conditions due to increased concentrations of CO_2 and carboxylic acids [64]. In contrast to poorly supplied areas with low proliferation, in tumor regions with good nutrient supply, there is a high rate of proliferation of cancer cells. From highly proliferating tumor cell areas, cells migrate to hypoxic areas, and die due to nutrient deprivation of the cells' inappropriate metabolism, resulting in necrotizing areas [65]. Furthermore, increased cell-cell adhesion is observed in tumor tissue, which leads to an increased density of tumor cells [66]. In addition, the reduced lymphatic function implicates a reduced clearance and thus increased intestinal fluid pressure (IFP) in tumor tissue [67]. These and other related alterations influence the effect of chemotherapy.

1.2.2 Drug penetration and resistance in peritoneal tissue with tumor invasion

Common chemotherapy regimes in terms of systemic application encounter limitations to sufficiently reach peritoneal tumor tissue, especially due to low vascularization of the parietal peritoneum. Nevertheless, enhanced angiogenesis within the tumor tissue may improve drug accessibility. In case of systemic administration of drug solutions, the fate of an applied active ingredient depends on its ability to penetrate tissue. Rather low selectivity for the tumor tissue causes systemic side effects. Instead, nanoscale drug delivery systems accompany with increased selectivity in transvascular transport and accumulation within the tumor tissue. This phenomenon is known as the enhanced permeation and retention (EPR) effect and is due to the mentioned fenestration of endothelia close to the tumor. In comparison, the openings of healthy endothelia have a size

of 10 nm, which only allows extravasation of dissolved active ingredients or small drug delivery systems [68]. Thus, these carrier sizes should be avoided in passive drug targeting. Instead, excessive particle sizes result in trapping in liver and spleen and opsonization by the mononuclear phagocyte system (MPS). Accordingly, a threshold of 150 - 200 nm seems to be meaningful for passive tumor targeting [69].

Intraperitoneal therapy allows direct and local access to the tumor tissue. This also increases the drug concentration in tumor regions with limited perfusion. In addition, drug concentration can be increased in hypoxic, small peritoneal metastases of less than 1 mm, which have no established vasculature and are therefore difficult to treat intravenously [70]. However, sufficient penetration of the cytostatic drug is required not only to reach surfaces of peritoneal disseminations but also tumor cells within the tumor nodules. In this context, optimal penetration depth depends on tumor size. Furthermore, the previously mentioned formation of tumor tissue (section 1.2.1), which results in hard, fibrotic tissue with increased IFP of 15 mmHg and higher, limits drug penetration [58, 67, 71]. Applying a capnoperitoneum with pressures around 12 - 15 mmHg during PIPAC procedure, counteracts the IFP, and thus, enhances penetration depths [4]. Increased penetration depths and concentrations of drugs are also reported for enhanced intraperitoneal pressures in laparoscopic HIPEC application [72]. Additionally, increased cell density in tumor tissue prevents drugs from penetrating into the tumor interior. There are drugs described decreasing the cell density. Paclitaxel (PTX) is reported to decrease cell density already at low doses, and thus, to reduce IFP. This allows the drug to improve its own and the penetration and distribution of other drugs into deeper tumor sites [73, 74]. However, an additional administration of corticosteroids such as dexamethasone are also known to reduce IFP in tumor tissue, facilitating the penetration of drugs [75].

To date, the extent to which particle sizes of particulate drug delivery systems influence penetration depth has been only incompletely described in the literature. Tang *et al*. report smaller particles of 50 nm penetrating deeper compared to bigger particles of 200 nm, whereas the mathematic model of Islam *et al*. shows low size-effects on penetration depth [76, 77].

1.2.3 Drug delivery on the cellular level

Apart from sufficient drug concentrations reaching the target tissue, the drug needs to be present in an active form and cellular uptake in case of an intracellular mechanism of action is indispensable. In this context, the altered microenvironment in cancer tissue also indirectly contributes to the efficacy of cytostatic drugs. For instance, the reduced oxygen concentration in hypoxic tumor tissue, is reported to decreases the cytotoxicity of superoxide-generating drugs, e.g., doxorubicin [78]. Instead, cytotoxicity of some prodrugs like mitomycin c require reduction under hypoxic conditions, and thus, effectivity of chemotherapy is preferentially increased in hypoxic tumor areas [79]. Glucose deprivation, which also occurs in tumor cells of transient hypoxic tissue, can disrupt correct protein folding in endoplasmic reticulum, and thus, increase resistance to drugs, which target functional proteins, e.g., topoisomerase II [80].

Different mechanisms allow small molecules to enter the cell. Besides the regulation of entry by specific channels, receptors or transporters, the bilayer of amphiphilic phospholipids represents an efficient selective barrier for passive diffusion. In general, membrane passage via passive diffusion is most effective for free, uncharged molecules. Slightly alkaline cytostatic agents, such as doxorubicin and mitoxantrone, are protonated in the acidified tumor environment and therefore only undergo a reduced cell uptake. In contrast, weakly acidic drugs such as cyclophosphamide and chlorambucil are subject to increased cell uptake. For PTX, representing a non-ionizable drug, cellular uptake is independent of the pH of the tumor tissue [81].

Apart from single molecules, nano-sized materials in a size range of ultra-fine particles (< 100 nm) are reported to overcome cell membranes by passive routes, such as diffusion and adhesive interactions [82]. Since particulate systems additionally use specific mechanisms for cell uptake, the cell membrane can be overcome by using them as drug delivery vehicles. In this way, active ingredients that otherwise have difficulty passing the membrane, due to their solubility or charge, can permeate into the cell. Figure 1.4 shows different cellular uptake mechanism of particulate systems. Endocytosis, especially, enables uptake of particulate systems through interaction with plasma membrane and ECM. Several mechanisms are distinguished here, provided that cellular uptake of particulate drug delivery systems is highly dependent on their physicochemical properties. In this regard, one important factor is the particle size. For large particles with a preferential size of 500 nm and larger, phagocytosis appears to be the predominant mechanism [83]. Phagocytosis serves as a defense from pathogens and for the removal of dead cells and cell fragments. It is mainly performed by immune cells such as macrophages, monocytes, neutrophils, or dendritic cells, but also to a less extent by fibroblasts, endothelial and epithelial cells. Opsonization of the particle surface by diverse blood proteins and ligand-receptor-interactions cause internalization by membrane invagination, budding and pinching off, forming endocytic vesicles (phagosomes). Macropinocytosis involves formation of large membrane extensions and ruffles by actin cytoskeleton rearrangement. This comprises non-specific uptake of extracellular fluid together with dissolved molecules and particles, and formation of vesicles of 200 - 500 nm. For most cells, macropinocytosis serves for incorporation of nutrients and solutes, meanwhile, immune cells use this pathway to sample molecules for antigen presentation [84]. Clathrin-dependent endocytosis and caveolin-dependent endocytosis form vesicles in lower size ranges. In clathrin-rich plasma membrane sites of the cell surface (up to 2 %), clathrin-dependent endocytosis is performed for uptake of nutrients and plasma membrane components, e.g., iron and cholesterol [85]. Hereby, vesicles are formed with typical diameters of 90 - 100 nm, but they can also reach sizes of up to 200 nm [86]. The caveolin-dependent endocytosis process involves vesicles of 50 - 80 nm for cell signaling, transcytosis and regulation of membrane components and tension [87]. Caveolae are flasked-shaped membrane invaginations, lined and stabilized with caveolin. They represent a substantial proportion of the cell membrane of endothelial cells and non-endothelial cells, such as adipocytes, fibroblasts and smooth muscle cells. Depending on the cell type, caveolae increase the membrane surface by about 70 % [88, 89].

For cellular uptake of PLGA particles of different sizes, Desai *et al.* determined a far more pronounced uptake for 100 nm NP compared to 1 and 10 µm microparticles. This was 2.5- and 6-fold

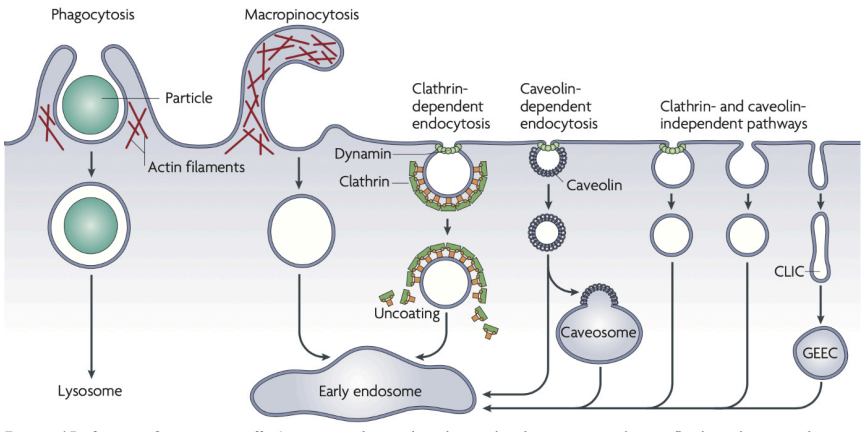

Figure 1.4: Cellular uptake mechanisms of particulate systems.

Particles of 500 nm and larger are taken up by phagocytosis, while smaller particles are incorporated by macropinocytosis (200 - 500 nm), clathrin- (up to 200 nm), and calveolin-dependent endocytosis (50 - 80 nm). Clathrin- and calveolin-independent uptake mechanisms are, for example, receptor mediated. Reprinted with permission [90]. Copyright © 2007 Nature Publishing Group.

higher on the basis of the weight, and more specifically, $2.7*10^3$ and $6.7*10^6$ fold higher in terms of particle numbers [91]. Additionally, extent and mechanism of cellular uptake depends on surface charge and particle shape. While negatively charged NP have a low rate of cellular uptake due to electrostatic repulsion with the negatively charged cell membrane, positively charged NP are incorporated rapidly and to a higher extent. In the literature, clathrin-dependent endocytosis and macropinocytosis are reported to be the main uptake mechanisms for positively charged NP. For negatively charged NP uptake, clathrin-dependent endocytosis or macropinocytosis are excluded and a definite mechanism remains unclear [92, 93, 94]. In human body fluids, surface absorption of biological molecules such as proteins (referred to as protein corona) can cause an increase in size and reduction in surface charge of particulate systems, and thus, additionally affect degree and mechanism of cellular uptake [95]. Influence of particle shape is controversially described in the literature. For example, Chithrani *et al.* repeatedly reported an increased internalization of spherical NP compared to rod-shaped NP in various cell types. Instead, other research groups determined the highest cellular uptake of rod-shaped and disc-shaped NP; spherical, cylindrical, or cube-shaped NP showing lower uptake rates [96, 97, 98, 99].

Incorporation of the drug delivery system, and uptake of the free or released active ingredient in the cell do not necessarily determine the exertion of its effect. Upon cellular uptake, the particulate drug delivery systems usually end up in uptake vesicles, which either transport their cargo to other intracellular structures, release it or develop into degrading vehicles [87]. In this case, constant proton influx causes acidification, leading to a pH gradient from the early endosome (pH approx. 6.5) to the late endosome (pH approx. 5.5) to the lysosome (pH approx. 4.5) [100]. In addition to milieu-dependent inactivation of cytostatic drugs, lysosomal sequestration of weakly basic cytostatic drugs such as anthracyclines, imidazoacridinones and tyrosine kinase inhibitors, as well as exocytotic release of cargo at the plasma membrane, result in lysosomal-mediated drug resistance, as the active ingredients fail to reach their site of action [101, 102]. However, lysosomal degradation can also be used as strategy for hydrolysis- or acid-triggered drug release of NP [103, 104].

Hydrolytic degradation of PLGA is increased at acidic pH, resulting in faster degradation of NP [105]. Another known mechanism of chemotherapeutic resistance of tumor cells is efflux of cytostatic agents out of tumor cells performed by the cell membrane transporter P-glycoprotein (P-gp). In tissue with transient hypoxia expression of P-gp is induced [106]. Consequently, an increased drug resistance to substrates of P-gp, e.g., taxanes, vinca-alkaloids and anthracycline such as PTX, vinblastine and doxorubicin, occurs [107]. Furthermore, an enhanced expression of dihydrofolate reductase in hypoxic tumor tissue is reported, which implicates the resistance against folate antagonists, e.g., methotrexate [108]. Overall, in tumor tissue several mechanisms may reduce the efficacy of the active substance or the particulate drug delivery system, and thus, limit chemotherapy effectiveness in cancer patients.

1.2.4 Peritoneal clearance

In addition to limited penetration into the tumor tissue, impeded cellular uptake into the target cell, specific drug resistance, and mechanisms of drug clearance may prevent desired effects in the targeted tissue. Main processes in peritoneal drug clearance involve diffusion through the peritoneal membrane and drainage by the blood and lymphatic system [109].

The peritoneal membrane has a thickness of around 100 µm and is highly permeable for molecules of less than 20 kDa, which corresponds to a minimal radius of 1.78 nm [110, 111, 112, 113]. This can be explained by the three-pore model of Rippe *et al.*, which implies that around 90 % of endothelial pores are "small pores" of 4 nm radius, while a small percentage are so-called "transcellular pores" with a radius of 0.3 - 0.5 nm and "large pores" of about 25 nm radius [114, 115]. Additionally, a pore-matrix model is discussed, whereby a glycocalyx of 400 - 500 µm thickness on the luminal side of endothelial cells determines permeability. Thereby, the highly negative charge of hyaluronan, a glycosaminoglycan and major component of glycocalyx restricts the passage of molecules and drug delivery systems with negative charge [116, 117]. Thus, clearance of particulate systems by diffusion crossing the peritoneal membrane can be considered as being negligible. Instead, transcytosis into the lymphatic system is expected to be the primary mechanism. Clearance via the lymphatic system enables drainage of the interstitial and peritoneal fluid. In this context, the fluid is mainly absorbed by LS, having opening diameters of several µm up to 50 µm, but also, to a less extent by submesothelial lymphatic capillaries [118, 119]. Accordingly, particles up to micrometer-range are cleared from the peritoneal cavity via the lymph, whereby the probability of drainage decreases and retention time within the peritoneal cavity increases with increasing particle diameter [120]. After entering the lymphatic system, size again affects particle fate. Hereby, particles with diameters of more than 500 nm remain in lymphatic nodes, while smaller particles pass the nodes and enter the systemic circulation [121]. Therefore, lymphatic targeting is a strategy to address tumors with lymphatic spread and metastasis [122]. In addition to direct penetration into the tumor tissue, nanoscale particles may indirectly re-enter the tumor tissue after peritoneal clearance and uptake into the systemic circulation, and thus, both well-vascularized and poorly vascularized tumors are accessible [123]. However, after penetration of particles into deep, poorly vascularized tumor tissue, lymphatic drainage is unlikely due to tissue

alteration in the tumor microenvironment, and thus, absent or restricted lymphatic vessels (section 1.2.2.1).

Apart from lymphatic clearance, tumor-associated macrophages (TAM), especially, are decisive for particle clearance from the tumor tissue. Interaction of various cell types causes secretion of growth factors and enzymes which promote tumor development, suppress the activity of the immune system and support tissue transformation [124]. Through uptake processes, such as phagocytosis and macropinocytosis, TAM internalize and clear particulate systems of various sizes from the target site. Here, opsonization, i.e., formation of a protein corona, is reported to be essential for recognition and particle uptake [125].

Until recently it was assumed that linking strongly hydrophilic molecules, such as polyethylene glycol (PEG), in high density to the particle surface ("stealth"-effect) reduces opsonization and respective clearance [126]. Instead, Schöttler *et al.* reported that PEGylation causes a switch in protein adsorption to clusterin proteins (apolipoprotein J) instead of fibrinogen, albumin and vitronectin, which is responsible for reduced uptake by TAM [127]. Today, PEGylation is discussed controversially as PEG can cause pseudo allergic reactions, complicates endosomal escape after cellular uptake, and antibodies against PEG (IgM) are formed after multiple administrations, causing accelerated elimination via the complement system [128, 129, 130, 131]. Additionally, Miller *et al.* refuted its potential to prevent particle uptake in phagocytosing cells, showing a significant uptake of particulate PLGA-PEG drug delivery systems (size: approx. 135 nm, ζ-potential: -23 mV) by TAM [132]. However, they reported that TAM may act as a local drug depot and continuously release cytotoxic agents, which can affect surrounding tumor cells. Accordingly, cellular uptake by TAM may also harbor strategical potential in tumor therapy.

1.3 Nanomedicines for drug delivery

Within the last decades, nanomedicines including drug delivery vehicles of lipid-based and polymeric-based NP became increasingly attractive for overcoming biological barriers and controlled delivery of chemotherapeutics to tumor cells, especially. This is primarily due to their size, versatility, and ability to modify their surface. According to the vocabulary of the International Organization for Standardization (ISO), nanoscale vehicles have dimensions between 1 and 100 nm, however, the term is often used for sizes of up to 500 - 1,000 nm [133, 134]. Since polymeric NP were used in this work, relevant manufacturing techniques and potential polymers are described in the following.

1.3.1 Techniques for NP preparation

Apart from salting-out and electrospray drying, solvent-antisolvent precipitation and single emulsion solvent-evaporation technique (SE) are commonly used methods for preparation of polymeric NP [135, 136]. The solvent-antisolvent precipitation technique, also known as nanoprecipitation (NPr), solvent displacement, or interfacial deposition, was developed in 1989 by Fessi

et al. [137]. For reasons of simplicity, high automation potential regarding the control of process parameters and future upscaling options, this technique is one of the most frequently used methods for NP preparation [138, 139, 140]. The principle is based on two completely miscible solvents of which only one (solvent) is capable to dissolve the polymer. By transferring the polymer solution into the antisolvent, the solvent rapidly diffuses into the antisolvent, and polymer chains become insoluble and aggregate to NP due to solvent depletion. A dispersion with milky, turbid appearance occurs resulting from the scattering of light by colloidal properties of NP. In case of hydrophobic drugs intended for incorporation, the application of hydrophobic polymers in an organic solvent and an aqueous phase (antisolvent) is appropriate for interaction and efficient drug loading [140, 141]. To prevent or minimize aggregation of NP, stabilizers such as polyvinyl alcohol (PVA), poloxamers, or polysorbates (PS) dissolved in the aqueous phase are frequently used to coat the particles [138, 140]. By means of a syringe pump, microfluidic system, or semi-automated nanoprecipitation-system (SAN-system), NPr can be conducted under controlled conditions [138, 142]. Washing of NP, e.g., by centrifugation and redispersion is necessary in terms of removing organic solvent, not-incorporated drug and excess stabilizer.

SE was developed for the preparation of hydrophobic, polymeric NP in 1979 by Vanderhoff *et al*. [143]. Both the hydrophobic polymer and the drug are dissolved in a volatile, partial water-immiscible solvent which is added to an aqueous phase (antisolvent). An emulsion is produced by energy input, e.g., ultrasound (ultrasonic probe) or mechanical shear forces (UltraTurrax®). For this technique, the addition of an emulsifier to stabilize the emulsion is of importance. After the addition of further aqueous phase and solvent evaporation under continuous stirring, hardened NP are formed and can be processed [144].

1.3.2 Polymers for medical application

Depending on the disease, treatment and site of application, biodegradable and non-biodegradable polymers are applied for drug delivery. In the case of implants and some oral medications, non-biodegradable polymers are used. However, in NP application, apart from the oral application route, biodegradable polymers are required to prevent trapping and accumulation in the human body. Furthermore, biocompatibility, non-toxicity and non-immunogenicity of the polymers should be ensured. The following tables provide an overview of biodegradable and biocompatible polymers or polymer groups (Table 1.1 and Table 1.2). Two degradation pathways into monomeric units are distinguished: hydrolytic and enzymatic degradation. Several polymers described as being biodegradable in the literature are only degradable in bacteria. However, some decisive bacterial enzymes are present in the human intestinal microbiome, allowing orally applied polymers, such as mannan, carrageenan and pectin, to be indirectly degraded in the human body. Other bacterially degradable polymers such as PEG, poloxamers and dextran, can still be excreted when applied systemically due to their water solubility.

Table 1.1: Hydrolytically biodegradable and biocompatible polymers or groups of polymers.

Hydrolytically degradable groups	Example of polymers or polymer subgroups	Ref.
Polyester		[145], [146]
Polycarbonates	Poly(trimethylene carbonate) (PTMC)	
	Poly(dihydroxyacetone)-[methyl poly(ethylen glycol)] (MPEG-pDHA)	
	Poly(desamino tyrosyl-tyrosine ethyl ester carbonate) (PDTE)	
Polyhydroxyalkanoates (PHAs)	Poly(glycolic acid) (PGA)	
	Poly(lactic acid) (PLA; PLLA/PDLA/PDLLA)	
	Poly(lactic-*co*-glycolic acid) (PLGA)	
	Poly(ϵ-caprolactone) (PCL)	
	Poly(propylene fumarate) (PPF)	
Microbial poly(β-hydroxyalkanoate)s	Poly(3-hydroxybutyrate) (PHB)	
	Poly(3-hydroxybutyrate-*co*-3-hydroxyvalerat) (PHBV)	
Polyphosphoesters		[145], [147]
Polyphosphonates		
Polyphosphates		
Copolymers	Poly(lactide-*co*-ethyl phosphate) (p(DAPG-EOP))	
Poly (ortho esters)	POE types I-IV	[145]
Polyacetals	Poly(oxymethylen) (POM)	[145]
Polyanhydrides		[145], [147], [148]
Aliphatic homo-polyanhydrides	Poly(sebacic anhydride) (pSA)	
Aromatic homo-polyanhydrides	Poly[1,3-bis (p-carboxy phenoxy) propane] (pCPP)	
Copolymers	Poly[1,3-bis(p-carboxy phenoxy) propane]-(sebacic acid) (p(CPP:SA))	
	Poly [1,6-bis-(p-carboxyphenoxy) hexane-*co*-sebacic acid] (p(CPH:SA))	
Polyphosphazenes	Poly[bis(trifluoroethoxy)phosphazene] (PTFEP)	[145], [149]
Other copolymers		[145]
Poly(ester ether)	Poly(*p*-dioxanone) (PDO)	
Poly(ester urethane)s		
Poly(β-amino ester)s (PBAEs)		

Table 1.2: Enzymatically biodegradable and biocompatible polymers or groups of polymers.

Enzymatically degradable groups	Example of polymers or polymer subgroups	Ref.
Synthetic polyethers	Poly(ethylene glycol) (PEG)*	[145]
	Poly(propylene glycol) (PPG)*	
	Poly(tetrahydrofuran)*	
	Poloxamers ([PEG]n-[PPG]m-[PEG]n)*	
	PEG diacrylate (PEGDA)*	
	PEG dimethacrylate (PEGDMA)*	

Enzymatically degradable groups	Example of polymers or polymer subgroups	Ref.
Peptides		[145], [147], [150]
Proteins	Albumin	
	Fibrin	
	Gelatine	
	Collagen	
	Elastin (recombinant human tropoelastin)	
Polypeptides	Elastin-like polypeptide (ELPs)	
Natural poly(amino acids)	Cyanophycin*	
	Poly(γ-glutamic acid) (γPGA)*	
	ϵ-poly(L-lysine) (ϵ-PL)*	
Synthetic poly(amino acids)	α-poly(L-glutamic acid) (αL-PGA)	
	α, β-poly[(N-2-hydroxyethyl)-D,L aspartamide] (PHEA)	
	Poly(aspartic acid) (PAA)	
Polysaccharides		[145], [150], [151], [152]
Human origin	Hyaluronic acid	
	Chondroitin sulfate	
	Other carboanhydrates: heparin-, keratin- and dermatan-sulfate	
Non-human origin	Chitin*, Chitosan	
	Alginic acid/alginate*	
	Starch, starch acetate	
	Cellulose*, cellulose acetate*	
	Carrageenan*	
	Pectin*	
	Mannan*	
	Agarose*	
	Inulin*	
	Dextran*	

* physiologically not biodegradable in humans due to lack of enzymes; enzymes of other origin are required, e.g., microbial origin

In the following, polymers relevant for the present thesis will be discussed in more detail. PLGA (Figure 1.5 A) is one of the most extensively studied polymers for the preparation of hydrophobic polymeric NP and a large variety of small molecules as well as macromolecules such as peptides, proteins, and DNA/RNA were already formulated [153, 154, 155, 156]. Already in the 1970s, the synthetically produced *co*-polymer of esterified lactic acid and glycolic acid was approved as inactive ingredient for use in various medical products such as implants and injections by the U.S. Food and Drug Administration (FDA) [157]. Hydrolysis of PLGA in aqueous environment results in formation of the respective monomers, which can be metabolized to CO_2 and H_2O in the human body. Depending on monomer proportions, degradation can be controlled. Thereby an increase in the lactic acid content leads to a slower degradation of the polymer [158]. Processed PLGA types (Resomers®) and respective physicochemical properties used for the present thesis, are listed in Table 1.3. According to the manufacturer, the time of degradation of the polymers is less than

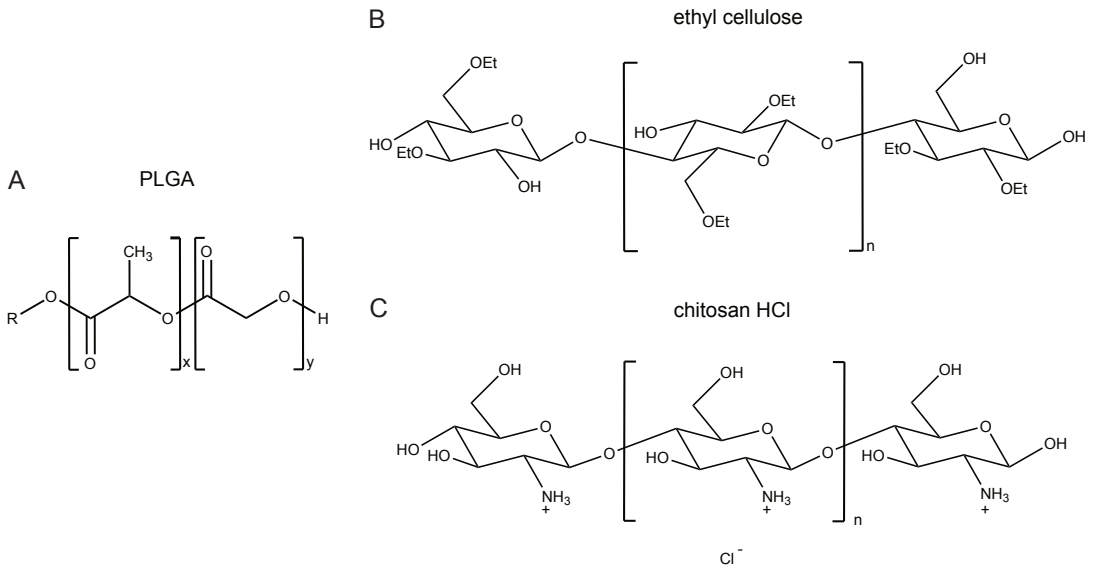

Figure 1.5: Chemical structures of PLGA (A), ethyl cellulose (EC) (B), and chitosan HCl (CS) (C).

x: number of lactic acid units. y: number of glycolic acid units. n: number of EC monomers or D-glucosamine units (CS). EC with a degree of substitution of two from three possible hydroxyl groups per cellulose monomer.

three months, in case of Resomer RG 753H less than six months [159].

Ethyl cellulose (EC; Figure 1.5 B) is a hydrophobic, water-insoluble cellulose derivative with ethoxy groups etherified hydroxyl groups and shows high physiological and storage stability especially regarding light and heat exposure. Due to its limited biodegradation behavior to bacterial enzymes but excellent compatibility in the human body, EC is commonly used and FDA approved, e.g., for coating of orally applied retard formulations, such as capsules and tablets [157]. EC types differ in terms of degree of substitution (DS) and viscosity. The grades used for this study (Ethocel™ Standard 4 and 10; in the following referred to EC 4 and EC 10) have an intermediate DS of approx. 49 % and low viscosities of 5.3 and 10.3 mPa*s [160]. The release behavior of EC-coatings depends on these properties, releasing less drug with higher molecular weight and lower DS. The addition of a plasticizer (e.g., dibutyl sebacate) increases the flexibility of the polymer, creates a less porous network, and thus, reduces the release rate, whereas pore formers can increase the porosity of the network and correspondingly increase the release rate [161].

The linear polysaccharide chitosan (CS, Figure 1.5 C) is a strongly polycationic derivative of poly-N-acetyl-D-glucosamine, known as chitin, which is found in the exoskeleton of crustaceans and in the cell wall of fungi and bacteria. As deacetylation of the N-acetyl groups results in free amino-groups, dissolving of CS requires low pH values for protonation [162]. However, CS chloride salt has good solubility in aqueous medium even at neutral pH values. In the human body, besides bacterial degradation in the intestine, the polymer undergoes lysosomal degradation [163]. FDA defines chitosan as generally recognized as safe (GRAS) substance [164, 165]. General approval for medical application by FDA is still pending; however, premarket notifications already address wound healing and tissue engineering [166, 167]. Despite its limited application so far, chitosan has been widely investigated as a polymer for NP production and DNA delivery due to its electrostatic attraction [168, 169].

Table 1.3: Overview of used PLGA types and their corresponding physicochemical different properties.

PLGA type	LA:GA ratio [%]	Inherent viscosity [dl/g]	M_w [g/mol]
RG 502H	50:50	0.16 - 0.24	07 - 17k
RG 503H	50:50	0.32 - 0.44	24 - 38k
RG 504H	50:50	0.45 - 0.60	38 - 54k
RG 653H	65:35	0.32 - 0.44	24 - 38k
RG 753H	75:25	0.32 - 0.44	22 - 36k

So far, various surface modification approaches have been used to add functionality to nanoparticulate drug delivery systems. For immobilization of targeting ligands on particle surfaces, two strategies are distinguished: (1) specific, stable chemical conjugation using functional groups, such as carboxylic acids, azides, and thiols, and (2) non-specific, non-covalent physical adsorption, using attractive forces between ligand and surface, such as electrostatic interactions, hydrogen bonding, and hydrophobic interactions. This allows macromolecules (polysaccharides, lipids, peptides, nucleic acids) and small molecules (steroids, vitamins, mono- and oligosaccharides) to be attached to the particle surface [170]. On the one hand, active targeting by means of the receptors expressed on the target cell can be achieved by functionalizing the particulate surface. In literature, antibodies and their fragments (e.g., against human epidermal growth factor receptor 2), folic acid (folic acid receptor), or estradiol (estrogen receptor), as well as human serum albumin and chitosan have been described as possible ligands [171, 172, 173, 174, 175, 176]. On the other hand, steric protection of NP against protein absorption, the associated phagocytotic uptake, and clearance can be reduced by stealth-coating materials, such as dextran, human serum albumin, heparin, and PEG (see section 1.2.4) [177, 178]. In addition, this steric effect can reduce aggregation of particles during storage [179]. Furthermore, surface modifications of NP have been already shown to reduce drug release [180, 181, 182]. Coating efforts for modifying drug release are described in detail in chapter 2.

1.3.3 Active ingredients for chemotherapy against peritoneal malignancies

Several active ingredients, approved for chemotherapy, are available commercially. In the context of immunotherapy, loading of NP with antibodies or modulators is principally also conceivable [183]. However, especially conventional chemotherapeutic drugs were used for intraperitoneal application so far, which includes platinum compounds, taxanes, anthracyclines and 5-fluorouracil [184]. Depending on the type of therapy, drugs with different mechanisms of action are suitable. For example, CRS requires purging chemotherapy with an acute cytotoxic effect for perioperative removal of tumor cells liberated by radical surgery, thus, preventing tumor recurrence [185]. For PIPAC therapy, drugs with a delayed-onset cell cycle-specific effect, such as PTX (Figure 1.6), can also be used.

PTX belongs to the group of taxanes and is naturally extracted from the bark of the Pacific yew (*Taxus brevifolia Nutt.*) [186]. Since the extraction of natural PTX has an extremely low yield

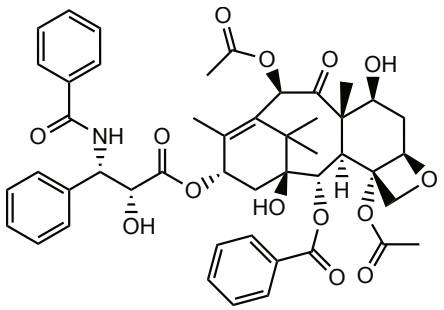

Figure 1.6: Chemical structure of PTX.

and the chemical synthesis is not industrially feasible for economic reasons, the semi-synthetic production of 10-deacetylbaccatin III, the precursor of PTX extracted from the needles of the European yew (*Taxus baccata L.*), offers a more cost-effective method of effectively obtaining PTX [187]. The mechanism of action is based on suppression of microtubules' dynamics by inhibiting their depolymerization. Thus, the cell cycle is blocked during mitosis and the proliferation of tumor cells is stopped [186, 188]. The poor solubility of PTX in aqueous medium of approx. 3.5 µg/ml at 37 °C is demonstrated by its logP value of 3.66 (decadic logarithmic partition coefficient in an octanol/water system) [189, 190]. Due to its hydrophobic properties, PTX seems to be an appropriate candidate for encapsulation within a hydrophobic polymer such as PLGA or EC. Furthermore, with 853.9 g/mol PTX has the highest molecular weight besides docetaxel among the mentioned cytostatic agents [184]. For intraperitoneal application, an approx. 1,000-fold area-under-the-curve (AUC) ratio of PTX in peritoneum vs. plasma is reported, while compounds with lower molecular weight showed significant decreased AUC ratios, such as cisplatin (300.1 g/mol) and doxorubicin (580 g/mol) with AUC ratios of 7.8 and 230, respectively [184, 191]. In terms of free or released active ingredient, the choice of a high molecular weight seems to be advantageous for long persistence in tumor tissue. Currently, PTX-containing drugs are approved for intravenous chemotherapeutic treatment of advanced AIDS (Acquired immunodeficiency syndrome)-associated Kaposi's sarcoma and combined with platinum-containing drugs for ovarian cancer and advanced non-small cell lung cancer. In combination with Gemcitabine, PTX is approved for first-line therapy of metastatic adenocarcinoma of the pancreas. In monotherapy or together with the humanized monoclonal antibody trastuzumab, PTX is administered for the treatment of (HER2 (Human epidermal growth factor receptor 2)-positive) metastatic breast carcinomas [192, 193]. For mentioned indications, intravenous dosages of 100 - 220 mg/m^2 (Taxol®) or 100 - 260 mg/m^2 (Abraxane®) are applied, as dosage is determined based on the calculated body surface area in systemic drug application. In local, intraperitoneal application, this scheme is usually adopted analogously. However, there is an incomplete correlation between the actual peritoneal surface area and the calculated body surface area. In addition, as described in section 1.1.1, there are gender differences in the peritoneal surfaces, which in turn affect the absorption properties of the active substance [194]. Currently, the favored concentration of PTX in IP application is being investigated and discussed. Williamson *et al*. recommended 175 mg/m^2 based on a dose tolerance study (phase I) for Nanotax®, a sterile nanoparticulate PTX powder, applied by IP

infusion [195]. Within a weekly application scheme, a maximal tolerated dose of 140 mg/m^2 PTX was determined by IP infusion of Abraxane® [196]. A phase I study (first in human), currently ongoing at Ghent University Hospital, investigates dose limiting toxicity of Abraxane® in PIPAC application in concentrations of 35 - 140 mg/m^2 PTX [197]. Due to reported high effective drug levels in tumor tissue after PIPAC application, lower concentrations of active ingredients might be sufficient [35].

1.3.4 Approved nanoparticulate drugs in cancer therapy

A number of nanoparticulate drugs are already available on the market, and a large number of new drugs or indications for use in cancer therapy are approved by the FDA every year [198, 199]. Currently, there are few clinically applied nanoparticulate drug delivery systems for use in cancer treatment despite extensive research over the past decades. Figure 1.7 indicates nanoparticulate drugs and medicinal devices so far approved by FDA or European Medicines Agency (EMA) for cancer therapy [200]. Moreover, it can be observed that with Abraxane® there is only one product consisting of polymeric NP. Drug development is known to be very time consuming and costly. A recent review by Wouters *et al.* found costs ranging from 320 million to 2.8 billion per drug, with anticancer and immunomodulatory drugs being the most expensive, and development times of 10 - 20 years are discussed [198, 201]. In the case of nanoparticulate formulations, the upscale of production with its batch-to-batch variations and characterization methods are currently costly and time consuming [198, 202]. Therefore, there is a need for improvement and optimization of classical analytical and production methods, and development of new large-scale methods to produce nanoparticulate drug delivery systems.

In addition, it should be mentioned that currently there are no approved medications for dedicated intraperitoneal application for cancer therapy, and thus, systemically applied drugs are used off-label for this purpose.

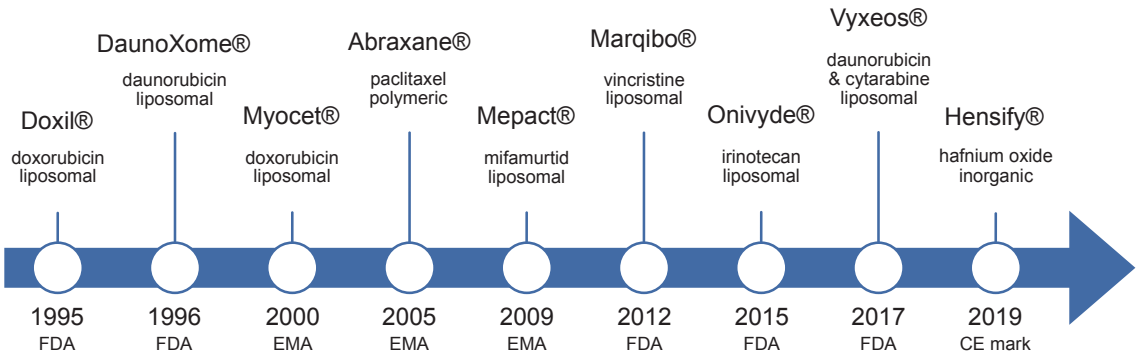

Figure 1.7: FDA and EMA approved nanoparticulate formulations in cancer therapy.

Only the initial approvals are indicated [200]. As Hensify® is an inorganic radioenhancer with a physical mechanism of action, it is approved on the European market as medical device [203].

1.4 Aim of work

PIPAC is a promising, novel therapy for peritoneal malignancies. However, despite its advantages, there are still improvements to be made in terms of prolonged cytostatic effects of the applied drug. The objective is to develop a formulation that can be primarily applied using the PIPAC technique, which requires, e.g., the presence of a sprayable liquid. After sufficient penetration into the tumor tissue, the active ingredient should reach the side of action, remain there and be efficient for a substantial period of time. This allows longer application-free time, and thus, higher quality of life for the patient within palliative treatment. Ideally, the release or action of the cytotoxic substance is delayed by approx. a week to allow healing of the tissue after laparoscopic surgery. To meet these requirements, drug-loaded, polymeric NP in a size-range of about 200 nm with modified release were to be developed. Within this size-range sufficient penetration and cellular uptake was expected. Formulations in the micrometer range were excluded in advance due to size limitations during application (impaired sprayability because of nebulizer blockage), and their negative side effects in terms of causing peritoneal adhesions and inflammation in the peritoneal tissue [204].

The first section of this thesis (chapter 2) deals with the preparation and characterization of biocompatible, drug-loaded, polymeric NP. Here, different preparation methods, carrier polymers, as well as coatings were investigated with respect to their colloidal and loading properties. Efficient drug loading and slow release from the hydrophobic carrier were aimed by selecting the drug PTX with its advantageous properties regarding tumoral tissue penetration, cellular uptake, reduced peritoneal clearance, and low water solubility. In the second section (chapter 3), a continuous manufacturing technique of loaded PLGA NP for potential industrial up scaling was investigated and compared with the conventional bench top (BT) NPr. In the third section (chapter 4), an *in vitro* setup was developed to study drug release, and diverse NP formulations of the first section were further characterized regarding their release profiles. Due to the incorporation of PTX in polymeric NP, Abraxane® represents a potentially desirable formulation, and therefore, was investigated in more detail in the fourth section (chapter 5). The last section (chapter 6) studies the sprayability of polymeric NP *in vitro* using devices of PIPAC application. Furthermore, this section contains *ex vivo* penetration studies with the aim to reveal sufficient penetration of polymeric NP. In this context, evaluation of penetration depths and prediction of the formulation's effectiveness were addressed.

2. Formulation development

2.1 Introduction

Formulation development for therapeutic use requires excipients being biocompatible, non-toxic, and non-immunogenic in the human body, ideally also being biodegradable after intraperitoneal application to ensure complete elimination. Apart from PLGA, which completely meets these requirements, EC was investigated in more detail as a carrier polymer. Due to presumed, altered solubility of PTX in ethanol (EtOH) instead of acetone (ACE), better loading properties in ethanol-soluble EC were intended. Steric stabilization of NP dispersions can be achieved, e.g., by PVA, a hydrophilic, water-soluble polymer with compatibility and biodegradability in human tissues and liquids [205].

Coating of NP is a promising strategy to achieve slower release and prolonged effects of an active ingredient [180, 181, 182]. For this, the polymers pectin and albumin represent potential candidates. Pectin is a strongly negatively charged polysaccharide, mainly consistent of poly galacturonic acids and the main component of the primary cell wall and the middle lamella of plants. Galacturonic acids in the backbone may be substituted with rhamnosyl residues or have highly branched side chains. Commercially, the polymer is used for gelling and thickening jam and dairy products. Different types of pectin are available regarding their degree of esterification of the galacturonic acids. In low methylated pectin (PEC), a high number of free carboxyl groups is present. Thus, the gelation of the polymer is pH-independent and does not require addition of saccharose, but has the potential to form complexes with bivalent ions such as Ca^{2+} ("egg box" model) [162]. Due to its gelation behavior, PEC may act as a hydrogel layer surrounding the NP, and thus, might temporarily delay or reduce drug release. Albumin (66 kDa), the most abundant plasma protein (35 - 50 g/l human serum) naturally transports, e.g., hormones, fatty acids, bilirubin, and bivalent cations such as copper (II), nickel (II), calcium (II) and zinc (II), and is essential for maintenance of the oncotic blood pressure [206]. Active transcytosis mediated by proteins such as albondin, the albumin receptor glycoprotein gp60 on endothelial cell surface and calveolae, allows direct transport of albumin into tumor tissue [207, 208]. Here, tumor cells utilize albumin for *de novo* protein synthesis, energy production, and thus, tumor growth [209]. Therefore, albumin coating of NP may both modify drug release and be suitable for targeted tissue penetration. Albumin has an isoelectric point of 4.6. Depending on pH, positively or negatively charged amino acids enable binding to the correspondingly counter-charged surface of NP. In addition, covalent crosslinking of primary amino groups mediated by crosslinkers such as glutar- and formaldehyde makes the coating more stable, more closely meshed, and ideally more impermeable, which could additionally prevent drug release [210, 211]. Adsorption of the coating polymers to the NP surfaces by electrostatic attraction forces requires positively charged NP surfaces for both PEC and albumin, and additionally a suitable pH of > 4.6 to evoke negatively charged amino acid moieties for albumin. For negatively charged coatings, introducing a positively charged polymer, such as CS, into the carrier particle represents a promising way to change the surface charge of nega-

tively charged NP. Due to the cytotoxicity of PTX, the use of a model substance is recommended for preliminary tests. The yellow-orange polyphenol curcumin (CUR) is isolated from the rhizome of the turmeric plant (*Curcuma longa L.*) and offers appropriate specifications to load and label PLGA NP [212]. Due to its hydrophobic, harmless, and fluorescent properties, application of CUR enables encapsulation in hydrophobic carriers and visualization of penetration depth in tissue (penetration studies in Chapter 6).

For storage and transport in medical application, formulations have to be protected from being degraded by aqueous dispersion media. Lyophilization is an efficient and frequently used method for this purpose. As reconstruction of the resulting lyophilized NP must be feasible to enable application as dispersion, lyo- and cryoprotectants, e.g., sugars such as glucose (Glc) and trehalose (Tre) are added. The high number of hydroxy groups in sugars facilitates the formation of hydrogen bonds to the product, and thus, stabilizes the NP from agglomeration during the freezing and dehydration process [213].

2.2 Material and methods

2.2.1 Material

The materials and equipment used for the experiments described here and in the following chapters are listed in chapter 8. Identification and purity of PTX was determined by nuclear magnetic resonance (NMR) spectroscopy performed by Dr. Josef Zapp (Pharmaceutical Biology, Saarland University).

2.2.2 Preparation and drug loading of polymeric NP

2.2.2.1 Plain PLGA NP

Plain PLGA NP were prepared by NPr as follows. 25 mg PLGA (Resomer RG 503H) were dissolved in 1.5 ml ACE for 10 min under rigorously stirring at RT (23 °C $\pm$ 1 °C). Then, the polymer solution was injected in 10 ml aqueous phase containing 2 % (w/v) PVA using a syringe pump with a flow rate of 0.5 ml/min. Particles were purified by centrifugation (2 x 10,000 RCF, 20 min, 20 °C). For investigations whether particle nebulization is feasible by PIPAC procedure (chapter 6) batch sizes were upscaled to 500 mg polymer with similar ratios and concentrations. Colloidal properties were measured by dynamic light scattering (DLS) and laser Doppler electrophoresis (section 2.2.4.1). Particle morphology was investigated by SEM (section 2.2.4.4).

2.2.2.2 CUR-loaded PLGA NP

For penetration trials (chapter 6) fluorescently labelled PLGA NP were used. For this purpose, a stock solution of 1 % (w/v) CUR in ACN was prepared and stored under light protection at 4 °C.

Batches of 500 mg PLGA (Resomer RG 503H) were dissolved in ACN for 10 min under stirring and the CUR-stock was added to reach an initial concentration of 1 % (w/w) of the polymer mass and a total volume of 30 ml. The further preparation of the particles followed the previously described, upscaled method for plain PLGA NP (section 2.2.2.1). Quality of CUR-loaded PLGA NP was determined by DLS laser Doppler electrophoresis and visualized by SEM and fluorescence microscopy. Drug loading (DL) and encapsulation efficiency (EE) were evaluated by fluorescence spectroscopy (direct determination).

2.2.2.3 PTX-loaded PLGA NP

Based on plain PLGA NP (section 2.2.2.1), the formulation development of PTX-loaded PLGA NP was initiated. A stock solution of 1 % (w/v) PTX in ACN was prepared and depending on the initial loading concentration, certain volumes were added to the volume of ACE, in which PLGA was dissolved and had to be adjusted accordingly to obtain a total volume of 1.5 ml. Independent of the initial PTX concentration, this preparation technique is referred to as “standard” in the following.

First feasibility trials were performed, investigating ACE and ACN as potential solvents as well as PVA (2 % (w/v)), PS 20 and 80 (1.25 % (w/v)), lecithin (0.5 % (w/v)), and poloxamer 188 (0.1 and 1 % (w/v)) dissolved in aqueous phase for stabilizing the resulting NP dispersion using 1 % (w/w) PTX concentration of the polymer mass.

Different preparation parameters were tested regarding the loading properties of PTX. First, types of different LA:GA ratios and PTX concentrations of 1 - 5 % (w/w) of the polymer mass were investigated using the standard NPr and were compared to SE. For the latter, 50 mg polymer were dissolved in EtOAc under stirring (approx. 800 rpm) for 10 min and 1 % (w/v) PTX stock (in EtOAc) was added to obtain a polymer concentration of 2 % (w/v) and a total volume of 2.5 ml. Then, the solution was added to 2.5 ml 2 % (w/v) aqueous PVA solution by slow, manual injection over 1 - 2 min. The obtained emulsion was covered and further stirred (approx. 800 rpm) for 1 h at RT before homogenization by ultrasonic homogenizer (500 J for 35 s). 20 ml of MilliQ® water was added and the emulsion was stirred under light protection for two days to completely remove residual EtOAc. The hardened NP were purified according to the standard NPr protocol.

Furthermore, different viscosities of PLGA (LA:GA 50:50), different amounts of Resomer RG 503H (10 and 40 mg) as well as tetrahydrofuran (THF) for solvent instead of ACE were tested using 2 % (w/w) PTX concentration in the standard NPr method. THF is a potential solvent for NPr due to its complete miscibility with H_2O and sufficient dissolution of PLGA and PTX. To prevent formation of precipitates and to investigate possible changes in DL, addition of EtOH to the aqueous phase was tested as a cosolvent. For this purpose, 0, 1, 3, and 5 ml of EtOH were mixed into the aqueous 2 % (w/v) PVA phase before injection of the drug-polymer solution containing 5 % (w/w) PTX of polymer mass. The samples were immediately purified after precipitation process to avoid PTX precipitates due to solvent evaporation and corresponding decrease in PTX solubility. PTX-loaded PLGA NP were evaluated regarding colloidal properties by DLS,

morphology by SEM, and loading behavior by HPLC.

2.2.2.4 PTX-loaded EC NP

EC NP were prepared by NPr using a modified protocol of Urbán-Morlán as described as follows [214]. 100 mg of EC 4 or EC 10 (higher viscosity for EC 10, see section 1.3.2) were dissolved each in 5 ml EtOH (2 % (w/v) for 2 h while stirring at RT. Using a syringe pump with a flow rate of 0.5 ml/min, the solutions were injected into 10 ml of a stirring (approx. 800 rpm) 5 % (w/v) PVA solution. For size tuning of EC 4 NP, polymer concentrations of 3, 3.5 and 4 % (w/v) were prepared using 100 mg polymer and volumes of 3.333, 2.857 and 2.5 ml of EtOH. A concentration of 3.5 % (w/v) EC 4 was chosen for loading trials with PTX. PTX concentrations of 1 - 20 % (w/w) of the polymer mass were tested. Therefore, a stock solution of 1 % (w/v) PTX in EtOH was prepared and depending on the initial loading concentration certain volumes were added to the volume of EtOH, in which EC 4 was dissolved and which had to be adjusted accordingly to obtain a total volume of 2.857 ml. After particle preparation, samples were purified by centrifugation (2x 20,000 RCF, 20 °C, 30 min with 20 ml MilliQ® water) and characterized regarding colloidal properties by DLS, morphology by SEM, and loading behaviors by HPLC.

2.2.3 Surface modification of polymeric NP

All coated, drug-loaded NP described in this section were investigated in terms of their loading, colloidal properties, and morphology (SEM).

2.2.3.1 CS-PLGA composite NP

As described in literature, the polycation CS can be added directly to the stabilizer solution for particle coating [215]. Therefore, 3.75 mg CS per 10 ml aqueous solution was dissolved in 2 % (w/v) PVA. The further preparation of the PLGA composite NP was similar to the standard one-step NPr. Following this protocol, NP with initially 2 % (w/w) PTX of the polymer mass were prepared. For manufacturing of positively charged fluorescent CS-CUR PLGA NP for penetration experiments (chapter 6), the procedure was upscaled to 500 mg polymer batches, which corresponds to an addition of 75 mg CS to the aqueous phase.

2.2.3.2 CS-EC composite NP

First, the setting of a suitable CS amount was investigated. 1, 5, 10, 15 and 25 mg CS per 10 ml aqueous solution were dissolved in 5 % (w/v) PVA. The remaining preparation of the EC 4 composite NP was adapted from the protocol for 3.5 % (w/v) EC 4 NP described in 1.2.2.4. For PTX-loaded CS-EC 4 composite NP 10 mg CS were dissolved in 10 ml 5 % (w/v) PVA solution. PTX-loading with initially 1 - 20 % (w/w) PTX of the polymer mass was tested.

2.2.3.3 PEC-coating of CS-PLGA composite NP

For PEC coating, 2 % (w/w) initially PTX-loaded CS-PLGA NP in a batch size of 500 mg were prepared and purified as described in section 2.2.3.1. After the last centrifugation step, particles were concentrated to a volume of 10 ml, slowly injected into 30 ml of 2 % (w/v) PEC solution, and incubated under stirring for 1 h. For preparation of PEC solution, 2 % (w/v) PEC was dissolved in aqueous medium by boiling at 100 °C for 1 h. To remove undissolved residuals, the solution was centrifuged (20,000 RCF for 30 min) and filtered (0.22 µm, polyvinylidene fluoride filter membrane). Then, samples were purified by centrifugation twice at 15,000 RCF for 30 min at 20 °C.

2.2.3.4 BSA-coating of CS-PLGA composite NP

In first coating experiments with bovine serum albumin (BSA), fluorescein isothiocyanate (FITC) fluorescently labeled BSA was used to verify a successful coating of NP by confocal laser scanning microscopy (CLSM). Additionally, different coating and crosslinking times were investigated regarding particle quality. For this, CS-PLGA NP in batches of 25 mg were prepared and purified. Then, NP were incubated with 2 mg BSA-FITC for 30 or 60 min at pH 6 under stirring (approx. 600 rpm). Then, samples were purified (2 x 10,000 RCF, 20 °C, 10 min with 20 ml MilliQ® water) and measured regarding size and ζ-potential by DLS and laser Doppler electrophoresis. Subsequently BSA was crosslinked with 10 µl 37 % formaldehyde for 1 h and purified again as described. Another sample was incubated with formaldehyde for 1 h without former purification. In addition to the CLSM tests, the samples were measured for their colloidal properties by DLS and laser Doppler electrophoresis. For final BSA-coated formulations, initially 2 % (w/w) PTX-loaded CS-PLGA NP in a batch size of 500 mg were prepared and purified as described in section 2.2.3.1. Then the samples were resuspended with MilliQ® water to a volume of 52.5 ml, 16.5 ml 0.4 % (w/v) aqueous BSA solution was added, and the pH was immediately adjusted to pH 6. After incubation for 30 min under stirring, half of the sample was either incubated with 90 µl 37 % formaldehyde for 1 h under stirring prior purification (2 x 10,000 RCF, 20 °C, 20 min with 20 ml MilliQ® water) or instantly purified.

2.2.4 Characterization of NP

2.2.4.1 Determination of colloidal properties

DLS, also referred to as photon correlation spectroscopy (PCS), is used for the optical sizing of smallest particles in liquids and thus, hydrodynamic diameter and polydispersity index (PDI) of NP can be evaluated. Apart from DLS measurements, the Zetasizer® NanoZS and Zetasizer® Ultra (Malvern Panalytical GmbH, Malvern, UK and Almelo, the Netherlands) were used for estimation of the particles' surface charges, expressed as ζ-potential, by laser Doppler electrophoresis. For Zetasizer® measurements, samples were diluted 1:500 with MilliQ® water and

filled into a disposable folded capillary cell (DTS 1070). The analysis was performed at backscatter angles of 173° and at 25 °C.

2.2.4.2 Quantification of CUR-loaded PLGA NP

CUR was quantified by fluorescence spectroscopy performed with an Infinite M200 plate reader (Tecan Trading AG, Männedorf, Switzerland). Emission and excitation wavelengths were set to λ_{em} = 515 and λ_{ex} = 415 nm, respectively, with a gain of 80 %. A calibration curve was prepared using concentrations of 0.1 - 1 µg/ml CUR in ACN. For evaluation of DL, aliquots of 1 mg freeze-dried NP were dissolved in ACN by vortexing for 5 min. Samples were filtered (0.45 µm, regenerated cellulose filter membranes), diluted to reach the concentration range of the created calibration curve, and volumes of 200 µl were measured in a solvent resistant 96-well plate. DL and EE were calculated as follows:

$$\text{DL [\%]} = \frac{\text{amount of recovered drug in NP aliquote [mg]}}{\text{amount of recovered NP in aliquote [mg]}} \text{ x } 100\ \%$$

$$\text{EE [\%]} = \frac{\text{amount of drug in total recovered NP [mg]}}{\text{initial amount of drug [mg]}} \text{ x } 100\ \%$$

Additionally, the limits of detection (LoD) and quantification (LoQ) were determined. For blank samples, plain PLGA NP, which were prepared and quantified in the same way, were used. Limits were calculated as follows (σ: standard deviation of blank samples, S: slope of calibration curve):

$$\text{LoD} = \frac{3{,}3 \text{ x } \sigma}{S}$$

$$\text{LoQ} = \frac{10 \text{ x } \sigma}{S}$$

2.2.4.3 Quantification of PTX-loaded NP

UV/Vis spectroscopy, a simple and fast method, was tested for quantification of PTX in addition to the more complex and time consuming HPLC technique. The quantification of PTX using UV/Vis spectroscopy involved the preparation of a calibration curve within a range of 5 µg/ml to 25 µg/ml PTX in ACN and measurement at a wavelength of 227 nm. Subsequently, the influence of PVA and PLGA on the measurement was tested. For this, 100 µg/ml PLGA alone or 100 µg/ml PLGA and 10 µg/ml PVA were mixed in PTX samples of 10 µg/ml ACN.

To separate possible affecting compounds such as PLGA or PVA within the sample under investigation, a HPLC procedure was used described by Furman *et al.* with adaption of parameters to the system [216]. At a flow rate of 0.5 ml/min, an injected sample volume of 20 µl was passed over a LiChrospher® 100 RP-18 column of an isocratic HPLC system of the UltiMate® 3000

model from Dionex Corporation (Sunnyvale, USA) at 30 °C. PTX was detected at a wavelength of 227 nm. A calibration curve of PTX in acetonitrile (ACN) was created using PTX concentrations from 0.05 µg/ml to 100 µg/ml. The influence of PVA (20 µg/ml) and PLGA (1 mg/ml) on the absorption of PTX (10 µg/ml) was investigated. LoD and LoQ were calculated as described in section 2.2.4.2 using pure ACN for blank measurements. For evaluation of loading behaviors, freeze-dried NP were dissolved in ACN by ultrasonication for 10 min. Samples were centrifuged at 24,000 RCF at 20 °C for 30 min, diluted to a NP concentration of 1 mg/ml and measured as described above. DL and EE were calculated as mentioned previously in section 2.2.4.2.

2.2.4.4 NP morphology and verification of fluorescence by microscopy

For the visualization of NP and evaluation regarding their morphology and topology, pin stubs were provided with a double-sided adhesive carbon disc and fitted with a silica wafer. Then, NP dispersions were diluted 1:100 with MilliQ® water and volumes of 5 - 10 µl were dropped on the wafer. Subsequently, the drop was carefully removed with a lint-free tissue to leave a thin film of NP dispersion on the wafer, and thus, to minimize the so called coffee-ring effect, the agglomeration of the NP due to the evaporation of the droplet [217]. Prior placing in the SEM chamber, the dried samples were sputtered with a thin gold layer of approximately 10 nm thickness in a Q 150R ES cathodic rotary-pumped sputter coater at 40 mA for 50 s (program: QT Time Gold) to make them electrically conductive for the subsequent SEM procedure by Zeiss EVO 15 or Zeiss EVO HD 15 using a working distance of 16.5 mm, an acceleration voltage of 5 - 20 kV and a secondary electron image detector. The fluorescence of FITC-BSA-coating of PLGA NP was verified by Zeiss CLSM LSM710 excited with an argon laser at 488 nm, the fluorescence of CUR-PLGA NP and CS-CUR-PLGA NP by Zeiss fluorescence microscope AX10 with an excitation wavelength of 470 nm.

2.2.4.5 Gelation trials of PEC and PEC-coated CS-PLGA composite NP

Prior to PEC-coating of NP, preliminary gelling experiments were carried out adding Ca^{2+} ions to PEC. For Ca^{2+} concentrations, a physiological concentration of 0.005 % (w/v), corresponding to an extracellular Ca^{2+} concentration of 1.1 - 1.4 mmol/l, and a higher concentration of 1 % (w/v) $CaCl_2$*$2H_2O$ were selected and added stepwise in 10 µl volumes to 0.5 ml of 0.1 and 1 % (w/v) PEC solutions, prepared as described in section 2.2.3.3. For investigation of the gelling behavior of PEC-CS-PLGA NP, 100 and 200 µl of a 1 % (w/v) CS-PLGA particle dispersion (corresponding to particle masses of 1 and 2 mg) were added to 1 ml of 0.5, 1 and 2 % (w/v) PEC solutions each and purified once or twice at 10,000 RCF for 20 min at 20 °C. PEC solutions were prepared as described in section 2.2.3.3. Resulting NP were characterized by DLS before and after the addition of 2 µl of 10 % (w/v) $CaCl_2$*$2H_2O$ solution. Single samples of 1 mg NP in 1 % (w/v) PEC solution, 1x and 2x purified, were additionally mixed and measured with larger volumes of 20 µl of $CaCl_2$*$2H_2O$.

2.2.4.6 Cell viability assay

Cell viability assays were performed with the help of Marijas Jurisic. The viability of HeLa cells (human cervix carcinoma cells) under the influence of PTX-loaded and unloaded EC 4 NP was investigated by their metabolic activity. Therefore, HeLa cells were cultivated in DMEM (high glucose) cell medium containing 10 % (v/v) fetal bovine serum and 1 % (v/v) antibiotics (PenStrep). 5,000 cells per well were seeded in sterile 96-well plates. The cell culture medium was removed, and the cells were washed with Hanks Balanced Salt Solution (HBSS) buffer and incubated with EC 4 NP and initially 1 % (w/w) PTX-loaded EC 4 NP in concentrations of 0.01 - 1,000 µg/ml for 24 h at 37 °C. Cell culture medium was used for negative control and 2 % Triton X-100 for positive control. After treatment, cells were washed with HBSS and incubated with HBSS containing 10 % (v/v) of the yellow 3-(4,5-dimethythiazol-2-yl)-2,5-diphenyl tetrazolium bromide (MTT reagent; 5 mg/ml) for 4 h at 37 °C. Then, the buffer was removed and DMSO was used to dissolve the formed blue formazan. A quantitative absorbance measurement was performed using an Infite®M200 plate reader at a wavelength of 550 nm. The cell viability was calculated using following equation:

$$\text{Cell viability (\%)} = \frac{\text{absorption sample - absorption positive control}}{\text{absorption negative control - absorption positive control}} \text{ x } 100\ \%$$

2.2.5 Redispersibility of NP formulations after freeze-drying

In terms of future commercialization, freeze-drying NP dispersions for storage and possibly transportation is a commonly used option. Since the redispersion into the original form is essential to ensure applicability, experiments regarding redispersibility after freeze-drying were performed. For this purpose, samples were frozen at -80 °C and then placed in a freeze-drying unit. Under a pressure of 0.2 mbar and a condenser temperature of -80 °C (Alpha 2-4 LSC) or -105 °C (Alpha 3-4 LSCbasic), samples were lyophilized over-night and redispersed within 48 h. All investigated samples were measured regarding their colloidal properties before and after being freeze-dried.

Fresh purified samples of plain PLGA NP, initially 1 % (w/w) CUR-loaded PLGA NP and initially 1 % (w/w) CUR-loaded CS-PLGA NP were freeze-dried and redispersed in MilliQ® water by vortexing for 5 min. For plain PLGA NP the addition of Glc was tested using a concentration of 50 mg/mg formulation. Initially 1 % (w/w) CUR-loaded PLGA NP were visualized by SEM in freeze-dried and redispersed state. The redispersion of initially 2 % (w/w) PTX-loaded EC 4 and PLGA NP, as well as the CS composites of both formulations, was tested. Therefore, aliquots of 1 mg/ml were prepared, freeze-dried and redispersed in 1 ml MilliQ® water by vortexing for 5 min. The effect of Glc and Tre addition before freeze-drying of the NP formulations were examined in concentrations ranging from 0.005 - 1 mg/mg formulation in case of PLGA NP types, corresponding to total concentrations of approx. 0.5 - 50 % (w/w) of the freeze-dried formulations. For EC 4 NP types Glc and Tre concentrations of 5 - 50 mg/mg formulations were investigated, corresponding to total concentrations of approx. 83 - 98 % (w/w) of the freeze-dried formulations.

The redispersibility of CS-EC 4 NP types was tested with Tre and Glc concentrations of up to 100 mg/mg formulation.

2.3 Results and discussion

2.3.1 Preparation and drug loading of polymeric NP

2.3.1.1 Investigations on PLGA NP

Preparation of plain PLGA NP according to existing protocols resulted in NP with hydrodynamic diameters of 197 $\pm$ 4 nm, a narrow particle size distribution (PDI of 0.054 $\pm$ 0.020), and a negative surface charge with a ζ-potential of -30.8 $\pm$ 4.1 mV. Figure 2.1 was obtained by SEM imaging and shows spherical, clean, and an agglomerate-free morphology of NP, providing excellent conditions for later trials. CUR-loading results are described along with those of CS-composite PLGA NP in section 2.3.2.1.

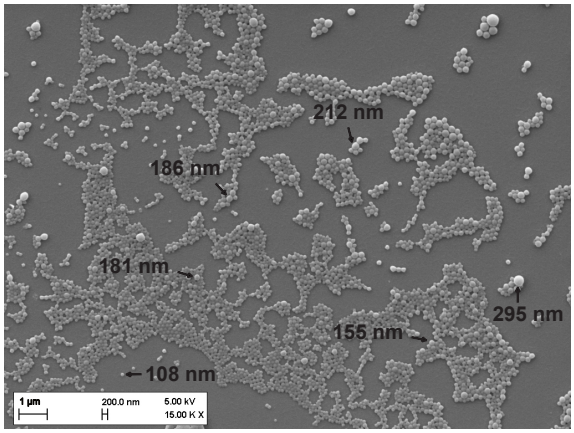

Figure 2.1: SEM image of purified PLGA NP.

Particle diameters measured with Fiji 1.0.

PTX-loaded particles, produced with ACN and PVA, could not be completely redispersed when purified by centrifugation and therefore, ACE was chosen as solvent. With 0.1 and 1 % (w/v) poloxamer 188 of flocculation of the produced particle dispersion was observed after a short time. Particles with PS 20 and 80 initially led to stable NP dispersions with sizes of 120 - 130 nm (PDI $<$ 0.1) and ζ-potentials of -30 to -35 mV. Using lecithin for stabilization, different size fractions of the unpurified particles (approx. 850 and 200 nm) indicated formation of agglomerates. Nevertheless, these NP dispersions could not be purified by centrifugation due to low redispersibility of the pellets. Only PVA led to stable, purifiable NP dispersions, and therefore, was used for the following experiments. Other methods for purification, such as tangential flow filtration, dead end filtration, and dialysis, would be conceivable for PS-stabilized NP. However, it must be considered that these techniques require larger amounts of aqueous rinsing solution and NP are exposed to them for several hours. This might cause loss of payload [218]. For this reason, these formulations were not further pursued.

In the following section, the influence of various parameters such as preparation method, solvent, initial drug concentration, and type and amount of polymer on particle properties is described. For SE, NP are slightly larger compared to NP produced by NPr and tend to have increasing sizes when raising initial PTX concentration (Figure 2.2 A). Using both methods, the polymer type did not influence particle size. PDIs of all samples were < 0.2 and represent narrow particle size distributions. SE led to considerably higher DL and EE for all tested PTX concentrations compared to NPr (Figure 2.2 B).

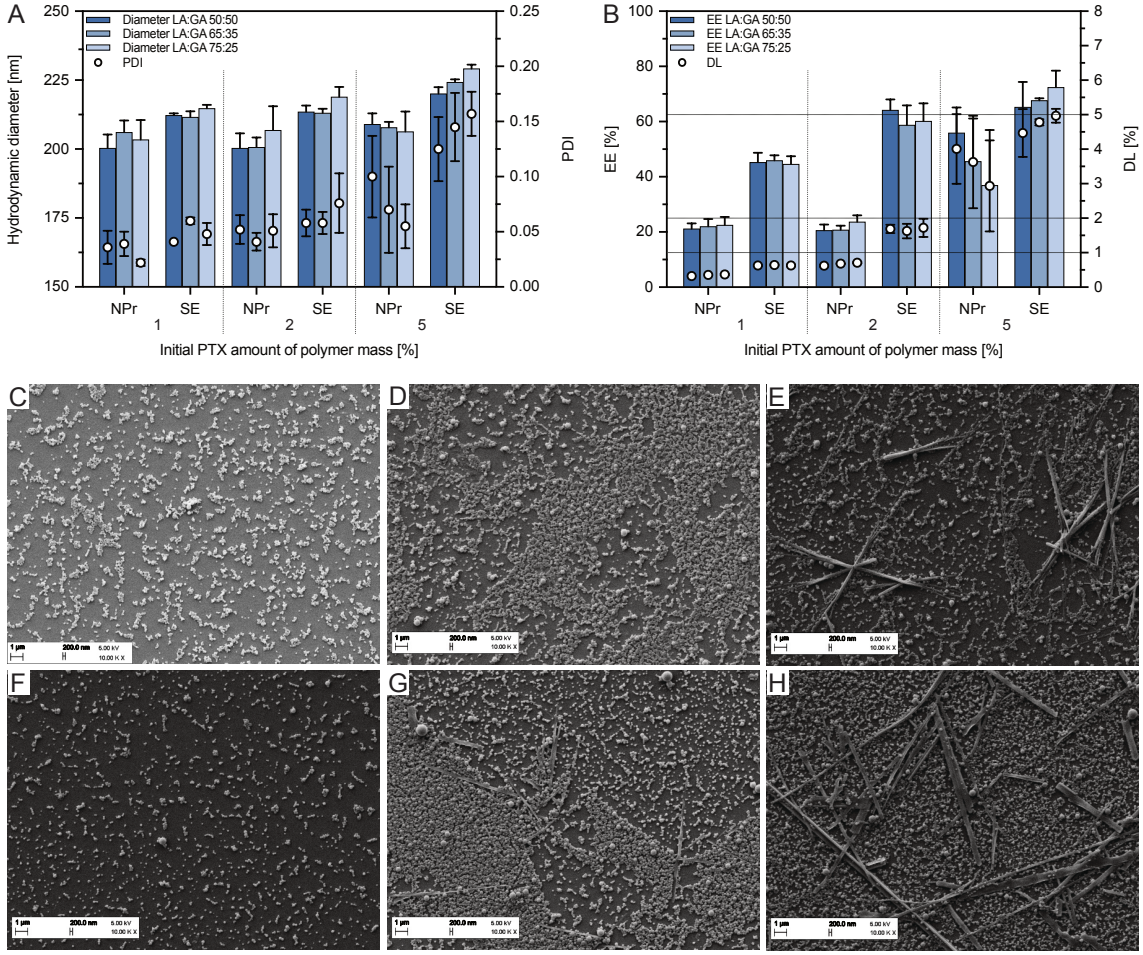

Figure 2.2: Characterization of PTX-loaded PLGA NP of different preparation methods, initial PTX amount and type of polymer regarding LA:GA ratio.

A: Colloidal properties. B: Loading properties. Horizontal auxiliary lines indicate the initial PTX mass with respect to the polymer mass. C-H: SEM images of NP made of PLGA with a LA:GA ratio of 50:50 and varying initial PTX amounts. C-E: NP of nanoprecipitation method. F-H: NP of single-emulsion evaporation method. C, F: 1 % (w/w) PTX. D, G: 2 % (w/w) PTX. E, H: 5 % (w/w) PTX.

At an initial PTX concentration of 5 % (w/w), EE and DL showed relevant fluctuations indicating inhomogeneity. SEM images (Figure 2.2 E, G, H) demonstrate that PTX precipitates obviously caused increased DL and EE at 5 % (w/w) PTX for NPr, and 2 and 5 % (w/w) for SE. Precipitates were identified consisting of PTX as precipitating dissolved PTX in 2 % (w/v) PVA solution without PLGA resulted in precipitates with similar morphologies (Figure 2.3). Varying LA:GA ratios of PLGA, morphology did not indicate noticeable differences. For this reason, only SEM

images of 50:50 ratio are depicted here (Figure 2.2 C-H).

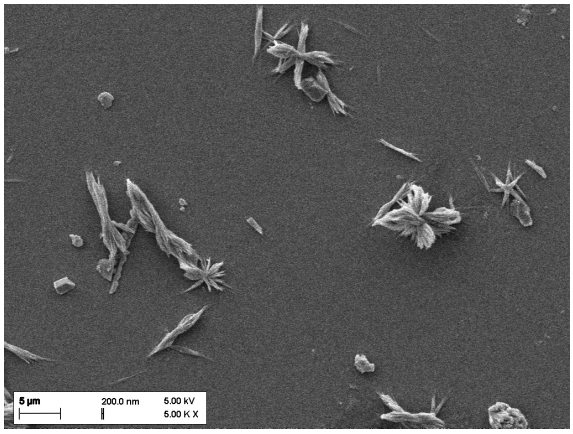

Figure 2.3: SEM image of pure PTX precipitates.

Morphology: 3 - 10 µm long rod-like structures, which aggregate into crosses, stars and bundles.

By changing parameters with respect to the standard NPr protocol (25 mg RG 503H in ACE), effects regarding colloidal and loading properties were evaluated. Using an initial PTX concentration of 2 % (w/w), PLGA of different viscosity and concentration as well as ACE and THF as solvents were compared. Resulting colloidal and loading effects are demonstrated in Figure 2.4. A higher PLGA concentration and use of THF resulted in larger particles, while less PLGA led to considerably smaller sizes. With lower PLGA viscosity (502H) a comparable particle size was received, while a higher viscosity (504H) led to slightly decreased sizes. All changes to the standard procedure resulted in narrow particle size distributions (PDI < 0.1). Using 10 mg of polymer, so far lowest loading properties in NPr were achieved while 40 mg led to highest results with DL and EE of 0.84 % and 32.2 %, respectively. Use of THF also resulted in slightly improved loading properties. Whereas for particle sizes (188 - 197 nm), the effect of PLGA viscosity on DL and EE was not very pronounced.

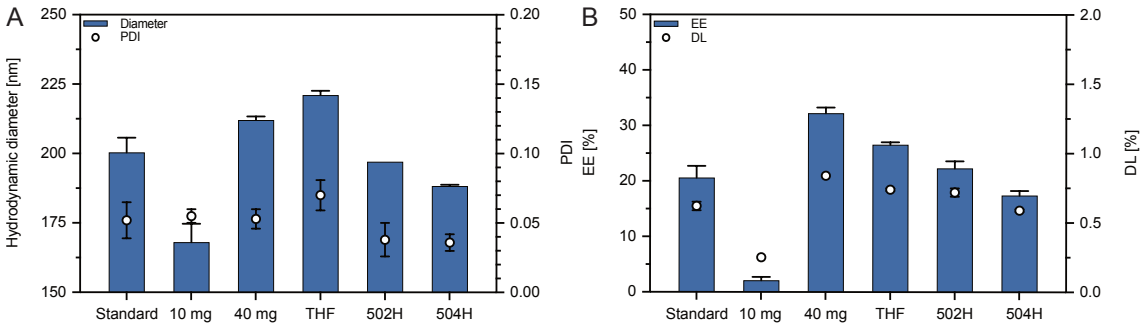

Figure 2.4: Characterization of PLGA NP with loading of initial 2 % (w/w) PTX of the polymer mass.

Comparison of NP prepared by standard NPr to variations regarding solvent type, PLGA amount and PLGA viscosity. A: Colloidal properties. B: Loading properties.

Especially the last described experimental series showed the tendency of larger particles to provide better loading properties. On the one hand, this can be attributed to a higher particle yield (16.7 vs. 75.6 % with 10 and 40 mg, respectively) due to the purification method used, and on the other

hand to an increased DL due to the larger particle volume. Both, DL and yield, again influence EE values. This relationship as well as the influence of solvents (THF and ACE) on the particle size are discussed in more detail in section 3.4.1.4.

Comparing the two NP preparation methods, an initially 2 % (w/w) PTX loading in SE showed precipitates while it did not in NPr. A presumably important difference is the solvent evaporation step by SE, which is necessary to cure the particles. In NPr, the dispersion can be purified immediately after injection and the free, dissolved PTX in the solvent-water mixture is instantly removed. In contrast, solvent evaporation reduces the solubility of the free, non-encapsulated PTX in aqueous medium, which leads to precipitates of the drug. Consequently, the subsequent purification step can no longer remove the µm-sized precipitates from the dispersion. This theory is supported by an opposite effect when a cosolvent is added. In NPr with initial PTX concentration of 5 % (w/w), the addition of EtOH to the aqueous phase before solvent injection reduced or avoided precipitate formation with increasing EtOH content (SEM images not shown). However, this was accompanied by reduced loading properties of 0.13 % DL and 1.42 % EE as well as formation of particle agglomerates adding 5 ml EtOH.

Overall, the loading is rather modest with DL below 1 % and EE of max. 45 % (SE) in the samples without precipitates of free PTX. Most PTX-loaded PLGA NP formulations described in the literature were initially loaded with 1 - 10 % (w/w) PTX and prepared with dichloromethane or chloroform and PVA-stabilized by SE, while in very few cases NPr was used [219, 220, 221, 222, 223, 224, 225, 226, 227, 228, 229, 230]. With particle sizes ranging from about 135 to 320 nm, DL of 2.7 - 5.8 %, and EE of 35 - 96 %, considerably higher loading properties were obtained than in the trials performed in the present thesis. None of these sources described the formation of PTX precipitates, so either better PTX encapsulation was obtained, possibly due to the chlorinated solvents used, or precipitates of free PTX were simply neglected. As the use of chlorinated solvents was to be avoided in the performed trials due to possible toxic residues in the final formulation, this option was rejected. For NPr, Esfandyari-Manesh *et al.* reported comparable particle sizes (190 nm) [222]. Although the EE of 80 % implies that PTX got lost, e.g., due to the purification method or adsorption on containers, a notably higher DL of 10.7 % compared to initially used 7 % (w/w) PTX concentration might indicate the presence of PTX precipitates.

Since the solubility of PTX in PLGA polymers was obviously rather low, the following experiments evaluated the loading of EC, which allows the solution of drug and polymer in EtOH.

2.3.1.2 Investigations on EC NP

The preparation method of EC NP following the protocol of Urbán-Morlán *et al.* was successful, although redispersibility during purification was more difficult compared to PLGA NP. Particles of 2 % (w/v) EC 4 and EC 10 resulted in slightly larger particle sizes of 152 nm and 222 nm, respectively, compared to the literature (Figure 2.5 A) [214]. Particle size distributions were wider than using PLGA with PDIs of < 0.2 and formulations showed agglomerate-free, spherical appearance

without impurities in SEM visualization (only 3.5 % (w/v) EC 4 NP are shown in Figure 2.5 B, except for 4 % EC 4 particles. This formulation showed large agglomerates with a net-like structure in the SEM (Figure 2.5 D), which probably was responsible for the in average increased PDI of 0.287. As EC 10 NP showed a relatively fast sedimentation within 1 - 2 min (inappropriate in terms of, e.g., the application process) and a particle size of approx. 200 nm was aimed for comparability with PLGA NP, the formulation with 3.5 % (w/v) EC 4 was selected for subsequent experiments. The ζ-potential measurements revealed values of 29.1 to 33.3 mV in all produced formulations, indicating stable dispersions.

When loaded with initial 20 % (w/w) PTX compared to 1 - 15 % (w/w) PTX, the particle size and PDI slightly increased and fluctuated, indicating the presence of PTX precipitates (Figure 2.5 C). Figure 2.5 E demonstrates DL, EE, and yield of loaded EC 4 NP. Initial 1 % (w/w) PTX loading in EC 4 resulted in higher DL (0.78 %) compared to PLGA with 0.62 % in NPr using initial 2 % (w/w) PTX, or 0.63 % in SE using initial 1 % (w/w) PTX. With higher initial amounts of PTX the DL increased continuously. At 10 % (w/w) initial PTX concentration a DL of 7.35 % was achieved without visible precipitates in SEM (Figure 2.5 F). A PTX concentration of initial 15 % (w/w) showed few single precipitates, while huge amounts of free PTX (precipitates) were visible with initial 20 % (w/w) PTX concentration (images not shown). Lower EE of approx. 35 % in EC 4 NP using initial 1 - 10 % (w/w) PTX compared to initial 1 % (w/w) PTX-PLGA NP prepared by SE can be explained by lower particle yields of around 45 %. Altogether, considerably higher DL could be achieved with EC 4.

To date, no loading values of PTX in EC NP have been reported, so it is not possible to tell whether these results are consistent with those of other laboratories. Nevertheless, it can be concluded that the solubility of drug and polymer is substantially better in this combination within NPr method using EtOH compared to PLGA formulations. As described earlier in section 1.3.3, a previous dosage of PTX in PIPAC has not yet been found, so it is not possible to conclusively evaluate whether a manufacturable and nebulizable amount of nanoparticulate formulation is possible and reasonable with the measured loading values. Nevertheless, a more than 10-fold higher amount of PLGA NP compared to the EC 4 NP can be assumed. Thus, a possible application with the doses of 35 - 140 mg/m^2 PTX (Abraxane®), currently investigated by Van de Sande within a dose-limiting toxicity study, might require 0.5 - 2 g/m^2 of initial 10 % (w/w) PTX-loaded EC 4 NP per application, and accordingly multiply higher amounts of initial 1 or 2 % (w/w) PTX-loaded PLGA NP by SE or NPr, respectively. A disadvantage of EC NP is the non-biodegradability of the polymer. Thus, elimination after peritoneal application is only possible via lymph and blood circulation. However, the extent to which this occurs is not yet predictable and further studies should be conducted in this regard. Due to the currently palliative application of the PIPAC procedure, issues regarding degradability or elimination are probably negligible.

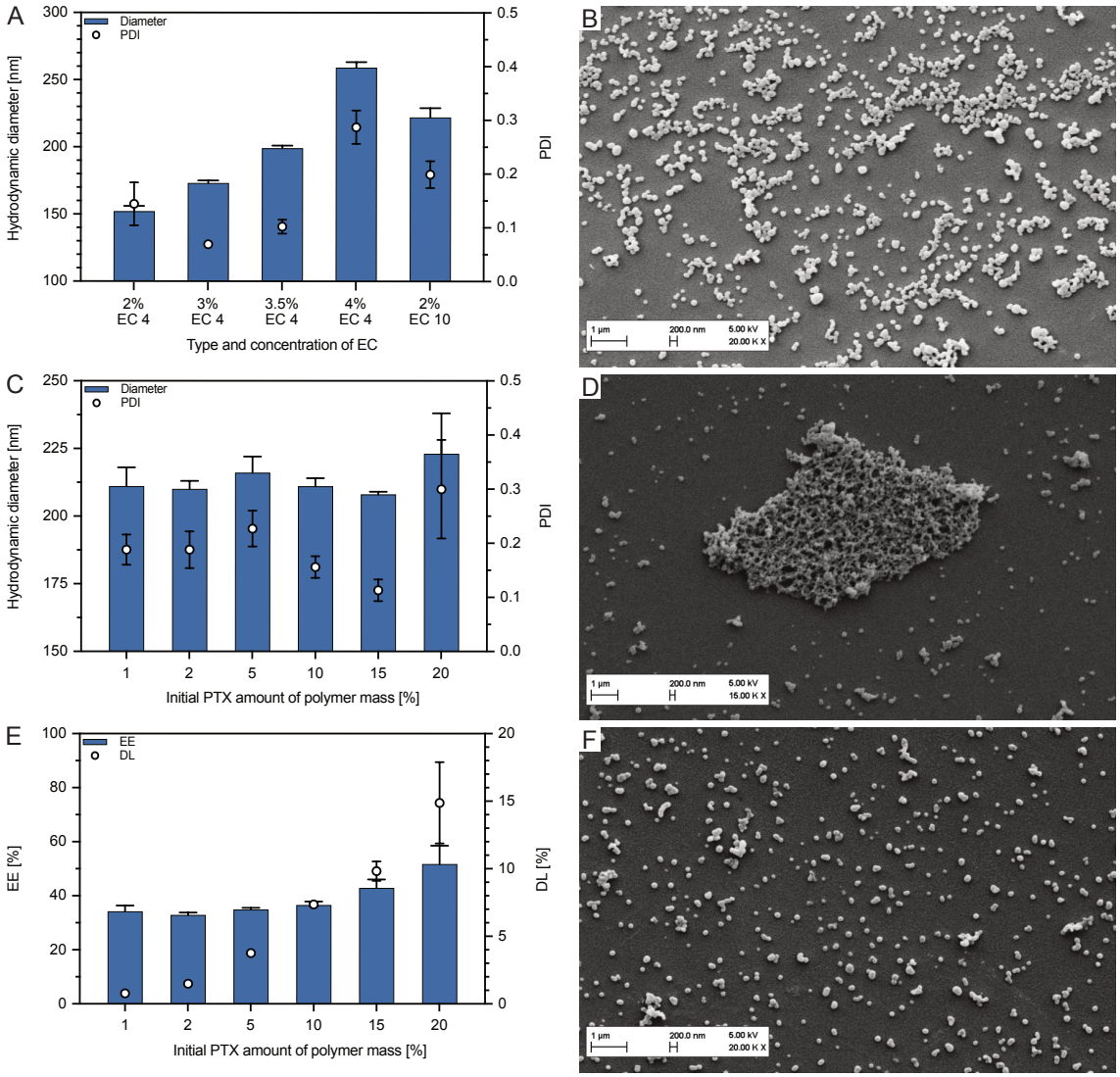

Figure 2.5: Characterization of diverse EC NP formulations.

A: Colloidal properties of plain EC NP using different polymer types and concentrations. B: SEM image of plain NP of 3.5 % (w/v) EC 4. C: Colloidal properties of PTX-loaded EC 4 NP. D: SEM image of plain NP of 4 % (w/v) EC 4. E: Loading properties of PTX-loaded EC 4 NP. F: SEM image of 3.5 % (w/v) EC 4 NP with loading of initial 10 % (w/w) PTX.

2.3.2 Surface modification of polymeric NP

2.3.2.1 Surface modification of CUR-loaded PLGA NP

The properties of negatively and positively charged CUR-loaded PLGA NP used for penetration trials are listed in Table 2.1. The combination of CS and PLGA led to a change in ζ-potential towards positive values compared to PLGA alone. Furthermore, particle size was approx. 20 nm larger, which probably caused higher yields and better loading properties. CS, with its numerous free positively charged amino groups, interacts electrostatically with the negatively charged carboxyl groups of PLGA, creating a positive charge on the surface and an increased volume of the NP. Nafee *et al.* obtained comparable surface charges with similar CS concentrations [215].

The fluorescence of CUR-loaded NP is shown in Figure 2.6 C and D. SEM images demonstrated spherical, agglomerates-free samples (Figure 2.6 A and B). Overall, the particles were stable, had a narrow particle size distribution, and can be evaluated in terms of their penetration depth according to surface charge in tissue after PIPAC application due to their fluorescence (chapter 6).

Table 2.1: Properties of CUR-loaded negatively charged PLGA NP and positively charged CS-PLGA composite NP. Colloidal properties were measured batch-wise (n = 18), quantitative properties were measured after particle pooling.

Type of carrier	Diameter [nm]	PDI	ζ-pot. [mV]	Yield [% (w/w)]	DL [% (w/w)]	EE [% (w/w)]
PLGA NP	189 ± 5	0.040 ± 0.018	-27 ± 2	36.9	0.45	16.8
CS-PLGA NP	210 ± 5	0.059 ± 0.013	+18 ± 3	59.7	0.57	33.1

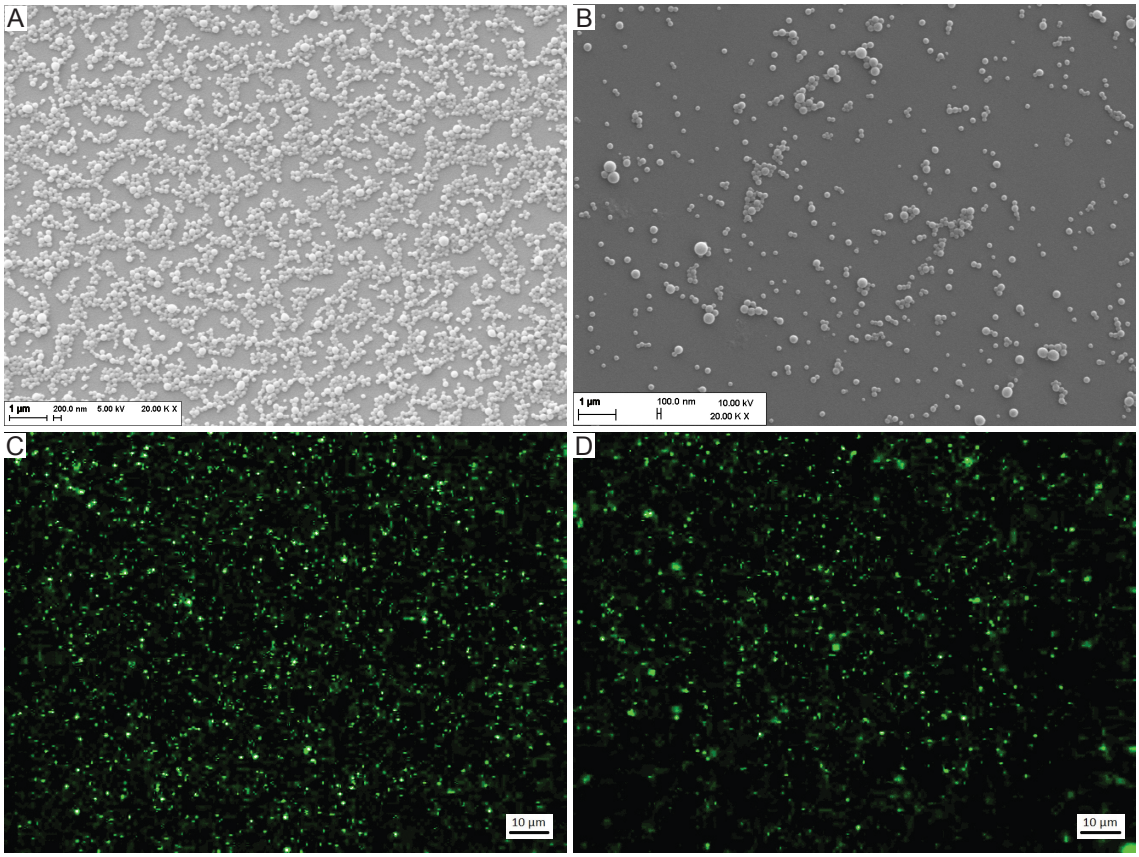

Figure 2.6: Visualization of CUR-loaded PLGA NP.

A and B: SEM images for morphology investigations. Spherical NP with relatively narrow particle size distribution were visible, appearing larger for CS coated particles. No impurities or excess CS were observed. C and D: Fluorescence microscopic examination of CUR-loaded NP. In both samples CUR fluorescence could be detected. Larger fluorescence spots indicate particle agglomeration. A, C: CUR-loaded PLGA NP. B, D: CUR-loaded CS-PLGA NP. Adapted from Nanomedicine (2021) 16(2), 109-120 with permission of Future Medicine Ltd. [231]

2.3.2.2 Surface modification of PTX-loaded PLGA NP

The surface modification of PTX-loaded NP and the corresponding change in drug release is the central objective of this work. To adsorb the negatively charged coating polymers PEC and BSA onto the surface of negatively charged PLGA NP, PTX-loaded CS-PLGA composite carriers with positive surface were prepared first. Colloidal properties of surface modified particles are demonstrated in Figure 2.7 A.

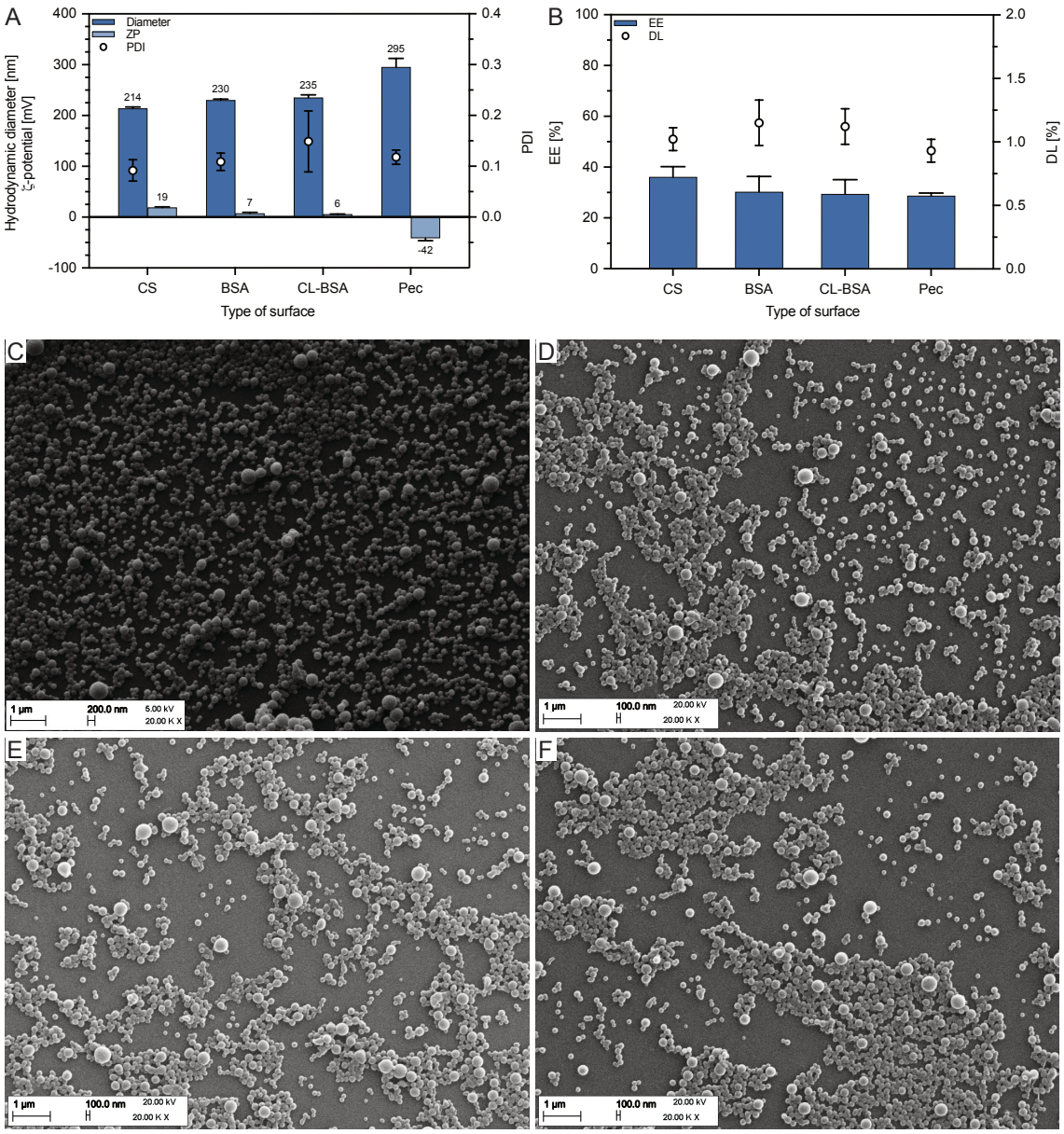

Figure 2.7: Characterization of initially 2 % (w/w) PTX-loaded PLGA NP with various surface modifications.

A: Colloidal properties. B: Loading properties. C-F: SEM imaging for morphological examination. C: CS-PLGA NP. D: BSA-coated CS-PLGA NP. E: Cross-linked BSA-coated CS-PLGA NP. F: PEC-coated CS-PLGA NP.

CS-composite NP loaded with PTX showed similar values as the previously described CUR-loaded CS-PLGA particles. DL and EE were increased by 50 % and 75 %, respectively, compared

to unmodified PLGA NP (Figure 2.7 B). Larger particle volumes and a possibly increased affinity of PTX to the CS-PLGA composition might account for this regard. Due to the better loading properties within SE, this was also tried for preparation of CS-PLGA composite NP. However, this was not successful as the CS coating did not seem to adhere effectively to the particles, and therefore, neither an increase in size nor a clearly positive ζ-potential were measured. Nevertheless, this contradicts the results reported in the literature [215]. The use of EtOAc in SE compared to ACE in NPr might result in an adsorption only at the particle surface, which might have been partially washed away during the harsh purification by centrifugation, and thus, explain the low surface potential. The ζ-potential measurement of unpurified NP by Nafee *et al.* might support this explanation since the slightly adherent CS layer was not washed away [215].

Subsequently, successful coating with BSA or PEC by electrostatic adsorption was confirmed by particle enlargement and the drop or change in ζ-potential (Figure 2.7 A). BSA coating considerably reduced the positive NP surface charge. Formaldehyde-mediated cross-linking of the positively charged amino acids did not affect the surface potential. The adjustment of the pH value to approx. 6 prevails a negative charge of BSA during the coating process (isoelectric point at pH 4.6) and a high positive charge of CS [232]. The negative moieties of BSA adsorb to the positive CS NP surface, whereas the few positively charged amino acids are repelled by the strongly positively charged CS molecules. The effective reduction of positive charge compared to the CS-coated surface leads to a reduction of the ζ-potential to low positive values.

Instead, PEC coating was generally pH-independent and clearly negatively charged particles were measured. Li *et al.* reported similar behavior in the context of liposome coatings in terms of particle enlargement and charge [233]. Regarding the loading properties (Figure 2.7 B), coated NP tended to lower EE, probably due to the additional purification steps. DL in BSA-coated NP was slightly higher compared to PEC. This might be due to the reported affinity between albumin and PTX causing a conformational change and loss of helical stability of the protein [234, 235, 236]. SEM images in Figure 2.7 C-F indicate spherical NP without visible residuals of CS or coating material.

To confirm successful coating with BSA, FITC-labeled BSA was used in preliminary experiments. The resulting particles were successfully examined using a CLSM (Figure 2.8). Moreover, different parameters in BSA coating were investigated (detailed results not shown). Overall, incubation times of 30 and 60 min of BSA in NP dispersion resulted in comparable colloidal properties of the coated NP, suggesting saturation of surface adsorption. Therefore, an incubation time of 30 min was selected. Purification prior to the cross-linking step also did not reveal any changed properties. Thus, additional purification was not carried out to circumvent possible particle loss.

2.3.2.3 Surface modification of PTX-loaded EC NP

As increased PTX loadings were achieved for CS-PLGA NP, the modification of EC 4 NP with CS was also investigated. The effect of different CS concentrations on the colloidal properties of plain CS-EC 4 NP is shown in Figure 2.9 A. For the lowest CS amount of 1 mg in the aqueous phase, a

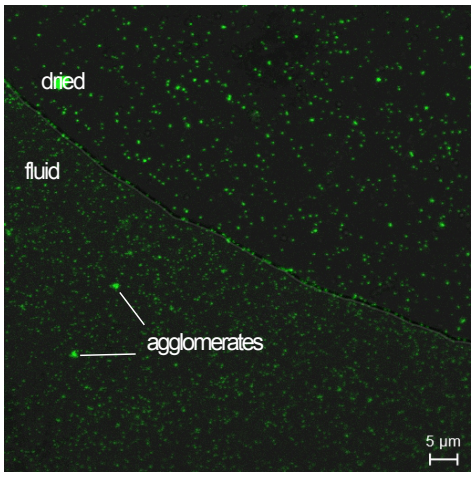

Figure 2.8: CLSM examination of CS-PLGA NP coated with FITC-labelled BSA and cross-linked by formaldehyde.

NP in liquid and after drying at magnification of 100x (oil). Bigger fluorescent spots indicate particle agglomerates.

markedly unstable particle dispersion was obtained, indicated by a very fast deposited dispersion with agglomerates and low positive ζ-potentials. Presumably, not the entire surface was covered with positively charged CS, whereby the negative charge of EC 4 led to an unstable dispersion. Higher CS concentrations revealed stable particle dispersions. 5 and 10 mg CS resulted in a particle size increase of about 50 nm compared to NP of EC 4 alone. 15 and 25 mg CS resulted in increasing sizes accompanied by free CS as demonstrated by SEM image in Figure 2.9 C. Therefore, an amount of 10 mg CS in the aqueous phase was used for further PTX-loading experiments. DL with initial PTX concentrations of 1 - 20 % (w/w) were comparable to EC 4 NP without CS (Figure 2.9 B). PTX precipitates were found in the SEM images at 15 % (w/w) initial PTX concentration (Figure 2.9 D). However, as for the CS-PLGA composite NP, higher EE was measured due to the substantially higher particle yield of about 70 %.

Obviously, CS does not improve encapsulation of PTX in terms of an increased affinity to the polymer blend. However, the pronounced size effect might improve loading.

2.3.3 Characterization of NP

2.3.3.1 Quantification of PTX and CUR

To quantify the (model) drug amount loaded into the NP, methods by UV/Vis spectroscopy and HPLC were investigated in the case of PTX, and fluorescence spectroscopy for CUR. Quantification of pure PTX dissolved in ACN was possible with both methods (Figure 2.10). However, the presence of PVA caused an absorption shift at the maximal absorption wavelength of PTX, resulting in a measurably higher concentration of PTX as contained at all (Figure 2.10 A and B). This influence was not measured for PLGA (Figure 2.10 B). Since the extent of the PVA absorption shift was concentration-dependent (experiment not shown) and PVA concentration itself depended on the effectiveness of purification, introducing PVA into background subtraction was not feasi-

ble. Instead, absorption of PTX was measured without an influence of neither PVA nor PLGA by HPLC benefiting from the chromatographic separation of the compounds (Figure 2.10 C).

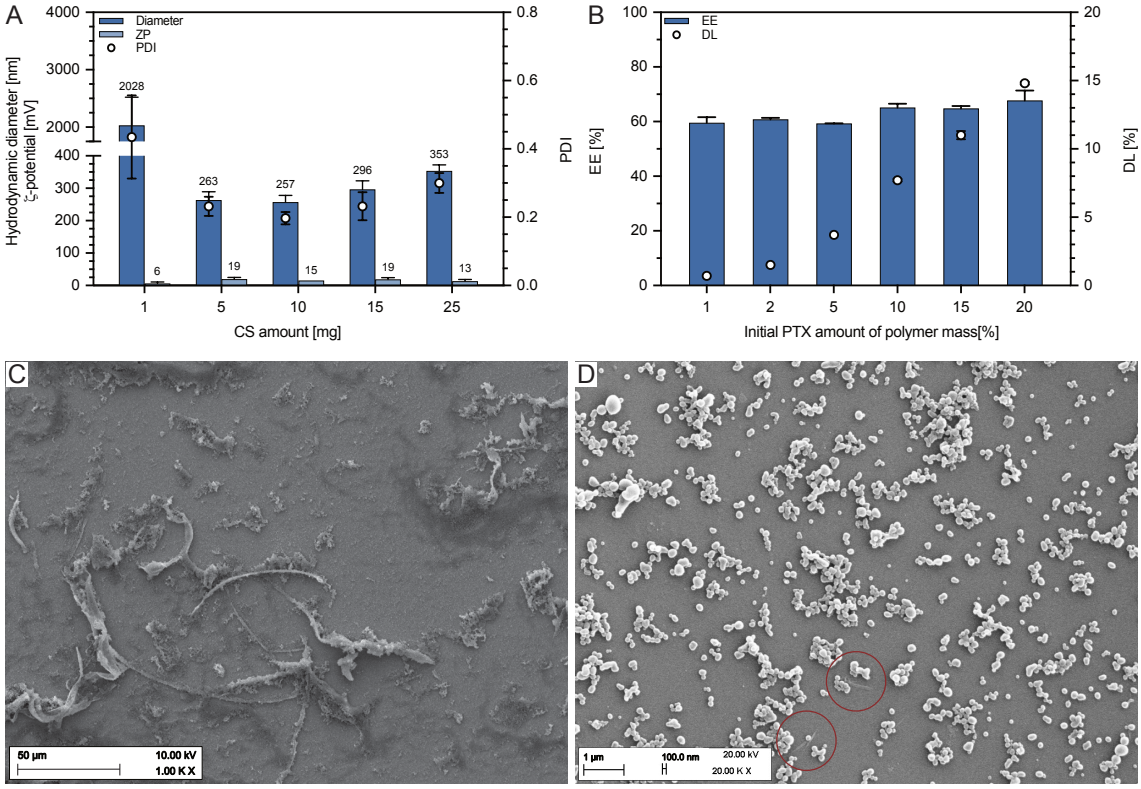

Figure 2.9: Characterization of plain and PTX-loaded CS-EC 4 composite NP.

A: Colloidal properties of plain CS-EC NP using varying amounts of CS in the aqueous phase (preparation by NPr). B: Loading properties of CS-PLGA NP using 10 mg CS in aqueous phase and varying amounts of PTX. C, D: SEM imaging of CS-EC NP. C: Plain CS-EC 4 NP with 25 mg CS showing residuals of free CS. D: CS-EC NP with 10 mg CS and initial 15 % (w/w) PTX. Red circles refer to PTX precipitates.

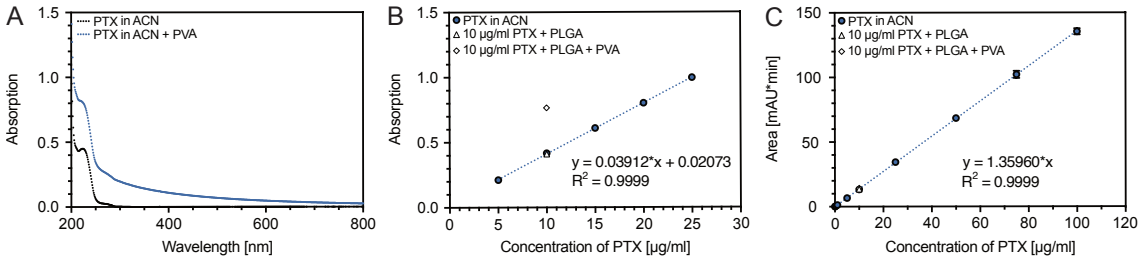

Figure 2.10: Quantification of PTX in ACN.

A: Absorption enhancement of PVA in wavelength scan by UV/Vis spectroscopy. B, C: Calibration curves and influence of additional PVA on the recovered PTX concentration. B: UV/Vis spectroscopy. C: HPLC.

Calibration curves, LoD and LoQ were calculated to examine CUR and PTX loadings (Table 2.2). The LoQ determined for PTX approx. agreed with 5 ng/ml as reported by Ibrahim *et al.* [237]. For both methods, high sensitivity allowed efficient measurement of NP loadings.

Table 2.2: Calculations of CUR and PTX quantification methods.

Quantified compound	Calibration curve	Correlation coefficient (R^2)	LoD	LoQ
CUR	y = 20.014x	0.9993	7.89 ng/ml	23.92 ng/ml
PTX (HPLC)	y = 1.3596x	0.9999	2.2 ng/ml	6.6 ng/ml

2.3.3.2 Gelation of PEC

Gelling properties of PEC and PEC-coated PLGA NP were investigated to estimate the extent to which a hydrogel layer forms around the coated particles. First gelling experiments of pure PEC with a physiological Ca^{2+} concentration showed visually no change in viscosity. Addition of 1 % (w/v) $CaCl_2$*H_2O solution to 1 % (w/v) PEC resulted in gelling clumps already after adding a volume of 20 µl ion solution (Figure 2.11 AI). The amounts of gelled clumps increased with further addition of ions until the PEC solution was completely gelled (Figure 2.11 AII). PEC solutions of 0.1 % (w/v) were not affected by addition of Ca^{2+} ions. Thus, a certain concentration of Ca^{2+} and PEC is necessary to perceive a visual gelation, consistent with reported concentration-dependent ionic gelation of PEC [238].

Figure 2.11 B illustrates gelation-mediated variation in sizes and PDIs of PEC-coated NP. All PEC-coated particles showed higher particle sizes than the CS-coated particles. When purified twice, an increasing particle size was visible with increasing PEC concentration. The addition of small amounts of calcium ions showed only slight changes in size. This tendency towards larger particles at higher PEC concentrations was also visible for particles purified once, except the 2 mg sample coated with 2 % (w/v) PEC. When small amounts of Ca^{2+} ions were added to once purified samples, an enormous increase in size was visible. This gelation behavior, which was not observed for NP purified twice, was probably caused by free PEC or PEC, which was weakly associated with the CS cations. High amounts of Ca^{2+} ions seemed to also gel PEC anions, which were associated stronger with CS cations, indicated by increased sizes of twice purified particles after addition of high amounts of Ca^{2+}. It is assumed that already during the coating process a gelation of PEC takes place due to the association with polycations (CS) adherent to the particle surface. Thus, the addition of the divalent ions might only lead to gelation of remaining free PEC. In high quantities Ca^{2+} might also lead to dissociation of PEC from the particle surface. Therefore, it is uncertain whether an addition of Ca^{2+} ions is necessary or in what quantities it should be applied. A higher concentration of free PEC, which gels after application of Ca^{2+} ions, might serve as an additional hydrogel layer instead of a liquid film in which the NP are embedded, and thus, could prevent or slow down drug release.

2.3.3.3 Cell viability

To ensure non-biodegradable EC 4 NP do not cause any toxic effects when remaining in the human body, plain EC 4 NP were examined within an MTT assay. Since PTX-loaded EC 4 NP were

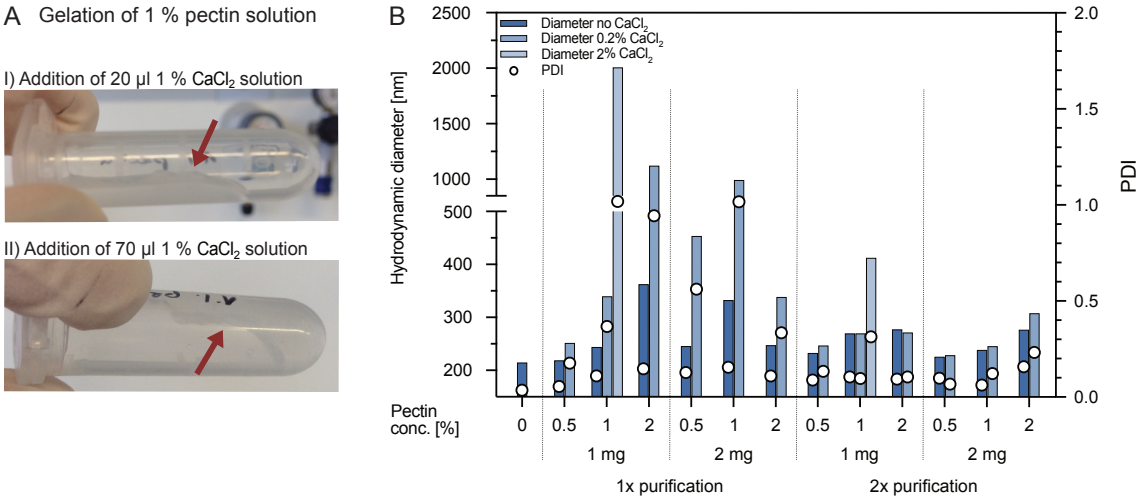

Figure 2.11: Gelation pre-tests of PEC and PEC-coated CS-PLGA NP.

A: Images of stepwise addition of 1 % (w/v) $CaCl_2$ solution to 1 % (w/v) PEC solution. B: DLS results of various PEC-coating parameters and influence of $CaCl_2$ on particle properties (n=1).

expected to cause toxic effects, these were also subjected to the assay. HeLa cells were selected being available in the laboratory and representing adenocarcinoma human cervix epithelial cells potentially, but rather atypically, spreading into the abdominal cavity and leading to peritoneal metastasis [239, 240]. Concentrations from 0.01 to 1,000 µg/ml of both NP formulations were investigated. Results of *in vitro* assays (Figure 2.12) showed a high viability of HeLa cells at all concentrations of plain EC 4 NP within 24 h indicated by values of 90 - 120 %. According to literature, cell viability above 80 % is considered as non-cytotoxic, 60 - 80 % as weak cytotoxic, 40 - 60 % as moderate cytotoxic, and below 40 % as strong cytotoxic [241]. Instead, PTX-loaded EC 4 NP appeared to have a concentration-dependent weak cytotoxicity. Up to 1 µg/ml NP, corresponding to 7.7 ng/ml PTX, non-cytotoxicity is given, while 10 - 1,000 µg/ml NP, corresponding to 0.077 - 7.7 µg/ml PTX, showed weak cytotoxic values.

Fonseca *et al*. demonstrated that both incubation time and concentration affect the *in vitro* cytotoxicity of PTX by cell viability trials of small cell lung cancer cells (NCI-H69) treated with Taxol® or PTX-loaded PLGA NP. Cell toxicity was higher for longer periods of incubation ($\geq$ 72 h) with PTX showing moderate cytotoxicity. This is in accordance with the mode of action of PTX as with longer incubation time a larger number of cells enter mitosis allowing PTX to become active [242]. Other cell lines revealed similar results [243, 244]. Thus, PTX-loaded EC 4 NP have dose- and presumably time-dependent cytotoxic effects. In contrast, unloaded EC 4 NP showed no cytotoxic effect.

2.3.4 Redispersibility of NP formulations after freeze-drying

Since the designed formulations including PTX can be most efficiently transported and stored in the dried state to ensure stability, redispersibility of NP was of great importance and is described in the following. As CUR-loaded PLGA and CS-PLGA NP were required for external penetration

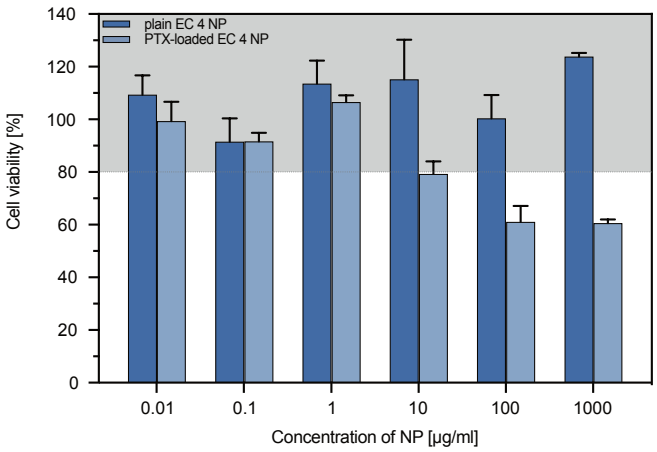

Figure 2.12: Cell viability of HeLa cells after 24 h incubation with plain and PTX-loaded EC 4 NP.

Non-toxic concentrations are considered with a viability above 80 % and are highlighted with a grey boundary.

tests, their redispersibility after freeze-drying was investigated first. Colloidal properties of freshly manufactured and redispersed NP (without storage or transport) showed a small but acceptable increase in size (Figure 2.13 A). SEM images (Figure 2.13 C and D) of freeze-dried CUR-loaded PLGA NP demonstrated that NP formed cylindrical and plate-shaped structures resulting from the process of water removal (sublimation). In the redispersed samples no or hardly any NP agglomerates were visible (Figure 2.13 E). Accordingly, a good stability and redispersibility was present. However, after transport to the cooperation laboratory in Tübingen and a storage time of about one year, redispersion of the freeze-dried NP cakes was not completely possible. Figure 2.13 B shows the presence of agglomerates in DLS measurements (micrometer range) that could not be redispersed. Long storage time and transportation might have led to time-dependent or mechanical destruction of the freeze-dried cake matrix, which normally prevents NP from agglomeration, making redispersion, and thus, application impossible. When considering the colloidal properties of plain PLGA NP, a substantial increase in size and size distribution was determined compared to the CUR-loaded formulations. Thus, CUR loading seems to have a stabilizing effect on the NP. The inclusion of Glc as a lyoprotector had pronounced effects on the redispersibility of NP (Figure 2.13 A). Therefore, the concentration-dependent stabilizing influence of Glc (monosaccharide) and Tre (disaccharide) was further investigated in subsequent experiments addressing the redispersibility of PTX-loaded NP.

For PLGA-based NP, concentrations of 0.005 - 1 mg/ml Glc and Tre were used. Redispersibility was possible at all concentrations (Figure 2.14 A and B) and, as already shown in the preliminary tests, without lyoprotector. PLGA NP showed slightly better stability with Glc compared to Tre, with size and size distribution increasing steadily below concentrations of 0.1 mg/ml. For CS-PLGA composite NP, redispersibilities with Tre and Glc did not differ noticeably. However, a detectable steady increase in PDI and particle size was observed with decreasing sugar concentrations. Nevertheless, even the lowest concentrations of lyoprotector or its omission resulted in particle sizes of about 270 nm and PDI of < 0.3, indicating redispersibility and possible application regarding colloidal properties. Due to considerably worse redispersibility of EC-based NP,

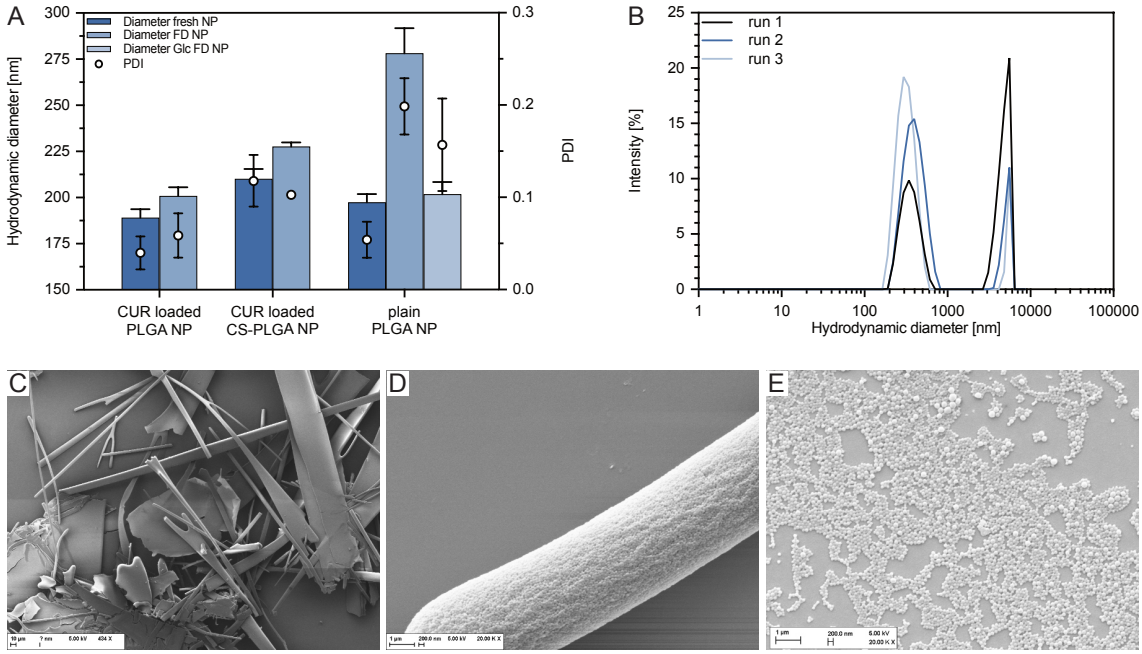

Figure 2.13: Stability of PLGA NP after lyophilization and redispersion.

A: DLS results of redispersed plain PLGA NP, CUR-loaded PLGA and CS-PLGA NP compared to freshly prepared NP. B: DLS curves of redispersed CUR-PLGA NP after transport and storage time of approx. one year. C-E: SEM images of CUR-loaded PLGA NP. C, D: Lyophilized NP. E: Dried NP after lyophilization and redispersion.

these were freeze-dried with higher lyoprotector concentrations. EC NP were lyophilized with concentrations of 5 - 50 mg/ml Glc or Tre and showed good to moderate redispersibility with Tre at all concentrations (Figure 2.14 C). Instead, Glc only demonstrated good stabilization of particles at concentrations of 30 mg/ml and above. In contrast, CS-EC NP, were not redispersible at any sugar concentration investigated (5 - 100 mg/ml). Thus, formulations of CS-EC 4 NP did not appear to be reasonable for a subsequently marketed product as the economic efficiency in terms of low storage time and high transport costs in the dispersed form of NP formulations would not be sufficient. To evaluate the effect of lyoprotectors on the stability of the NP over longer storage periods and during transport, further investigations are required. Furthermore, when adding a lyoprotectant, it should be considered for later application that the formulation's osmolality increases. In order to prevent fluid influx into the peritoneum and thus, possible leaching of NP or drug from the peritoneal tissue, the human body's physiological osmolality of approx. 285 osmol/l (reference range 275 - 300 osmol/l) should be targeted [245]. This approx. corresponds, e.g., to a Glc concentration of 50 mg/ml (278 osmol/l) or a NaCl concentration of 9 mg/ml (308 osmol/l) [246, 247]. Depending on the redispersed particle volume, the osmolarity should be adjusted by means of *aqua ad injectabilia* or the addition of ions or sugar.

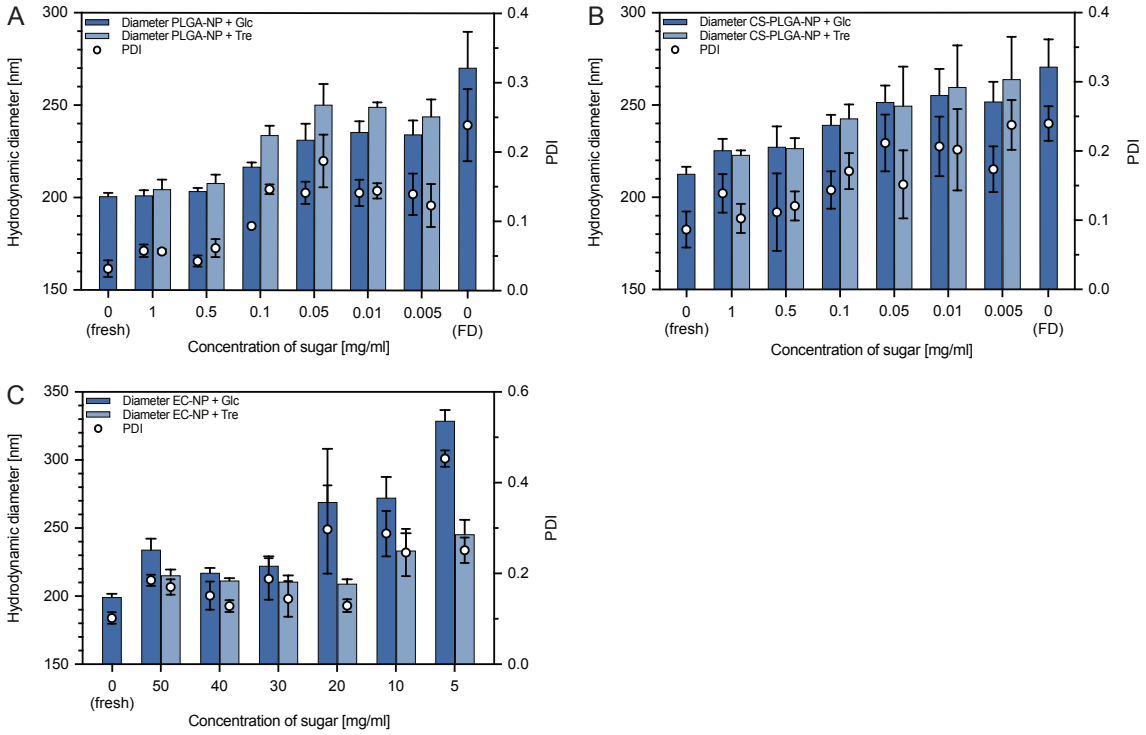

Figure 2.14: Stability of different NP carriers, lyophilized with various concentrations of Glc or Tre.

DLS results of freshly purified and redispersed NP loaded with initial 2 % (w/w) PTX. A: PLGA NP. B: CS-PLGA NP. C: EC NP. FD: freeze-dried.

2.4 Conclusion

Overall, the encapsulation of PTX in polymeric NP showed relatively low loading properties, which vary depending on polymer and solvent, presumably due to different solubility or affinity behavior of PTX to the polymer. EC NP revealed best loading properties, while cellular toxicity was excluded, thus, providing a promising platform for subsequent EC-based pharmaceutical products. Successful modifications of the particles and their surface led to the development of auspicious formulations with advantageous properties such as mucoadhesiveness (CS), gelling ability (PEC), and increased tumor cell uptake (BSA) [207, 248]. Regarding development of a commercially available and stable product, lyophilization of the NP formulations was investigated being a commonly used method for systemically applicable drugs. For this, results indicate the need of lyoprotectants.

3. A spinning disc system for continuous production of PLGA NP

3.1 Introduction

Within the last three decades, a considerable amount of research has been devoted to polymeric biomaterials, with PLGA being among the most extensively studied. As mentioned above, the biocompatible and biodegradable polymer has been approved by the FDA for decades, and meanwhile there is a selection of approx. 20 depot formulations available such as the microparticulate Lupron Depot®, the solid implant Propel® and the *in situ* forming gel Perseris™ [249]. Additionally, PLGA is the most widely used polymer for nanoparticulate drug delivery vehicles. However, so far there are no therapeutics on the market that use PLGA in nanoparticulate formulations. This might be due to the fact that no cost- and time-efficient mass production process for pharmaceutical manufacturers has been well established so far, which limits the potential clinical application. Currently, there are a few approaches for large-scale production of PLGA NP, e.g., the SAN-system developed by Rietscher *et al.* [138], the NPr system based on MicroJet Reactor (MJR) technology [250], and the SE modified by Schiller *et al.* [251] using focused ultrasound or microfluidic approaches in general [252, 253]. As NP must be subsequently purified from solvents or stabilizers before application, this represents a further time and cost consuming factor for commercial production.

A spinning disc is a multifunctional device promising automated mass production at reasonable costs for the manufacturer. These systems provide a continuous flow process in which centrifugal forces are used to disperse the liquid impinging on the rotating disc into a thin film, thus, creating a large surface to volume ratio of the liquid. This technology has been used for decades, e.g., to carry out various fast chemical reactions in so-called spinning disc reactors (SDR), including reactions of polymerization [254], neutralization [255], and re-crystallization [256]. In addition, a large number of nanosized chemical compounds were produced via reactive precipitations, e.g., hydroxyapatite [257], TiO_2 [258], ZnO [259], as well as magnetic Fe_3O_4 [260, 261]. As described in literature, spinning disc technology has been successfully used for ionic gelation of CS NP [262] and for NPr of NP consisting of beta-carotene [263], starch [264], or pure CUR [265]. What they have in common is a two-phase feeding of the reacting liquids, thus, taking advantage of the fast and homogenous micromixing capability of the rotating disc [257, 266]. In addition, this technology enables an increased and controllable heat and mass transfer, which supports many syntheses and processes that are otherwise limited in this respect [267]. This also applies to concentrate liquids, as described by Akhtar *et al.* [268], representing a gentle method due to short contact time to a heated plate.

In the literature the mechanism of NPr is described as a four-step process: supersaturation, nucleation and growth by condensation, and coagulation. The addition of the dissolved polymer to the antisolvent, in which the solvent is fully miscible, results in reduced solubility and leads to super-

saturation when the equilibrium saturation concentration is exceeded. Above the critical supersaturation concentration nucleation is induced [269]. For the modified NPr technique of the present thesis, only one starting solution is necessary: the polymer is dissolved in a solvent-antisolvent mixture containing a small amount of antisolvent. The thin film formed by the centrifugal forces increases the interface for solvent evaporation. Choosing a suitable solvent (e.g., ACE) with a low vapor pressure leads to supersaturation and particle nucleation. As a result, a NP dispersion in the antisolvent (e.g., H_2O) is obtained.

This chapter describes the manufacturing of PLGA NP of uniform and tunable sizes in an experimental spinning disc system (SDS) by evaporation controlled NPr. Parameters were tested regarding their influence on particle properties. Loading properties of NP were evaluated using CUR as hydrophobic, fluorescent model drug and PTX as potentially applicable formulation in comparison to the classical BT NPr approach. Transferability to a more advanced system, which allows a continuous NP production, was additionally investigated. Some of the experiments described as follows were performed by Marie-Sophie Ehrlich in context of her master thesis. This includes the testing of the different parameters in the production of unloaded PLGA NP in prototype I and II, and parts of stability trials and CUR-loading experiments.

3.2 Design and functionality of the developed SDS

Figure 3.1 A (left scheme) shows the developed prototype I, which was composed of several modules with a modified, propellerless computer fan (12x12 cm) representing the core of the system. A petri dish base (15x100 mm), which was inserted into the lid, was fixed using a rubber in between the dishes and served as an exchangeable precipitation and collection vessel. The lid of the glass petri dish was permanently fixed upside down on the engine of the fan as a holder for the petri dish base. To adjust the rotation speed of the fan, and thus, the petri dish, a laboratory power supply unit was connected to the fan and was used with varying voltage. Due to the operation of the fan by means of voltage, the rotational speed of the inserted petri dish had to be determined and adjusted separately using a Voltcraft® DT-10L tachometer. The polymeric solvent-antisolvent mixture was filled in a syringe (5 ml) and inserted in a syringe pump to control the feeding flow rate onto the inserted, rotating petri dish. The syringe with the fixed-on cannula (0.55x25 mm) was positioned approx. 3 mm above the inserted petri dish. To produce NP, the fan-petri dish system was forced to rotate, and the rotational speed was set prior starting the syringe pump. After the syringe was completely emptied, the SDS was stopped, the inserted petri dish was removed, and the NP dispersion was collected from the rim of the dish (Figure 3.1 B).

Since the first prototype was not able to produce larger batches of NP due to its limited collection volume (petri dish rim), and was therefore only usable for laboratory scales, a second prototype (II) was developed. It was constructed using a special fabricated glass vessel for continuous sample collection. As presented on Figure 3.1 A (right scheme), the vessel included a round recess for the engine of the fan with indentations as protection against leakage and an outlet tube for sample release at the bottom. First experiments were conducted using 20 ml syringes inserted in a syringe

pump. The sample mixtures were dripped on a glass petri dish lid (15x80 mm), which was fixed in proper alignment on the fan's engine. The idea behind this prototype II was to continuously remove the product from the collection site. Connecting of a pumping system with a huge feeding reservoir (instead of a volume limiting syringe pump) might allow upscaling of PLGA NP production to industrial scales in the future.

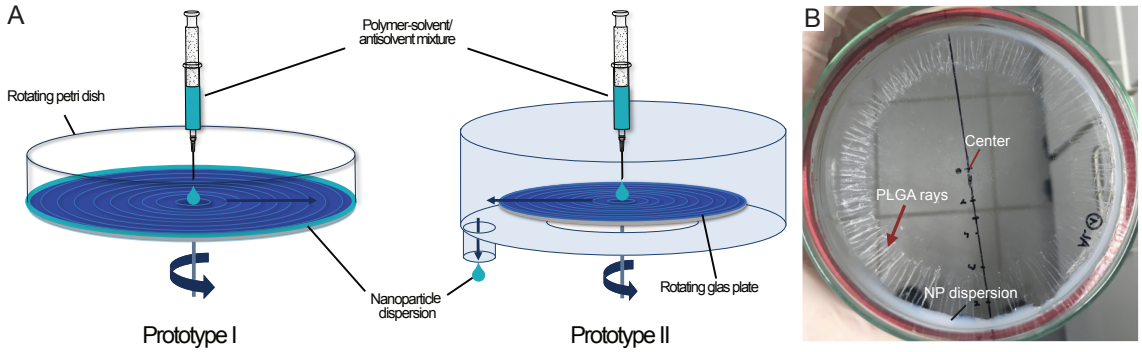

Figure 3.1: NPr by solvent-evaporation in an SDS.

A: Schematic illustration of spinning disc setups. Blue arrows display movements of the plates and the fluid. B: Petri dish after NPr with centred dropping position. At a certain distance from the centre of the plate, radially arranged dried polymer residues were observed (red arrow). NP dispersion accumulated at the rim of the dish.

3.3 Methods

For preparations of polymeric NP by standard procedure, a polymeric solvent-antisolvent mixture of 2 mg/ml was prepared with 10 mg Resomer RG 503H dissolved in ACE while stirring rigorously for 10 min before adding MilliQ® water in an ACE to H_2O ratio of 9:1. The laboratory power supply unit was started at a voltage of 5 V corresponding to a measured rotational speed of approximately 841 rpm. At a flow rate of 0.5 ml/min the solution was applied to the center of the rotating, inserted dish of prototype I. Before, the dish was coated with 2 % (w/v) PVA solution by drying at ambient conditions to stabilize the precipitated NP in dispersion. The resulting dispersion was removed from the rim of the inserted petri dish. The standard procedure was used in the following investigations unless otherwise stated.

3.3.1 Control of particle size

First, the influence of system specific settings on particle size was investigated. Therefore, spinning speeds of 841 rpm (5 V), 2,051 rpm (5.5 V), and 2,727 rpm (7 V), and distances of the cannula from the center of the inserted petri dish to the rim of 0, 1.5, and 3 cm were tested. Moreover, the dependence of polymer type, polymer concentration, and solvent composition on NP size was investigated. Different molecular weights of 50:50 LA:GA ratios (Resomers RG 502H, 503H, 504H), LA:GA ratios (Resomers RG 503H, 653H, 753H) and Resomer RG 503H concentrations of 0.5 - 22 mg/ml were precipitated. The influence of solvent and antisolvent was investigated comparing ACE, ACN and THF as solvents and MilliQ® water, EtOH, methanol

(MeOH), and isopropanol (iPrOH) as antisolvents. Colloidal properties were measured by DLS and laser Doppler electrophoresis (section 2.2.4.1). Particle morphology was investigated by SEM (section 2.2.4.4). The colloidal properties of resulting NP produced by SDS were compared with those of NP prepared by BT NPr as described in section 2.2.2.1. For this purpose, 10 - 40 mg of Resomer RG 503H and 25 mg of different PLGA types (Resomers 502H, 503H, 504H, 653H, and 753H) were dissolved in 1.5 ml ACE. Besides, for examination of the evaporation effect on particle formation, solvent-antisolvent mixtures were prepared as described above and dried on silica wafers for SEM imaging. 30 randomly chosen particles per resulting image were measured with Fiji for size evaluation. The yield was determined freeze-drying the collected NP dispersion prepared by concentrations of 2, 6 and 12 mg/ml for 24 h.

3.3.2 Colloidal stability

The stability of NP prepared with and without PVA coating of the inserted dish was investigated for prototype I. For this reason, dispersions were stored at 4 °C and their quality was evaluated with respect to the colloidal properties of freshly prepared NP, stored for 7, 14, 21 and 28 days. For prototype II, the stability was only investigated for non-coated disc conditions.

3.3.3 Loading of CUR and PTX

For preparation of CUR-loaded NP, CUR was dissolved in ACE to yield a 1 % (w/v) stock solution. In SDS (prototype I), Resomer RG 503H was dissolved in ACE, and the CUR solution was added to obtain concentrations of 2, 6 and 12 mg/ml, and an initial content of 1 % (w/w) CUR with respect to the polymer. Moreover, PLGA concentrations of 6 mg/ml with initial CUR contents of 1, 2 and 5 % (w/w) of the polymer were prepared. The resulting NP dispersions were collected, centrifuged (10,000 RCF, 20 °C for 20 min), and the pellet was investigated for DL and EE as described in section 2.2.4.2.

For comparison with BT NPr, CUR-loaded NP were prepared as described in section 2.2.2.2 with an initial PLGA concentration of 12 mg/ml and initial CUR concentrations of 1, 2 and 5 % (w/w) of the polymer mass. SDS samples of 5 mg/ml Resomer RG 503H and initial PTX contents of 1, 2 and 5 % (w/w) of the polymer mass were prepared. The resulting NP dispersions were collected, centrifuged (10,000 RCF, 20 °C for 20 min), and the pellet was investigated for DL and EE as it is described in section 2.2.4.3. In SEM, the samples were analyzed for PTX precipitates. Results were compared with PTX-PLGA NP prepared by BT NPr with the same initial PTX concentrations (Chapter 2.3.1.1).

3.3.4 Investigations on prototype II

For testing the transferability of colloidal properties of NP to prototype II, polymeric solvent-antisolvent mixtures were prepared in an amount of 20 ml and precipitated under the same system parameters as used for prototype I. As the amounts of coating material, used in prototype I, was

not sufficient for larger amounts of polymer as used in prototype II, the spinning disc was not coated with PVA. The collection vessel was pre-wetted before dropping started to increase the liquid volume and allow the resulting dispersion to be collected.

3.4 Results and discussion

Based on a modified NPr it was possible to produce particles using an SDS. The large surface of the rotating plate triggered extensive evaporation of the applied solvent (ACE). Thus, NP precipitated and produced a milky, highly concentrated dispersion in the small amount of antisolvent. However, a loss of polymer on the rotating plate was visible in forms of radicular rays (Figure 3.1 B), being thoroughly described in section 3.4.1.5. Volumes of 5 ml sample mixture prepared as described in section 1.3 resulted in a dispersion volume of 0.3 - 0.4 ml. Assuming that the solvent component (4.5 ml) almost completely evaporated, which was also indicated olfactorily, 60 - 80 % of the aqueous phase were recovered.

3.4.1 Control of particle size

Depending on the dosage form and target site of the drug delivery system to be applied, different particle properties, such as particle size, can be advantageous. Therefore, the range of particle sizes which can be achieved with the developed evaporation triggered method using PLGA as carrier system was investigated by varying preparation parameters.

3.4.1.1 Effect of PLGA concentration

As shown in Figure 3.2 higher PLGA concentrations resulted in larger particles as expected for SDS and BT method. In BT, however, the effect was much smaller. Huang and Zhang described this dependence of particle size on polymer concentration for BT [270]. In SDS sizes of approx. 120 - 380 nm were achieved within the tested concentration range (Figure 3.2 A). An almost linear relationship between polymer concentration and particle size was observed up to a concentration of 16 mg/ml. Above this concentration, limited reproducibility is displayed by fluctuating sizes of 335 - 380 nm, indicating that a plateau was reached, or a maximum controllable particle size was exceeded. Indicated by an increasing PDI from 0.016 to 0.2, the particle size distribution became wider with increasing polymer concentration, correlating with the particle size. However, in the linear range, the PDI did not exceed a value of 0.2 still indicating a narrow distribution [271]. Particle sizes of approx. 150 - 220 nm with very narrow size distributions (PDI < 0.1) were achieved using the BT method (Figure 3.2 B). With masses of 50 mg PLGA and more dissolved in 1.5 ml ACE to produce larger NP, no homogeneous NP dispersion was achieved, and directly at the tip of the cannula visible precipitates were formed. Bilati *et al.* also reported unsuccessful NPr at higher concentrations in the BT method, and Huang and Zhang did not report any further increase in particle size with higher concentrations than 20 mg/ml, just an increase

in particle size distribution by measuring individual, larger particles [270, 272]. Higher polymer concentrations may accelerate supersaturation, and thus, precipitation of the polymer is faster induced. Within the BT NPr system higher concentrations lead to shorter diffusion distances of the polymer molecules away from each other, and thus, increase the probability of collision and larger particle formation. In SDS, diffusion should not affect the solution due to its premixed state. The formation of a thin film of liquid leads to particle divergence, instead. The precipitation process with higher polymer concentrations starts at a lower distance from the center of the spinning disc because the distance between the polymer chains is lower and therefore their collision probability is higher [263]. Mainly due to a higher coagulation rate, this results in a more intensive particle growth and larger particles [269]. Furthermore, the probability of growth through agglomeration is statistically increased by the higher number of polymer chains per volume, which is associated with the increase in concentration. It appears that the distances of the polymers to each other in SDS have a more pronounced effects on particle size than the reduced diffusion in the BT NPr system.

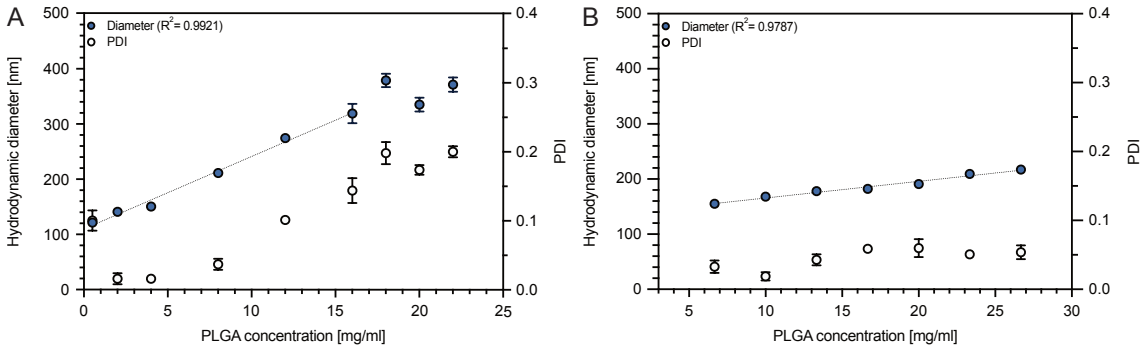

Figure 3.2: Effect of polymer concentration on NP size precipitated by SDS and BT.

A: DLS results using SDS. Trend line (R^2 = 0.9921) indicates a nearly linear relationship between polymer concentration up to 16 mg/ml and particle size. B: DLS results using BT setup.

3.4.1.2 Effect of PLGA types

Figure 3.3 shows that PLGA types did not markedly influence the investigated particle size in BT NPr. Particle sizes were constant around 180 - 195 nm and uniform. Budhian *et al.* also reported unchanged particle sizes at different LA contents and inherent viscosities in BT NPr [273]. In contrast, the evaporation triggered SDS method led to considerably larger particles with increasing LA content in the polymer (Figure 3.3 A). A higher proportion of LA in the polymer implies lower number of possible hydrogen bonds and increased hydrophobic interactions leading to a lower solubility of the polymer in the aqueous medium. Thus, a faster supersaturation is achieved as previously described for polymer concentration, however, without changing the number of polymers. This effect is probably so minorly pronounced in BT NPr that no or no remarkable differences in particle size were detected. In case of changing parameters such as a different solvent, the LA:GA ratio might also affect particle sizes in BT NPr method as described by Bilati *et al.* [272].

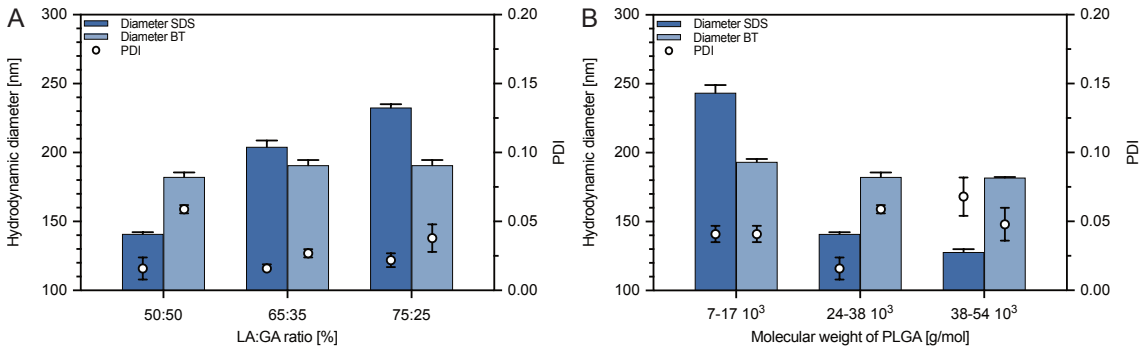

Figure 3.3: Effect of polymer types on NP sizes precipitated by SDS and BT.

A: Different LA contents of PLGA. B: Different molecular weights of PLGA.

In SDS, smaller particles were obtained with increasing viscosity or increasing molecular weight (Figure 3.3 B). The highest molecular weight (38,000 - 54,000 g/mol) resulted in particles almost half the size of particles produced with the lowest molecular weight (7,000 - 17,000 g/mol) (243.3 $\pm$ 5.7 nm vs. 127.7 $\pm$ 2.2 nm). Instead, the difference in size of 10 - 15 nm between the medium molecular weight PLGA (24,000 - 38,000 g/mol) and the highest molecular weight PLGA was rather small. The overlap of the molecular weights of both polymers might explain this. In BT NPr, opposite behavior was reported by Crucho and Barros [274]. According to their data, a higher polymer viscosity led to an impeded diffusion and thus, formation of larger particles. Due to the pre-fabricated solvent-antisolvent mixture used in SDS this argument of solvent diffusion does not apply. Presumably, the increased probability of collision at lower molecular weight explains the measured size differences. At constant polymer concentration and lower molecular weight, the number of polymer molecules in solution and thus, the collision probability is considerably higher. In contrast, precipitating different molecular weights in BT NPr only appeared to have minor influence (193.3 $\pm$ 2.1 nm with 7,000 - 17,000 g/mol vs. 181.7 $\pm$ 0.5 nm with 38,000 - 54,000 g/mol), probably due to only minimal effects of diffusion. SEM demonstrating differences in particle size obtained using different types of PLGA; images are displayed in Figure 3.4 A-E.

3.4.1.3 Effect of spinning speed and dropping position

The spinning speed could only be adjusted indirectly via voltage on the applied power source and not on a continuous scale. Three reproducible rotational speeds with maximized discrimination were selected. Produced NP had similar sizes (841 rpm: 140.9 $\pm$ 1.3 nm, 2051 rpm: 146.5 $\pm$ 11.2 nm and 2727 rpm: 139.2 $\pm$ 9.4 nm) with small size distributions (PDI $<$ 0.05). In contrast, Sana *et al.* as well as Khan and Rathod reported smaller particles at higher rotational speeds of 400 - 1,200 and 500 - 3,000 rpm, respectively [264, 265]. Due to the increased centrifugal forces on the plate this was argued with an increased micromixing, which reduced the probability of collision and thus particle growth [266]. Furthermore, varying dropping positions had no relevant influence or correlating tendencies in NP size (0 cm: 140.9 $\pm$ 1.3 nm, 1.5 cm: 126.4 $\pm$ 2.0 nm and 3 cm: 134.0 $\pm$ 2.4 nm). This contradicts De Caprariis *et al.* who revealed a

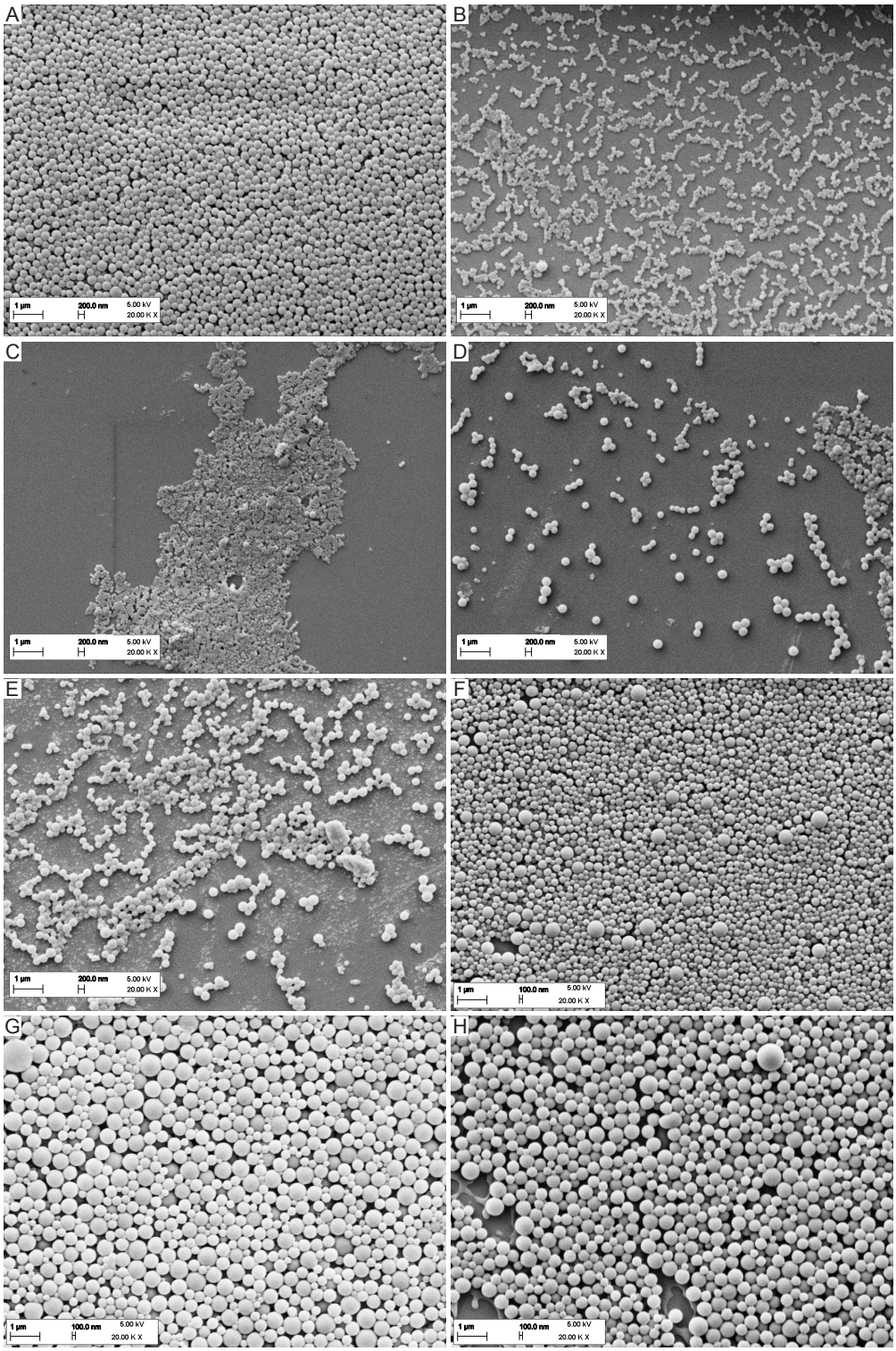

Figure 3.4: SEM images of PLGA NP.

A-E: Different PLGA types in ACE and H_2O precipitated by SDS. A: Resomer RG 502H (50 % LA content, 7 - 17,000 g/mol), 241 $\pm$ 34 nm. B: Resomer RG 503H (50 % LA content, 24 - 38,000 g/mol), 127 $\pm$ 21 nm. C: Resomer RG 504H (50 % LA content, 38 - 54,000 g/mol), 84 $\pm$ 20 nm. D: Resomer RG 653H (65 % LA content, 24 - 38,000 g/mol), 198 $\pm$ 38 nm. E: Resomer RG 753H (75 % LA content, 24 - 38,000 g/mol), 227 $\pm$ 45 nm. F-H: Resomer RG 503H precipitated in different solvent-antisolvent mixtures by drying on silica wafers. F: ACE and H_2O, 183 $\pm$ 65 nm. G: ACN and H_2O, 386 $\pm$ 115 nm. H: ACE and EtOH, 348 $\pm$ 86 nm.

decrease in particle size with increasing distance from the center of the rotating disc [257]. Again, the argument was a more efficient micromixing with increasing distance. This discrepancy with our own results can be explained by setup variations. Since two separate feeding jets were applied in the referenced literature, micromixing had an essential influence on NP size. In our setup, micromixing did not affect or just to a very limited extend affected NP size because pre-mixed, homogeneous liquids were applied to the rotating disc. Nevertheless, with increasing distance of the dropping position from the center of the spinning disc or with an increased rotational speed, the dripped solution is faster forced to the rim but on an increasing surface, and thus, the polymers faster increase distance between each other. Thus, smaller particle sizes can be expected. However, increase of the rotational speed may accompany faster evaporation of the solvent due to thinner films of liquid, and therefore, faster precipitation of polymers to larger particles might occur. Thus, the resulting constant particle size might be explained by a balance between those opposite effects at the experimentally realizable speeds.

3.4.1.4 Effect of solvent and antisolvent type

Appling different types of solvent and antisolvent, a change in particle size was observed in DLS and SEM (Figure 3.5 and Figure 3.4 F-H). Using ACE smaller NP (approx. 140 nm) were formed than with ACN and THF (approx. 230 nm). Huang and Zhang also reported the influence of solvents on particle size in the BT process [270]. In accordance with their findings, ACE and ACN resulted in equal particle sizes, while THF formed larger NP. This phenomenon was probably caused by different diffusion coefficients of the solvents in H_2O. However, this effect does not account for the resulting particle sizes in SDS since pre-mixed solvent-H_2O mixtures were applied. Instead, the solvents' surface tensions might have decisive influence on NP sizes. Decreasing surface tension might distribute the polymers to be concentrated, and thus, distance the polymers to each other to a higher extend on the spinning disc with the same contact time. The probability of collision and particle growth is more limited. Average values for surface tensions of 23.122 nm^{-1} for ACE, 27.340 nm^{-1} for THF and 29.143 nm^{-1} for ACN can be found in the literature [275]. In agreement, changing the solvent from ACE to ACN or the antisolvent from H_2O to EtOH, a visual increase in NP size already resulted during the drying process alone on silica wafers (Figure 3.4 F-H).

Replacing H_2O with alcohols (MeOH, EtOH and iPrOH) while ACE remained as a solvent, an increase in NP size resulted (Figure 3.5). This might be attributed to the interaction of polymer and antisolvent, described by the Hansen solubility parameters: PLGA 20.20 $mPa^{1/2}$, H_2O 47.8 $mPa^{1/2}$, EtOH 26.52 $mPa^{1/2}$, MeOH 29.61 $mPa^{1/2}$ and iPrOH 23.58 $mPa^{1/2}$ [276, 277]. In general, the hydrophobic PLGA is insoluble in both H_2O and alcohols. According to the Hansen solubility parameter, PLGA is significantly less soluble in water than in the investigated alcohols. Consequently, the precipitation process in alcohols might occur slower, and thus, particle growth lasts for a longer time. In contrast, precipitation in water is completed earlier, with a lower growth rate, and thus, smaller NP. Further investigations should be carried out to support this hypothesis.

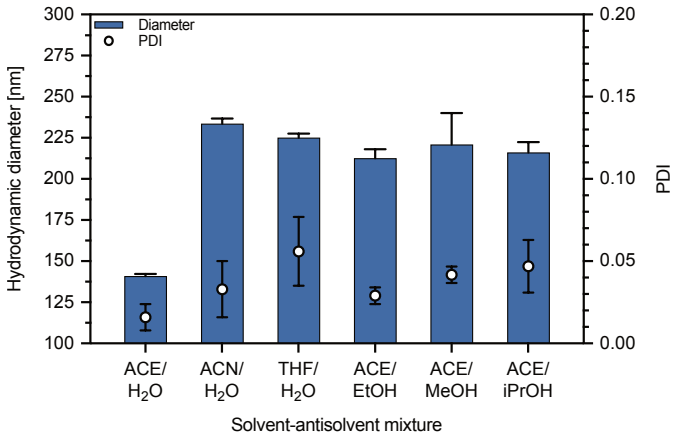

Figure 3.5: Effect of solvent and antisolvent types on NP size in SDS.

Resomer RG 503H dissolved in different solvent/antisolvent mixtures.

3.4.1.5 Yield of SDS produced NP

The evaluation of the recovered NP amounts revealed lower particle yields with higher polymer concentrations (Table 3.1). Polymer loss can be explained by dried PLGA particles on the spinning disc (Figure 3.1 B). With higher concentrations, visually more PLGA dried on the disc before reaching the rim for collection. No or a rather small amount of PLGA seemed to remain on the plate up to a center distance of approx. 3 cm. With higher distances, the resulting NP dispersion flowed radially towards the edge indicated by polymer dried in rays. Probably, the different areas on the disc might be caused by a change in surface tension and thus wettability of the liquid due to the evaporation of the solvent. Furthermore, it is assumed that precipitation of the particles already occurred before reaching the rim, and thus, an adjustment of the plate diameter could help to reduce the loss. Particle loss also applies to the BT method due to the need of subsequent purification. For example, using a centrifugation method, the yield depends on centrifugation parameters and particle size. Contrary to SDS, here smaller sizes tend to more particle loss. Moreover, particle quality suffers due to formation of aggregates and partially incomplete redispersibility after centrifugation [278]. Comparing both prototypes, particle yields are tendentially lower with prototype II. This is discussed in more detail in section 3.4.4.

Table 3.1: Comparison of particle yield recovered with prototype I and prototype II. Deviation of yields was calculated using initially 2, 6 and 12 mg/ml polymer for particle production.

Polymer concentration [mg/ml]	**2**	**6**	**12**
Yield prototype I [%]	88.8	72.8	40.6
Yield prototype II [%]	78.7	69.9	25.4
Deviation [%]	10.1	2.9	15.1
Mean [%]		9.4	
Standard deviation [%]		5.0	

3.4.2 Colloidal stability

All investigated samples did not show any visible or measurable change in stability, such as caking of agglomerated NP, a decrease in ζ-potential, and subsequent increase in particle size and PDI due to agglomeration (Table 3.2). The maximum size deviation of all investigated NP ranged between 2 - 6 nm after 28 d stored at 4 °C as dispersion, and thus, the particle size remained constant over the measured time. The size distributions displayed slight fluctuations but all PDIs remained below 0.1. The average maximum decrease in ζ-potential was 5.6 and 7.6 mV for PVA-coated plates and not coated plates, respectively. In total, all measured ζ-potentials were below values of -30 mV (-39 ± 2 mV) indicating good stability even after 28 days. Hence, comparing the data obtained for both types of discs, it can be concluded that the coating of the disc with a stabilizer (e.g., PVA) is not necessary to maintain particle quality, at least, for reviewed storage time of 28 days. Further studies should be performed for verifying longer storage periods. The stability of the particles produced in prototype II was assured with uncoated plates and tested under same conditions (max. deviations from the fresh NP in size: 2 nm, in PDI: 0.023, and in ζ-potential: 8.1 mV).

Table 3.2: Colloidal stability of PLGA NP prepared by SDS and stored at 4 °C for 28 d. Maximum deviations occurring within 28 d in particle size, PDI and ζ-potential (ζ-pot.) of the freshly prepared NP.

Batch sample	**PVA-coated plates**			**Non-coated plates**		
	Δ in size [nm]	**PDI**	**ζ-pot.** [mV]	**Δ in size** [nm]	**PDI**	**ζ-pot.** [mV]
Batch 1	6	0.0089	5.5	2	0.016	5.2
Batch 2	4	0.0145	5.5	4	0.0234	8.8
Batch 3	3	0.0132	5.7	2	0.0244	8.7
Mean	4	0.012	5.6	3	0.021	7.6
Standard deviation	1	0.002	0.1	1	0.004	1.7

3.4.3 Loading of CUR and PTX in SDS

As in both SDS and BT NPr, particle sizes of 1 % (w/w) CUR-loaded PLGA NP (Figure 3.6 A and B) were similar to those of unloaded PLGA NP (Section 1.4.1.1, Figure 3.2 A and B), drug loading in these concentration ranges did not seem to have influence on the particle sizes. Increasing the polymer concentration with a constant initial CUR concentration of 1 % (w/w) of polymer mass resulted in an increased DL in SDS (Figure 3.6 A) and in case of 6 mg/ml compared to 2 mg/ml in a higher EE. Choi *et al.* also described higher DL for larger particles [278]. Since larger particles lead to larger particle volumes, it is not surprising that higher drug amounts were found. In contrast, increase of polymer concentration above 6 mg/ml caused reduction in EE. Since EE was calculated by multiplying the amount of drug recovered in 1 mg formulation and the yield of the formulation to obtain the total amount of drug recovered in formulation, EE directly correlates to the yield. Apparently, the increased DL did not compensate for the much higher particle loss (79.6 % vs. 43.5 % yield).

To be able to compare loading properties between the two manufacturing methods, polymer concentrations were selected according to results of section 3.4.1.1 to obtain similar particle sizes. Particle sizes in SDS and BT developed conversely with increasing CUR concentrations (Figure 3.6 B). While the particle size in SDS increased with higher CUR concentrations, it decreased in the BT process. Figure 3.6 C shows that higher DL and EE could be achieved using SDS compared to BT NPr. DL of SDS particles was twice as high as BT DL with values of 80 - 90 % of the initially used CUR mass. Also, EE of SDS particles was markedly higher than that of BT particles. On the one hand, this is due to the mentioned particle loss during the purification step in BT, which is linked to the resulting EE. On the other hand, 20-fold larger volumes of the aqueous phase are used in BT (10 ml vs. 0.5 ml in SDS), and thus, more CUR may be lost. Furthermore, the aqueous phase in BT NPr contains surfactant (2 % (w/v) PVA) and herewith enables more solubilized CUR not being available for encapsulation in the particles.

Also, PTX loading was higher in SDS compared to BT NPr with DL being more than twice as high for 1 and 2 % (w/w) initial PTX concentration (Figure 3.6 D). EE were 3 - 3.5-fold higher with values of about 70 and 60 %, respectively, without forming PTX precipitates (Figure 3.6 E and F). Apart from DL improvements, the enormous EE can also be attributed to yields above 80 %, implying higher values of 15 - 20 % higher than in the BT NPr. However, for 5 % (w/w) PTX, the amounts of both particle yield and PTX loading clearly decreased and were below BT NPr values. This can be explained by precipitation of PTX (Figure 3.6 G), which presumably occurred mainly on the spinning disc, and thus, did not end up in the collected fraction to be measured at the rim of the disc.

3.4.4 Further development of the SDS

With a size of 135.5 $\pm$ 5.5 nm, a PDI of 0.017 $\pm$ 0.002, and a ζ-potential of -29.2 $\pm$ 3.2 mV, the resulting particles prepared by prototype II had comparable properties to those produced with prototype I (140.9 $\pm$ 1.3 nm, PDI 0.016 $\pm$ 0.008, -28.3 $\pm$ 2.7 mV) using the same parameters. The stability of particles was also successfully investigated over a period of 28 d at 4 °C (section 3.4.2). During the manufacturing process using an initial volume of 20 ml, it was difficult to collect the produced NP due to the low final volume of dispersion. Therefore, the collection vessel was additionally moistened with water. This increased the final volume and diluted the final NP dispersion. The outlet enables implementation of larger or even unlimited volumes, and thus, continuous harvest of the particles and obtainment of larger amounts of particle dispersions. Accordingly, moistening might be omitted. Examination of the yields displayed an average reduction of 9.4 $\pm$ 5 % compared to the yield in prototype I (Section 3.4.1.5, Table 3.1). This was probably attributed to the collection vessel, which provides more surface area for particle loss. For the production of larger quantities, the losses should become less relevant.

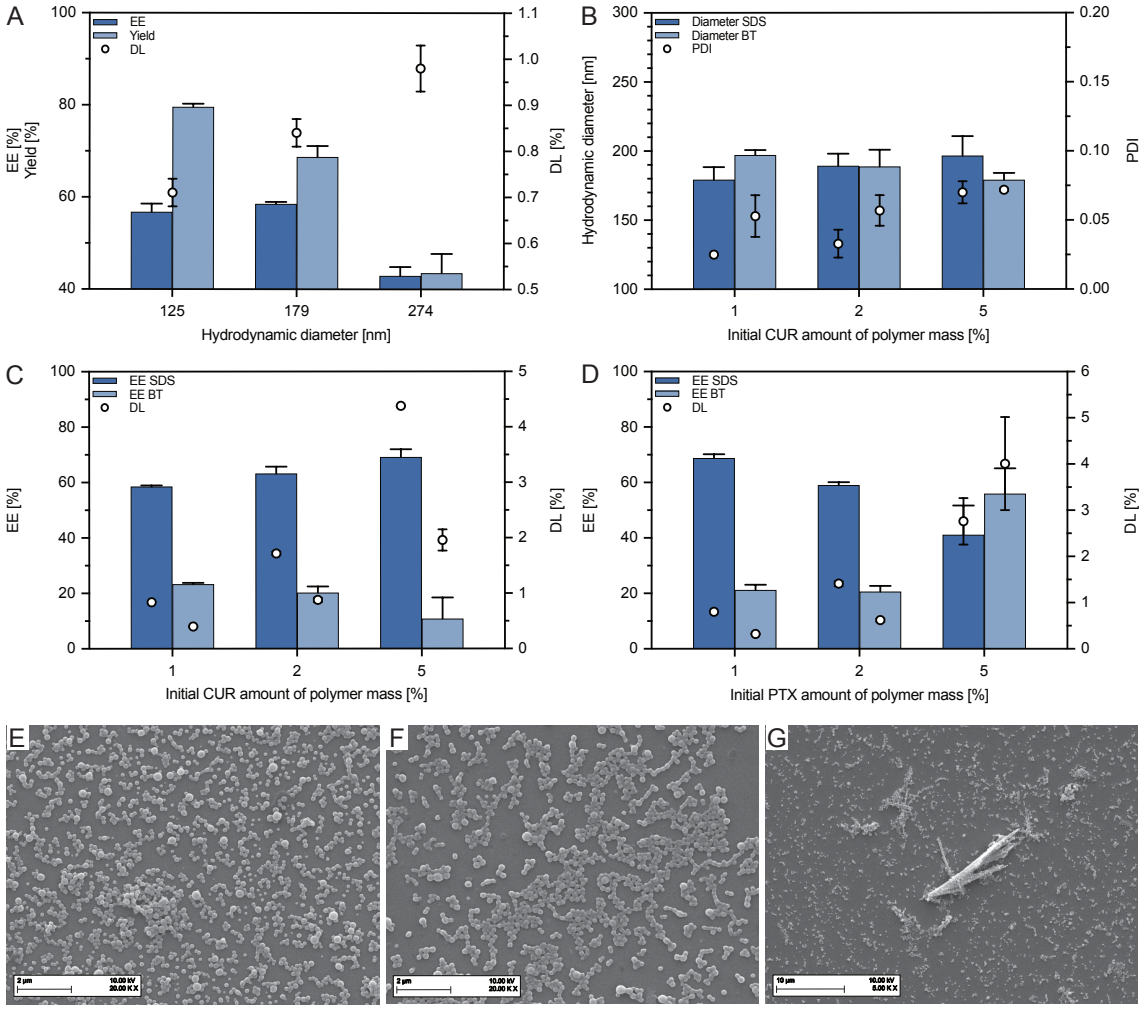

Figure 3.6: CUR and PTX loading trials in SDS and BT NPr.

A: Quantification of CUR-loaded PLGA NP according to different particle sizes in SDS. Particles were prepared with an initial CUR content of 1 % (w/w) of polymer mass. B: DLS results of different CUR loadings in SDS and BT. C: Loading properties of different CUR loadings in SDS and BT NPr. D: Loading properties of different PTX loadings in SDS and BT NPr. E-G: SEM images of PTX-loaded PLGA NP prepared by SDS method with different initial PTX contents. E: Initial 1 % (w/w) PTX content of the polymer mass. F: Initial 2 % (w/w) PTX content of the polymer mass. G: Initial 5 % (w/w) PTX content of the polymer mass.

3.5 Conclusion

The developed prototypes allowed stable particles to be tuned within a larger size range than in classical BT NPr (120 - 380 nm vs. 150 - 250 nm). It has been demonstrated that the yields in SDS depend on the particle size with 70 - 90 % being achieved at sizes < 200 nm. Future optimization, e.g., variation of the size of the rotating disk, might further increase the yield, especially with larger particles. Additionally, the loading of both tested substances CUR and PTX revealed a satisfying success and a markedly higher efficiency compared to the BT process. Nevertheless, further studies and improvements should be carried out regarding purification of loaded particles and possible surface modifications in terms of coatings and composition with other polymers such as CS. The continuous evaporation triggered NPr method in SDS investigated here represents a

potential platform for large-scale industrial production of PLGA based NP, and thus, could lead away from batch production and the problems associated with.

4. Drug release from PTX-loaded NP

4.1 Introduction

For decades it has been common practice to submit release kinetics of the corresponding drugs in the registration dossiers of regulatory agencies. The drug release kinetics provide information about the behavior of dosage forms and are basic parameters to obtain information on a drug's safety and efficacy. Release trials are intended to evaluate the influence of formulation design and manufacturing methods on the drug product as well as routine quality control for batch authorization and product uniformity. Furthermore, *in vitro* release kinetics are used to predict *in vivo* release, also known as *in vitro-in vivo* correlation/relation (IVIVC/R), whereas an *in vivo* release is difficult to simulate *in vitro* due to extremely complex physiological processes in the human body. In addition to the stability of the active ingredient in the release medium, the setup also plays a pivotal factor influencing the release from the drug delivery system. For classical dosage forms, such as tablets, capsules, or transdermal patches, setups using apparatuses such as the basket, paddle, reciprocating cylinder, or flow cell are prescribed in the pharmacopoeias, whereas no standardized, appropriate setup is yet recommended for nanomedicines [279, 280, 281]. In this context, the main challenge is the size of the formulation as the released and to be analyzed compound must be separated from the nanosized particulate drug delivery system. Hereby, most of the release methods mentioned in the literature are based on dialysis or sample and separate principle [222, 223, 224, 225, 226, 227, 228, 229, 281, 282]. For separation, methods such as filtration, centrifugation, and solid phase extraction are commonly used [225, 283, 284]. Since the release of an active ingredient of a formulation depends particularly on its solubility and diffusion in the surrounding medium, it is obvious that saturation in the medium must not be reached during release experiments. So-called sink conditions should be pursued, as they usually apply to the human body due to constant inflow and outflow of fluid. There are different possibilities to obtain sink conditions in *in vitro* release experiments. These include a sufficient volume of release medium, the constant exchange of release medium, e.g., through an "open system" as in the flow cell, or by addition of detergents which increase the solubility of the active ingredient.

The first section of this chapter evaluates the preliminary experiments conducted to establish an appropriate setup and release conditions for measuring the drug release of PTX-loaded NP. Subsequently, the release kinetics of the developed formulations of sections 2.2.2 and 2.2.3, which were investigated under the previously selected release conditions, are discussed. Here, the focus is on sustaining the release by modifying the formulation with respect to the carrier polymers and the surface modification of the NP.

4.2 Methods

4.2.1 Development of a convenient release setup for PTX-loaded NP

In preliminary experiments, three different release setups were investigated, and advantages and disadvantages were evaluated. Therefore, artificial peritoneal fluid (APF; Table 4.1), isotonic saline, and isotonic glucose medium containing 0.2 % (w/v) sodium lauryl sulfate (SLS) or PS 80 were investigated as release media. PTX-loaded PLGA NP were used to establish appropriate release parameters. Since the formulation to be applied in the human body is isotonic at best, NP were isotonized before dispersion in release medium. The influence of both the release medium's pH on PTX stability and sink conditions when adding the detergents PS 80 and SLS were analyzed. To estimate the release under physiological conditions (*in vivo*), the saturation of PTX in human ascites (*ex vivo*) was measured. For this purpose, ascites samples, taken from two patients with peritoneal malignancies, were provided by Prof. Reymond (UKT Tübingen).

Table 4.1: Composition of APF (Physioneal 40, Baxter) [285].

Ingredient	Final solution after mixing [g/l]
Anhydrous glucose	22.7
Sodium chloride	5.38
Calcium chloride (dihydrate)	0.184
Magnesium chloride (hexahydrate)	0.051
Sodium bicarbonate	2.1
Sodium lactate	1.68

4.2.1.1 Tested setups for drug release

The first tested setup investigated drug release in microcentrifuge tubes. NP were diluted to a concentration of 10 mg/ml, isotonized with sodium chloride, and then dispersed in release medium in a ratio of 1:10, corresponding to 1 mg/ml NP. Several aliquots of 1 ml volume were filled into 1.5 ml microcentrifuge tubes and incubated at 37 $\pm$ 2 °C and 80 rpm under light exclusion using an incubation shaker. At each time point one tube was removed and cooled for three minutes at approx. 37 °C to prevent further release from the particles. The samples were centrifuged (40,000 RCF, 30 min, 4 °C) to obtain a particle-free supernatant, which was then extracted with ACN (1:1) and quantified by HPLC (section 2.2.4.3). For each medium a calibration curve was determined to calculate the released drug amount.

The second tested setup did not base on separate sampling, but on the repeated extraction out of a bulk sample. For this purpose, 100 mg NP were dispersed in isotonic media, resulting in a total volume of 10 ml. The dispersion was incubated with 90 ml release medium in an Erlenmeyer flask with stopper at 37 $\pm$ 2 °C and 80 rpm under light exclusion using an incubation shaker. Volumes of 1 ml were collected at each time point and were replaced with fresh release medium. The extracted samples were proceeded and analyzed as described above.

The third release setup was tested and evaluated using dialysis tubings with a molecular weight cut off (MWCO) of 12 - 14 kDa. In this setup, 100 mg NP were dispersed and isotonized in 10 ml, then filled into soaked and cleaned dialysis tubings, and closed to reach a certain length of approx. 2.5 cm. In the following, the samples were placed in 225 ml screw-cap glasses and completely covered with the release medium. This required 140 ml, resulting in a total volume of 150 ml. Samples were incubated as previously described. At certain time points, samples of 1 ml volume were removed and replaced by the same volume of fresh medium. The samples were directly extracted with ACN (1:1) and analyzed as described above. In preliminary tests, the interaction of PTX in dissolved state and loaded in PLGA NP with the dialysis tubings was tested. Hydrophilic tubings made of regenerated cellulose with very low adsorption properties were used, which should minimize a possible influence on the release. Since a complete distribution of the drug in the medium, and also a complete release from the particles could be measured, it was concluded that the tubings do not or only to a minor extent interact with PTX.

4.2.1.2 pH-dependent stability of PTX

The PTX peaks observed in the HPLC chromatogram using APF (pH 7.4) as release medium were further examined by ultrahigh-performance liquid chromatography coupled to orbitrap mass spectrometry (UHPLC-MS). For sample preparation, PTX was dissolved in ACN to obtain concentrations of 10 and 20 µg/ml. The sample with 20 µg/ml PTX was mixed with APF containing 0.2 % (w/v) SLS. 20 µl of each sample was injected, analyzed at a wavelength of 227 nm and chromatogram peaks were identified by their masses. The analytical experiment was performed by Dr. Stefan Böttcher (Institute for pharmaceutical and medicinal chemistry, Saarland University). The extend of PTX degradation depending on the pH of the release medium was investigated. Therefore, APF containing 0.2 % (w/v) SLS was adjusted to pH 6,7 and 7.4 before 1 ml hereof was mixed with 100 µl of 0.1 % (w/v) PTX-ACN stock. After 24 h incubation (37 °C, 80 rpm) samples were filtered (0.2 µm), extracted with ACN 1:1 and analyzed by HPLC (section 2.2.4.3).

4.2.1.3 Saturation concentrations of release media and *ex vivo* ascites fluids

The solubility of PTX in release medium containing different detergents of various concentrations was investigated. Excess of PTX was given in microcentrifuge tubes and 1 ml of release medium containing PS 80 or SLS in concentrations of 0 - 0.5 % (w/v) was added. Isotonic saline containing 0.1 M acetic acid/acetate buffer (pH 4.75) was used as release medium. The sample tubes were horizontally aligned and incubated (37 ± 2 °C, 80 rpm) for 24 h. The samples were filtered (0.2 µm) and extracted with ACN 1:1 before HPLC analysis (section 2.2.4.3).

Ascites fluids of two cancer patients were investigated regarding their pH and their PTX solubility. First, volumes of 20 ml ascites samples were centrifuged (20 min, 10,000 RCF, 20 °C) and filtered (0.2 µm) to remove cells and tissue residuals. Excess of PTX was given in microcentrifuge tubes, 1 ml of ascites was added, and it was proceeded as described above. After extracting the samples

with ACN 1:1, precipitates were centrifuged (30 min, 30,000 RCF, 20 °C) and supernatants were collected for HPLC analysis. Calibration curves of both ascites fluids were prepared in ascites 1:1 diluted in ACN and samples were centrifuged as described prior HPLC analysis (section 2.2.4.3).

4.2.2 Release kinetics of PTX-loaded NP

Release kinetics of PTX-loaded PLGA and EC 4 NP were investigated in dialysis tubing setup described in section 4.2.1.1. Isotonic saline containing 0.1 M acetic acid/acetate buffer and 0.2 % (w/v) SLS was used as release medium. The following nanoparticulate formulations were investigated: uncoated PLGA and EC 4 NP, composite-NP of CS and PLGA or EC, as well as BSA-, CL-BSA-, and PEC-coated CS-PLGA NP. Furthermore, PEC-coated NP were examined with and without the addition of Ca^{2+} ions. Therefore, a physiologic concentration of Ca^{2+} (1.15 - 1.35 mmol/l extracellular; 1.25 mmol/l corresponds to 25.676 mg $CaCl_2$*$2H_2O$ per 140 ml release medium) was added before dialysis tubings were inserted into the screw-cap glasses. Formulations based on PLGA had an initial PTX loading of 2 % (w/w) regarding polymer mass. EC 4 NP were tested with different PTX loadings (1, 2 and 10 % (w/w) regarding EC 4 mass) and particle concentrations (10, 50 and 100 mg). In order to compare release kinetics of EC 4 and PLGA NP, similar drug loadings were chosen (EC 4 based NP with an initial PTX loading of 1 % (w/w) regarding polymer mass, PLGA based NP with an initial PTX loading of 2 % (w/w) regarding polymer mass). All formulations were prepared as described in sections 2.2.2 and 2.2.3. At pre-determined time points (0, 1, 2, 4, 8 and 24 h, and 2, 4, 7, 10, 14 and 17 d) samples of the release medium were collected and HPLC samples were prepared as described above (4.2.1.1). Drug contents were analyzed, and the cumulative release was calculated.

4.3 Results and discussion

4.3.1 Development of a convenient release setup for PTX-loaded NP

4.3.1.1 Evaluation of release setups

Experimental results using the microcentrifuge tube setup demonstrated, that PTX concentrations can be determined in the release medium even with small amounts of particles (data not shown). Since no medium was renewed in this setup, sink conditions were only obtained by the solubility of PTX in the initial volume of release medium. Therefore, the addition of a detergent was of importance, which in turn accelerated the release by leaching out the drug. The observed values within a measurement series and between identical measurement series fluctuated. This might be due to visually observed deposition of particles on the tube vessel surface above the release medium. The tube surface in relation to the filled volume is considerably larger for this setup than for the other two setups investigated. In this way particle losses can occur to a much greater extent, and thus, the amount of active ingredient released varied between samples. However, also the vessel material might be a reason for adherence of hydrophobic drug. The microcentrifuge tubes

consist of hydrophobic polypropylene, while hydrophilic glass vessels were used for the other two setups. Sampling in the bulk setup (Erlenmeyer flask setup) was carried out by exchanging the volume at each time point of extraction, which improved sink conditions. In addition, NP were removed but not returned. Thus, calculation of drug release required double extrapolation. To keep the error as small as possible, large amounts of NP (100 mg per release sample) were used. Remarkable for both tested sampling and separate methods with distinct principles was a rapid (burst) release (at least 80 %) within the first hours after dispersion ($<$ 24 - 48 h). This phenomenon has been documented repeatedly for PLGA NP and therefore met the expectations [286, 287, 288].

In contrast, considerably lower release rates of approx. 80 % in 7 d were measured in the dialysis setup. In the literature, dialysis is one of the most commonly used methods for drug release of nanoparticulate carriers. However, there is multiple evidence that the membrane slows down transport (permeation) of the drug into the external medium (receiver compartment), and thus, the measured drug release does not correspond to the actual release within the dialysis tube (donor compartment) [289]. Although the system contains 50 % more medium (150 ml total liquid), the release out of the NP only occurs in the donor compartment with 10 ml volume instead of 100 ml (compared to Erlenmeyer setup) and is determined by local solubility and saturation. Thus, it is reasonable to assume that the sustained release is due to a markedly higher particle concentration (10 fold) and respective PTX concentration within the donor compartment. The influence of the particle concentration is discussed in more detail in section 4.3.2. An important factor is an uniform filling of the membrane (here a length of 2.5 cm) to obtain reproducible filling volumes and surfaces to the receiver compartment. Despite the slowed drug release due to membrane permeation and the higher particle concentration in the donor compartment, a valid IVIVC was observed by D'Souza *et al.* [290]. Moreover, changes in sustained release can be measured more precisely over time, and thus, this setup was chosen to compare release kinetics of the different carrier systems.

4.3.1.2 pH-dependent stability of PTX

In the course of evaluating different release setups, various release media were additionally examined. One artificially occurring problem in this process was microbial growth associated with performing experiments at 37 °C for prolonged periods of time. This was most pronounced for release medium containing 5 % (w/v) Glc, e.g., growth on dialysis membranes accompanied with decreasing PTX concentrations after 1.5 - 2 weeks. For APF, which primarily consisted of Glc, NaCl, and buffering substances (sodium bicarbonate and sodium lactate; Table 4.1), no visual microbial growth occurred. Although no microbial infestation was visible, a minor peak in HPLC analysis was observed with a retention time of 3.6 - 3.7 min and increasing by duration of the release experiment (Figure 4.1 A and E). To demonstrate the extent of the side peak, both main and side peak were added for calculations in Figure 4.1 A. A decrease of PTX in APF due to buffered pH of 7.4 was suspected. When using unbuffered release media such as 0.9 % (w/v) NaCl solution, the pH decreased over time with values of pH $<$ 4 already after 24 h (Figure 4.1 B), and

no relevant side peak was detected. To identify the substance causing the side peak, a release sample was collected after 24 h and analyzed by UHPLC-MS (Figure 4.1 C). Besides PTX (exact mass of 853.331 g/mol plus 1 g/mol protons), a substance with 281.27 g/mol (plus 1 g/mol protons) was detected. The Pharmacopoeia Commentary describes a degradation of PTX to the ineffective Baccatin III (Figure 4.1 D) in basic pH (> pH 8) [291]. The deprotonated side chain cleaved from Baccatin III has a mass of 281.069 g/mol, comparable to the observed mass in mass spectroscopy. This substance is also the chromophore of PTX and can be measured by the UV/Vis detector of HPLC at approximately the same absorption wavelength. Since the extinction coefficient of the degraded substance is unknown, it is uncertain whether the two peaks (main and side peaks) can be added 1:1 for calculations. Further analytical investigation would be required to ensure correct evaluation. As degradation was already assumed at pH values of 7.4, the degradation in APF was investigated at lower pH. As shown in Figure 4.1 E, the side peak minimized at decreasing pH values to a minimum of 6 % of the main peak at pH 6. Accordingly, a pH of < 6 was targeted in subsequent release trials of different formulations to avoid degradation. As Tian and Stella reported a pH optimum of about 4 for PTX, medium was buffered in this range using an acetic acid/acetate buffer at pH 4.75 [292]. Physiologically, a pH of approx. 7.4 is assumed, which means that a long-lasting effect in the tissue after the release of PTX can only be expected to a limited extent due to its instability. After penetration of the particles in tumor nodules with a pathophysiologically lower pH, the stability of PTX can be expected to improve.

4.3.1.3 Saturation concentrations in release media and *ex vivo* ascites fluids

To ensure that sink conditions prevailed during the release experiments, two detergents of different concentrations were tested regarding their saturation concentrations. Using detergents, large volumes and medium exchange could be minimized to avoid problems encountering with quantification of the released PTX in terms of sensitivity and detectability in lower concentrations. With both PS 80 and SLS, a linear correlation between added concentration (0 - 5 mg/ml) and dissolved PTX concentration (saturation concentration) was observed (Figure 4.2). In concentrations of 2 mg/ml of the detergents, PTX concentrations of approx. 40 and 5 µg/ml were measured with SLS and PS 80, respectively, which corresponds to an 8-fold higher solubility of PTX in SLS compared to PS 80. This corresponded to a saturation concentration for 100 mg formulation of initially 2 % (w/w) PTX-loaded PLGA NP in 150 ml release medium containing 2 mg/ml PS 80 (dialysis setup). Since the European Pharmacopoeia specifies that sink conditions prevail when the volume of the release medium is at least 3 to 10 times higher than the saturation volume, PS 80 was not considered being adequate at the concentrations tested [279]. For this reason, a concentration of 2 mg/ml SLS was selected for subsequent release tests, which ensured sink conditions with respect to European Pharmacopoeia.

The analysis of the ascites fluids revealed pH values of 7.5 and 8 and variable saturation concentrations as presented in Table 4.2. Determination of PTX saturation concentrations indicated that the solubility in the physiological medium was substantially higher compared to, e.g., pure water. This was probably due to proteins dissolved in ascites, such as albumin, which increased

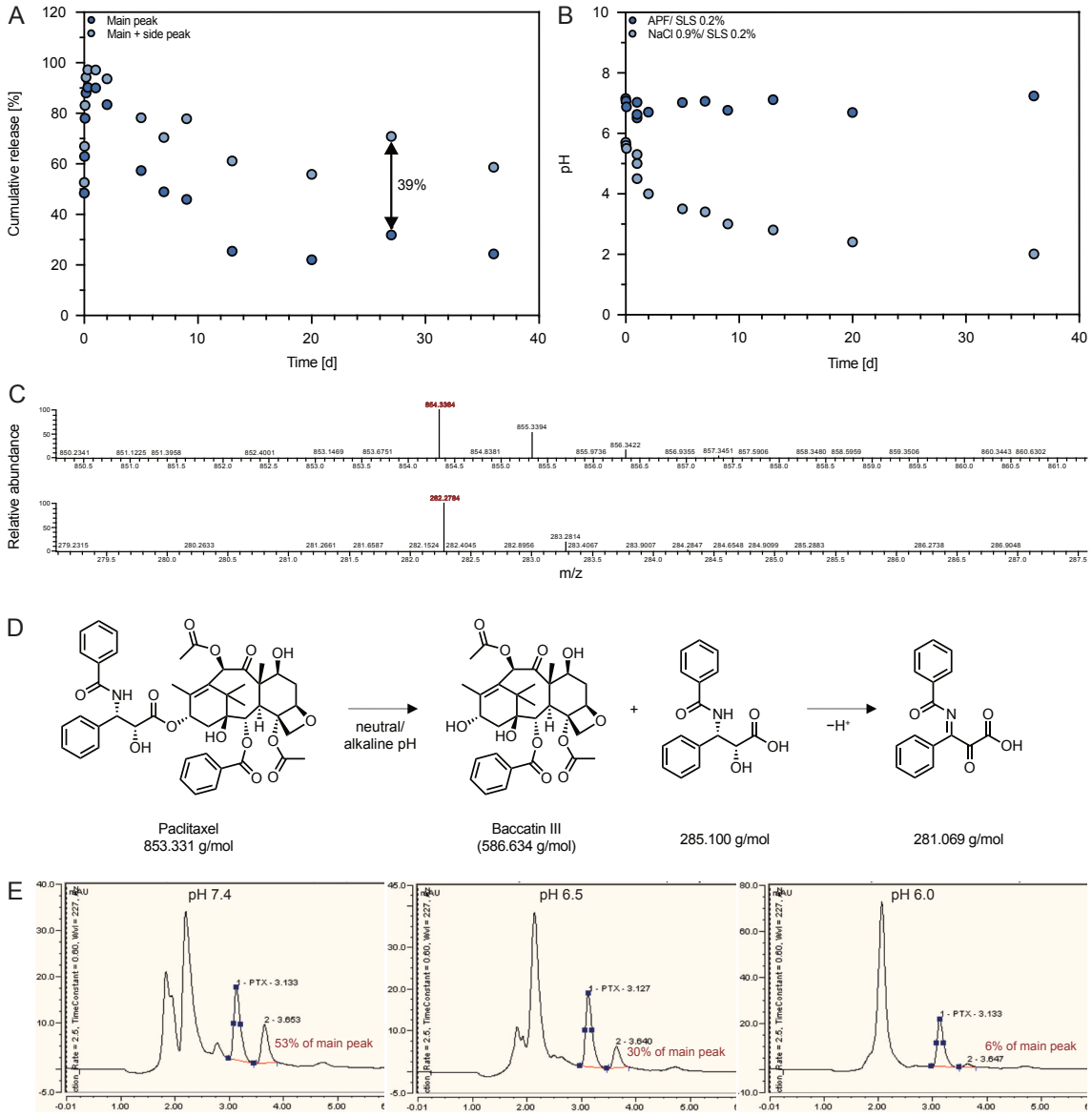

Figure 4.1: Influence of pH in release medium on stability of PTX.

A: Cumulative release of PTX-loaded PLGA NP in APF buffered at pH 7.4. For calculation of released PTX amounts, areas of main peaks (HPLC) and summed areas of main and side peaks were used. Thus, the distances between the calculated concentrations represents the extent of the side peaks and correspondingly the amount of degraded PTX. B: pH trends during release using APF (pH 7.4) and NaCl 0.9 % (not buffered) as release media. C: PTX (upper part) and its degradation product (bottom part) detected by UHPLC-MS. D: Structural formula of the possible degradation product matching the detected mass. E: Dependence of pH within the release medium on the extent of PTX degradation and the associated side peak in HPLC.

PTX solubility as already described previously. The solubility differed substantially between the investigated ascitic liquids, probably attributed to different pH values and respective PTX stability. Accordingly, in ascites 2 with a higher pH of approx. 8, parts of the dissolved PTX might have been degraded after 24 h incubation. This corresponded to side peaks visible in the HPLC quantification (not shown). Comparing the PTX solubility data between *ex vivo* (ascites fluids) and *in vitro* conditions, the solubility in 0.2 % (w/v) SLS was 2 - 5 times higher, whereas PS 80 would require higher concentrations of about 3 - 7.5 mg/ml to meet the physiological conditions.

In the literature, *in vivo* conditions are specified with peritoneal fluid volumes of 5 - 20 ml and extracellular fluid exchange of 500 ml/h in peritoneal tissue [293]. Compared to the *in vitro* dialysis setup with 150 ml fluid and only few ml fluid exchange, a correlation is doubtful. Regarding the altered pathophysiological conditions in the tumor with its heterogenic tissue, as described in section 1.2.1, a correlation is even more unpredictable. Thus, release experiments performed in the present study mainly serve to compare release kinetics between the different formulations and to assess the effectiveness of different modifications of the particle surface.

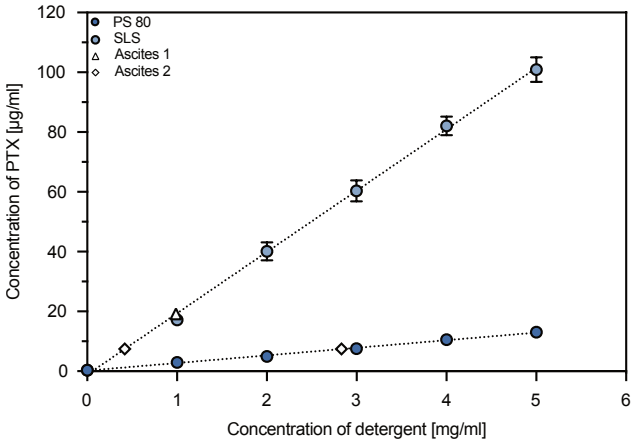

Figure 4.2: Saturation concentrations of PTX in different media and detergent concentrations.

The media investigated were PS 80 and SLS in concentrations of 0.1 - 0.5 % (w/v), and ascites fluid of two patients with peritoneal malignancies. PTX concentrations in ascites were compared with corresponding detergent concentration. As the saturation concentration of PTX in ascites 1 was higher than all determined saturation concentrations in PS 80, only SLS was compared to ascites 1 (triangle symbol).

Table 4.2: Analysis of ascites fluids. For transferability to the *in vitro* release medium, the corresponding PS 80 and SLS concentrations that would be required to dissolve the *ex vivo* measured saturation concentration of PTX were calculated.

Sample	pH	PTX saturation concentration [µg/ml]	Corresponding PS 80 concentration [mg/ml]	Corresponding SLS concentration [mg/ml]
Ascites 1	7.56	19.18	7.46	0.99
Ascites 2	8.07	7.42	2.83	0.42

4.3.2 Release kinetics of PTX-loaded NP

Once suitable release conditions for PTX-loaded NP were established, the nanoparticulate formulations developed in sections 2.2.2 and 2.2.3 were evaluated. The release of PTX from PLGA NP occurred at a substantially higher rate than from EC 4 NP (Figure 4.3 A). While after 10 d the largest portion of PTX (93 %) was released from the PLGA NP, only about 60 % was released from the EC 4 NP at the same period. Composition with CS reduced the release of PTX from PLGA NP by more than half to 44 % compared to unmodified NP. For EC 4 NP, however, CS composition did not markedly change the release kinetics. As for the loading behavior of PTX in EC 4 (section 2.2.3.2), CS obviously did not influence the release of PTX. In addition to release-sustaining effects of CS, Lu *et al.* reported that the release was dependent on the CS quantity in

the particle system, and thus, the release decreased with increasing CS quantity [288]. Attempts were also made to include higher amounts of CS in composite PLGA NP. However, this resulted in NP with low redispersibility after centrifugation and free CS (SEM; results not shown) and was therefore abandoned.

Since different DL were easily generated in EC 4 NP, varying particle concentrations with different DL were tested while keeping the total PTX amount constant in the release system (Figure 4.3 B). The lowest number of particles with the highest DL (10 mg, initial 10 % (w/w) PTX) showed the highest release rate and *vice versa*. In addition, EC 4 NP with doubled total amount of PTX were investigated (100 mg, initial 2 % (w/w) PTX) and comparable release kinetics were measured as with the same amount of particles and half the load. Thus, the particle concentration also has a pronounced effect on the release of PTX. It can be assumed that diffusion of released PTX and thus, the removal from the diffusion layer around the NP occurs more quickly at lower particle quantities than at a high particle concentration with much smaller distances to the neighboring particles. This possibly hinders mutual release. Furthermore, substantially more PTX might be on the surface or near the surface of the initial 10 % (w/w) PTX-loaded EC 4 NP compared to initial 1 and 2 % (w/w) PTX-loaded NP. This proportion of PTX is released much more quickly from NP. However, to confirm the effect of the increased particle concentration on a slower release, further investigations should be carried out.

Coating experiments with BSA and its cross-linked counterpart did not markedly effect PTX release (Figure 4.3 C). However, albumin-coatings might still improve uptake and accumulation of NP in tumor tissue as reported in the literature [222]. Nevertheless, it is reasonable to assume that the occurrence of a protein corona has little or no effect on drug release from NP after application to human body fluids. In contrast, PEC-coatings (without Ca^{2+} ions) reduced the drug release to approx. 30 % after 10 d (Figure 4.3 D). For comparison, the release from unmodified PLGA NP (Figure 4.3 A) was more than 200 % higher. Thus, the hydrophilic hydrogel layer around the NP exhibits a beneficial effect and prevents a rapid release of the hydrophobic PTX. In the presence of Ca^{2+}, however, this effect was not apparent or only appeared after more than one week to a substantially lower extent. As described for gelation experiments in section 2.2.4.5, the hydrogel layer, which adheres to the CS-modified particle surface via electrostatic attraction, probably detached from the particle surface by the electrostatic attraction of the Ca^{2+} ions in the solution. This might especially occur with PEC molecules that are more distant from the NP surface, strongly reducing the effect of PEC. Transferred to the application in the human peritoneal cavity, initially lowered Ca^{2+} levels in the peritoneum after application are gradually restored to an equilibrium through extracellular fluid exchange. Accordingly, the effect of the PEC hydrogel layer around the NP is not expected to have much influence on PTX release during medical application.

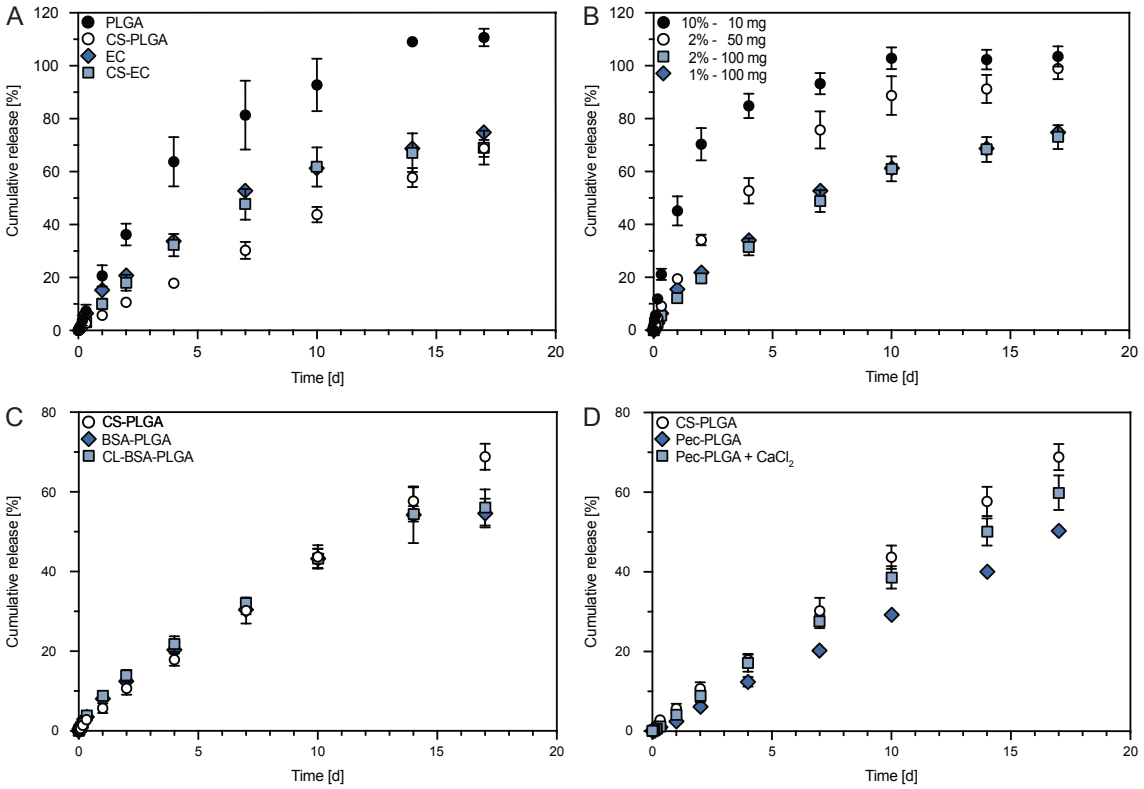

Figure 4.3: Release kinetics of PTX-loaded NP.

A: Release of unmodified and CS-modified NP using PLGA and EC 4 loaded with 2 or 1 % (w/w) PTX, respectively. B: Effect of NP quantity on release behaviour of EC 4 NP loaded with PTX in initial concentrations of 1, 2, and 10 % (w/w). C: Effect of BSA-coating on release behaviour of CS-PLGA NP. D: Effect of PEC-coating on release behaviour of CS-PLGA NP.

4.4 Conclusion

The establishment of a suitable release setup for PTX-loaded NP revealed relevant difficulties. Both the stability of the active ingredient and its detectability in the released concentration are required. It is also obvious that a standardized apparatus or functional setup adapted to nanoparticulate formulations must first be established before data between different research groups can be compared. In this context, release experiments with dialysis tubes based on results of the present thesis show promising potential. The dispersion releaser, combining the paddle apparatus, which is approved by pharmacopoeias, and dialysis technique is a current approach by Wacker and Janas [294]. The release of PTX could not be completely delayed by several days with the developed formulations in the tested setup. Nevertheless, the release of PTX could be sustained by using EC instead of PLGA and by composition of PLGA with CS. Hydrogel coating with PEC also succeeded regarding sustaining PTX release. Physiological Ca^{2+} concentration in the human body might limit clinical application. However, the results offer promising inspiration for future sustained-release formulations.

5. Characterization of Abraxane®

5.1 Introduction

Abraxane® is a solvent-free formulation of PTX stabilized with albumin as polymeric NP. It is the first approved formulation based on nanoparticle albumin-bound (nab™) technology (Abraxane® for Injectable Suspension, ABI-007, manufactured by Abraxis BioScience, LLC, a subsidiary of Celgene Corporation, Summit, USA) [295]. It is designed to increase efficacy and reduce toxicities associated with conventional solvent based PTX. Taxol® (Bristol-Myers Squibb, New York, USA) was the first product containing PTX, being authorized by FDA for the treatment of metastatic ovarian cancer in 1992. It consists of EtOH and Cremophor® EL [296]. The detergent is known to cause serious hypersensitivity reactions and neuropathy [297]. Additionally, the detergent can prevent the desired effect through inclusion of the drug in micelles [298]. Abraxane® additionally eliminates the need for pre-medication, which is necessary for Taxol® applications to prevent hypersensitivity reactions. The role of albumin in tumor progression mentioned in the previous chapters shows further advantages of the nab™ technology used in Abraxane®. Today, nab™-PTX is approved for the treatment of patients with metastatic breast cancer, locally advanced or metastatic non-small cell lung cancer and metastatic pancreatic adenocarcinoma in the United States, the European Union, Japan, and several other countries worldwide. In Japan, nab™-PTX is also approved for the treatment of advanced stomach cancer [299]. Abraxane® is of interest as it is an approved NP formulation of PTX and has already been successfully tested in the PIPAC application [197]. To assess whether this existing formulation already provides intended benefits such as delayed drug release, Abraxane® was characterized regarding *in vitro* release kinetics and further properties of nab™-PTX.

5.2 Methods

5.2.1 Reconstruction procedure

The freeze-dried formulation was reconstructed as described in the package insert and the company's technical information. Using a sterile syringe and cannula, 20 ml of a Braun® isotonic sodium chloride solution was slowly injected into the vial over a period of 2 min. The liquid jet was directed to the inner wall and not directly onto the powder, to prevent foaming. After complete addition, the vessel was left for 5 min to ensure good wetting of the dried powder. Then, the bottle was slowly and carefully swiveled and inverted for 2 min. As no foam formation was visible, the sample was suited for further experiments.

5.2.2 Methods for characterization

5.2.2.1 Determination of morphological and chemical properties

The appearance of both, the freeze-dried as well as the reconstructed formulation, was recorded including their morphology by SEM imaging. For this purpose, a few chunks of the freeze-dried NP cake were carefully removed through the vial using a sterile cannula to avoid opening the vial. After reconstruction, different approaches were tested to remove the sodium chloride for crystal-free imaging in dry state. First, sample preparation was carried out using a compressed air gun. For this purpose, 10 µl of a 1:10 dilution of the freshly reconstructed Abraxane® dispersion was dropped directly onto a silica wafer. After 15 min of settling time, the liquid was blown off using 2 bar air pressure. Another sample was desalinated by dialysis. Therefore, 1 ml sample was filled into a soaked and cleaned dialysis tubing and placed into 800 ml stirred MilliQ® water for 4 h with renewing the fluid after 2 h. A third sample was prepared centrifuging 1 ml twice (10,000 RCF, 20 °C, 30 min) redispersing the pellet in MilliQ® water.

Furthermore, pH, viscosity, and osmolarity of the reconstructed formulation was measured. For pH measurements, the pH glass electrode of the EL20 benchtop pH meter was dipped directly into the dispersion in primary packaging. For viscosity measurements, the reconstructed dispersion was filled with 4.5 ml to the lower filling mark of a micro-Ubbelohde viscosimeter and forced into the capillary tube. Then, the flow time between the measuring points through the capillary was determined. To evaluate the functionality and correct handling of the device, MilliQ® water and EtOH, liquids of known viscosities, were measured. The osmolarity of 50 µl Abraxane® aliquots were determined by freezing point depression using an Osmomat 010.

5.2.2.2 Determination of colloidal properties

Freshly reconstructed dispersions were diluted with MilliQ® water and with 0.9 % (w/v) sodium chloride solution (Braun®) 1:500 for examination of size and PDI. Both, dialyzed and centrifuged samples prepared as described for SEM imaging in section 1.2.2.1, were used for ζ-potential measurements. In addition, the colloidal properties were repeatedly measured after storage for 24 h at 4 °C.

5.2.2.3 Determination of DL

To determine the mass of the formulation, three aliquots of 1 ml reconstructed Abraxane® each were lyophilized in tared tubes and the amount of added NaCl was subtracted of total measured weight. The PTX-loading was investigated several times due to insufficient measured amounts. Best fit was obtained using freeze-dried, weighed aliquots, reconstructed in 1 ml MilliQ® water and centrifuged at 60,000 RCF, 20 °C, 30 min. The pellet was dissolved in ACN. The supernatant was precipitated by adding 1:1 ACN and mixing. Centrifugation was repeated . Both samples

were quantified by HPLC (section 2.2.4.3) and calculated concentrations were summed up for drug loading values.

5.2.2.4 Drug release of Abraxane®

For drug release trials, small amounts of freshly reconstructed Abraxane® were used due to high DL. Sample and separation setups described in section 4.2.1.1 were used. In microcentrifuge tube setup an aliquot of 100 µl Abraxane® was dispersed in 1.9 ml isotonic sodium chloride solution and added to 18 ml release medium containing 0.9 % (w/v) sodium chloride, 0.2 % (w/v) PS 80, and 0.1 M acetic acid/acetate buffer (pH 4.75). For bulk setup using 100 ml Erlenmeyer flasks, 200 µl sample were dispersed in 9.8 ml 0.9 % sodium chloride solution and added to 90 ml release media with the same composition as in the microcentrifuge tube setup. Samples were collected after 0, 1, 2, 4, 8, 24, 48 h and 7 d, and were analyzed by HPLC.

5.3 Results and discussion

5.3.1 Appearance of the nab™-PTX formulation

Abraxane® is provided as freeze-dried formulation to maintain the stability of the formulation over a longer period of time. By removing water, decomposition and degradation of NP, hydrolytic degradation of the active ingredient, especially, is reduced as far as possible. Less important, but still worth mentioning, is the reduction in the weight of the product in the lyophilized state, which ensures a lower energy and transport cost.

During first visual inspection of the vial, nab™-PTX appeared as a white-yellowish, fluffy freeze-dried cake (Figure 5.1 A). It was broken into several pieces, probably due to transport, and showed rough, fibrous surfaces at the fracture areas. The SEM visualization (Figure 5.1 B) revealed large, planar structures. At higher magnification (Figure 5.1 C), the surface structure was visible with embedded particulate structures indicated at the fractured areas. The resulting reconstructed, milky white yellowish (ivory) dispersion appeared homogeneous without any not reconstructed residuals.

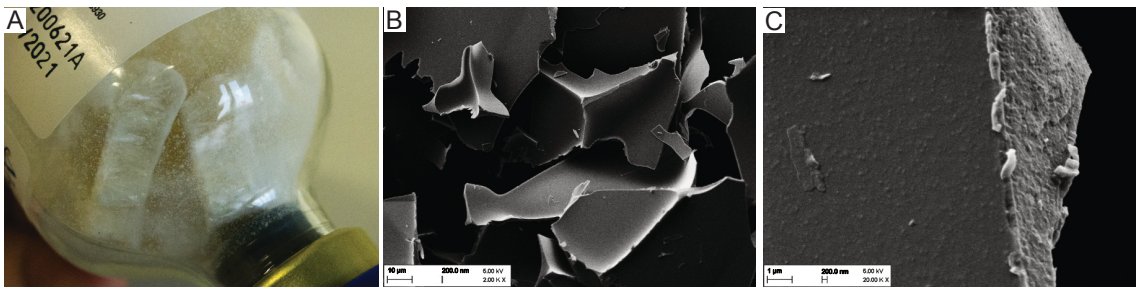

Figure 5.1: Abraxane® powder in original, lyophilized condition.

A: Photography of the vial. B, C: SEM visualization of the powder.

SEM images of differently prepared Abraxane® aliquots are presented in Figure 5.2. All three sample preparations were free of sodium chloride crystals as intended. The sample treated with compressed air showed spherical particles which might fit into the desired size range considering the dried state and the low-pressure conditions of the SEM (Figure 5.2 A). The dialyzed aliquot showed a higher particle concentration, but the particles mostly caked and not all NP had still spherical appearances (Figure 5.2 B). Presumably, the particles lost their stability within the 4 h of dialysis with large amounts of MilliQ® water (2 x 800 ml per 1 ml aliquot). Thus, the particles started to lose their shape or to disintegrate, as it is also described in the literature [299]. The centrifuged aliquot showed mainly precipitates of PTX in SEM (Figure 5.2 C), which in some cases stuck together to form larger structures, probably due to albumin residues. Apparently, the PTX bound to albumin precipitated at the bottom of the tube probably due to the harsh centrifugation conditions and supersaturation as dissolved albumin in the supernatant was removed.

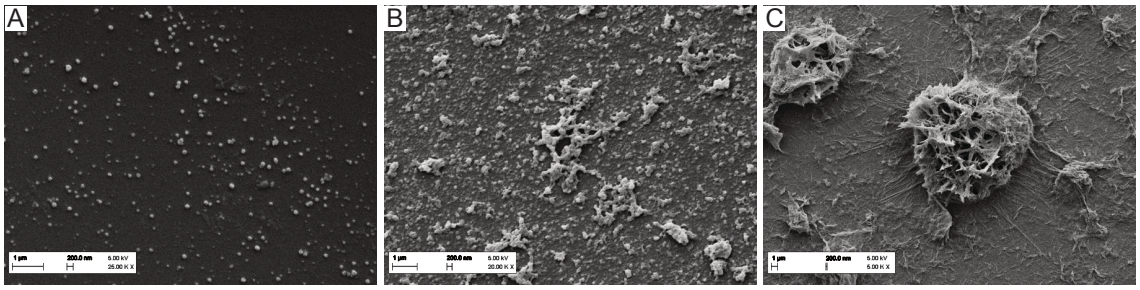

Figure 5.2: SEM visualization of Abraxane® after reconstruction and desalination procedures.

A: Sample prepared by compressed air. B: Sample prepared by dialysis. C: Sample prepared by centrifugation.

5.3.2 Properties of dispersed nab™-PTX formulation

Table 5.1 lists the results of the investigated properties of freshly reconstructed Abraxane® formulation. The measured pH value of 6.84 is within the range specified by the manufacturer from weakly acidic to weakly alkaline (pH 6 - 7.5). With an osmolality of approx. 293 mosmol/kg water, this is just below the range indicated (300 - 360 mosmol/kg), but should not cause any problems with intravenous application, as the physiological value of the blood plasma can be found at 275 - 300 mosmol/kg water [245]. The kinematic viscosity of Abraxane® was determined with a value of almost 1.2 mm^2/s at room temperature (RT; approx. 22 - 23 °C). The precision and reliability of the measurement was successfully verified using liquids of known viscosity (data not shown). In the literature, the particle size is described to be 130 nm. However, neither information on the particle size distribution nor the measured medium can be found. For this reason, the particles were measured in MilliQ® water as well as in isotonic saline solution. With 133 nm in water and 139 nm in saline, both measured sizes are close to the reported particle size. With PDIs of 0.117 in water and 0.114 in saline narrow particle size distributions were observed. A ζ-potential of about 6 mV (dialyzed) and 8.5 mV (centrifuged) indicated a rather low surface charge of the particles. The dry weight of the formulation after lyophilization and subtraction of the added sodium chloride is 47.38 mg/ml on average, just a bit below the

calculated theoretical value of 50 mg/ml:

$$m_{theoretical} = \frac{100 \text{ mg PTX} + 900 \text{ mg albumin}}{20 \text{ ml dispersion}} = 50 \text{ mg/ml}$$

Observed values for PTX concentration of 4.907 ± 0.099 mg/ml, were also slightly below the declared 5 mg/ml, but still within the permitted range of 15 % deviation (European Pharmacopoeia). These lower values for both the total weight of the formulation and the drug can be explained by losses, for example, at the tip of the pipette, or deviations of the balance by gravimetric measurement of particle weights. Nevertheless, the DL of 10.24 % corresponded to the value of 10 %, as described by the manufacturer [300].

Table 5.1: Properties of Abraxane® measured after reconstruction and 24 h after reconstruction. The experimentally determined values were compared with available values in the literature.

Properties	Measured	Literature
freshly redispersed		
pH	6.84	6 - 7.5*
Viscosity [mm^2/s]	1.197 ± 0.002	n.a.
Osmolality [mosm/kg]	293 ± 1	300 - 360*
size in H_2O [nm]	133	130*
size in saline [nm]	139	(medium unknown)
PDI in H_2O	0.117	n.a.
PDI in saline	0.114	n.a.
ζ-potential (dialysed sample) [mV]	-5.95	n.a.
c (PTX) [mg/ml]	4.907 ± 0.099	5*
DL [%]	10.24 ± 0.20	10**
24 h after redispersion		
z-average size in H2O [nm]	105	n.a.
z-average size in saline [nm]	126	n.a.
PDI in H2O	0.212	n.a.
PDI in saline	0.153	n.a.
ζ-potential (dialysed sample) [mV]	-5.85	n.a.
c (PTX) [mg/ml]	4.824	5*
DL [%]	10.52	10**

* Data taken from the product information/packaging [192]

** Data taken from FDA full describing information on Abraxane® [300]

Within 24 h after reconstruction and storage at 4 °C, the appearance of the dispersion did not change noticeably. Depending on the medium, the particle size decreased by 28 nm (H_2O) and 13 nm (saline). The PDIs, on the other hand, increased by 0.095 (H_2O) and 0.039 (saline). The ζ-potential of 5.85 mV of the dialyzed sample, as well as the PTX content of 4.824 mg/ml which corresponds to a DL of 10.52 %, reflected a nearly constant result. Despite a slight tendency towards degradation or dissociation of the particles, which was indicated by the decreasing particle size and worsening PDI, distinct and probably applicable particles were still present after 24 h. No comparative values were found due to lack of data in the literature.

PTX release from Abraxane® formulation was tested in both the Erlenmeyer and microcentrifuge tube setups and was calculated according to the specific drug loading of 10.24 %. In both release setups, high release rates of 83 and 95 % at release start were detected (Figure 5.3). At release start the concentration was approx. 12 % lower in the Erlenmeyer setup than in the microcentrifuge tube setup. An insufficient mixing of the formulation with the release media due to the immense total volume of 100 ml might be a reason for this. Within the first 48 h, the released PTX concentration fluctuated around a value of 100 %. Therefore, it can be concluded that PTX was released completely from the albumin NP right at the beginning of the experiment. This is in clear contrast to the substantially delayed release observed for PTX-loaded PLGA and CS-PLGA NP. Despite the high burst release within the first day, the developed NP formulation exhibited a sustained release and released drug for more than 4 h in contrast to Abraxane®. Thus, the release was slowed down by a factor of 4 and more.

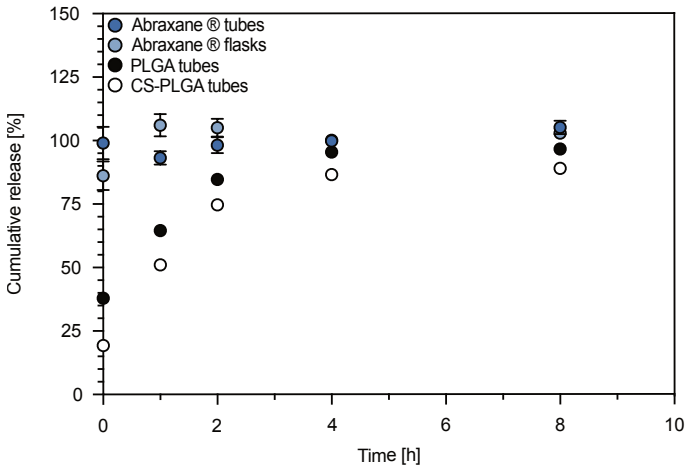

Figure 5.3: First 8 h of PTX release of Abraxane® performed in different setups and for comparison of PLGA and CS-PLGA NP performed in microcentrifuge tubes.

According to the literature, nab™-PTX should disintegrate after application in terms of a „dynamic dissolution process into smaller NP and eventually to mostly albumin-bound PTX complexes and a small fraction of unbound PTX", and the active ingredient bound to albumin should be transported to the site of action (Figure 5.4) [299]. For protein bound and unbound PTX about 94 % and 6.3 %, respectively, were reported. A "rapid" release is mentioned [299].

Due to degradation of the particles and the remaining PTX associated to albumin, PTX is present in dissolved form and can therefore be quantified in the release experiments. After seven days, white precipitates formed strings and settled to the bottoms of the microcentrifuge tubes. PTX concentrations decreased to values of around 35 %. After some time, PTX probably dissociated from the albumin exceeding the solubility limit of the release medium, and precipitated.

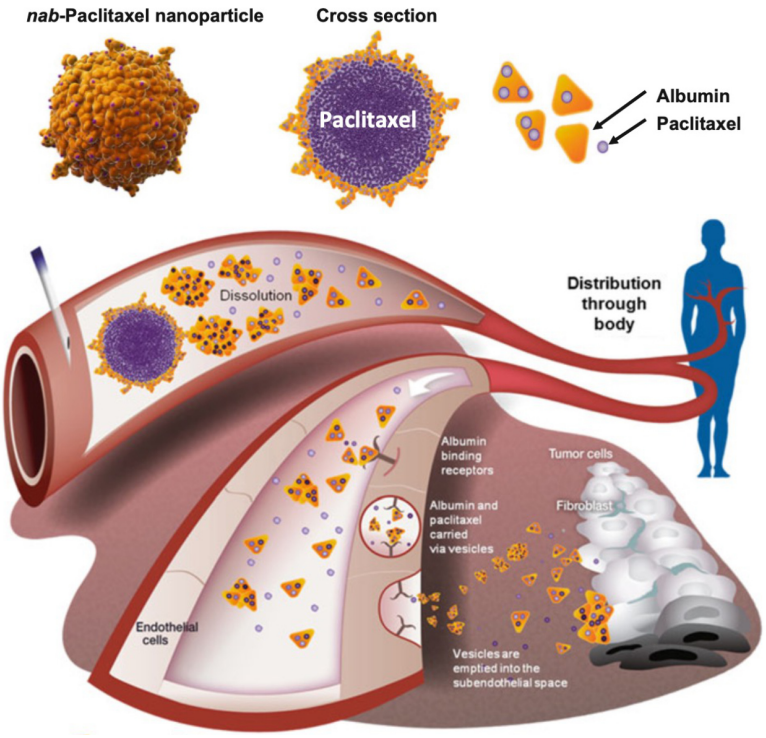

Figure 5.4: Schematic illustration of Abraxane® and mechanisms for the transport of Abraxane® into tumours.

Dissolution of nab™-PTX after intravenous application is displayed. Reprinted with permission [299]. Copyright © 2016, Springer Science+Business Media Singapore.

5.4 Conclusion

The particle properties for Abraxane® formulation described in the literature were confirmed as far as available. Both dialyzed particles of the SEM imaging and release samples indicated rapid particle decay. This suggests a dependence on liquid volume, temperature, and the duration particles persist in solution. As release experiments revealed an immediate decay of particles, a release can no longer be considered, but rather a dissolution of the drug by strong binding to albumin. Accordingly, the formulation is not suitable for the desired therapeutic purpose in PIPAC. Despite the high burst effect of PLGA NP, which was measurable by sample and separation setups, the formulations developed in the present work are based on a genuine drug release compared to the commercially marked Abraxane® formulation. Therefore, polymeric NP based on PLGA provide a more appropriate basis for further development of a sustained release formulation.

6. *In vitro* nebulization and *ex vivo* penetration of polymeric NP

6.1 Introduction

Since the proposed nanoparticulate formulation is to be applied within the PIPAC therapy, stability and sprayability of the polymeric carrier systems during the process are essential. As only limited data is available on the nebulization of polymeric NP using devices of PIPAC application (Figure 6.1), influence of the pressure conditions on the stability of NP was investigated during the spraying process.

Distinct delivery rates (flow rates) in volume per time (ml/s) can be adjusted at the angioinjector. During the injection, the pressure in the system increases, which is calculated based on the required motor current and plotted on the display of the angioinjector (one value per 300 ms). Thus, the injector constantly monitors the pressure and compares the value with a pressure limit set by the user. When this limit is reached, the pressure control of the injector intervenes and adjusts/reduces the delivery rate or aborts the application process [301]. In PIPAC application, flow rates of 0.5 - 0.7 ml/s are currently used during spraying application and a pressure limit of 21 bar is preset in the angioinjector system [302]. Via a tube system, the angioinjector delivers the applied liquid to the nebulizer, the so-called CapnoPen®. Pressure forces the liquid to enter the CapnoPen® and a pin is pressed against the release opening, causing the liquid to be nebulized in a spray cone (Figure 6.1, pin shown in red).

In addition to the application capability of the nanosized carriers, their penetration ability was also investigated using an enhanced inverted bovine urinary bladder (eIBUB) model established previously by the cooperating working group of Prof. Reymond at UKT [306]. Being an intraperitoneal organ, the urinary bladder is almost completely covered with visceral peritoneal tissue. In the eIBUB model the outside is turned in, which lines the cavity through the peritoneum. Due to the enormous size of the bovine urinary bladder, the eIBUB (2 - 3 l) occupies almost the volume of the human abdomen (3 - 5 l) after insufflation with CO_2. As doxorubicin applied in the eIBUB exhibited similar properties in terms of tissue concentration and depth of penetration compared to a human patient, transferability can be assumed [307]. Although the homogeneous distribution of active ingredients already improved, gravity, drag, and inertial impaction still prevent a desirable distribution with PIPAC [52, 308]. As reported by Van de Sande *et al*, further development to ePIPAC can additionally improve the spatial homogeneity of the aerosol and increase tissue penetration [52]. For this reason, the penetration properties of both PIPAC and ePIPAC were investigated in the eIBUB model. The penetration depth of CUR-PLGA NP of different surface charge (non-modified negatively charged and CS-modified positively charged NP) were measured via their fluorescent properties (Figure 2.6). The penetration studies were conducted in cooperation with the UKT coordinated by Dr. Ranjita Sahoo (Capnomed®). Thereby, the application of NP in the eIBUB model was performed by Yaroslaw Sautkin, the preparation and examination of

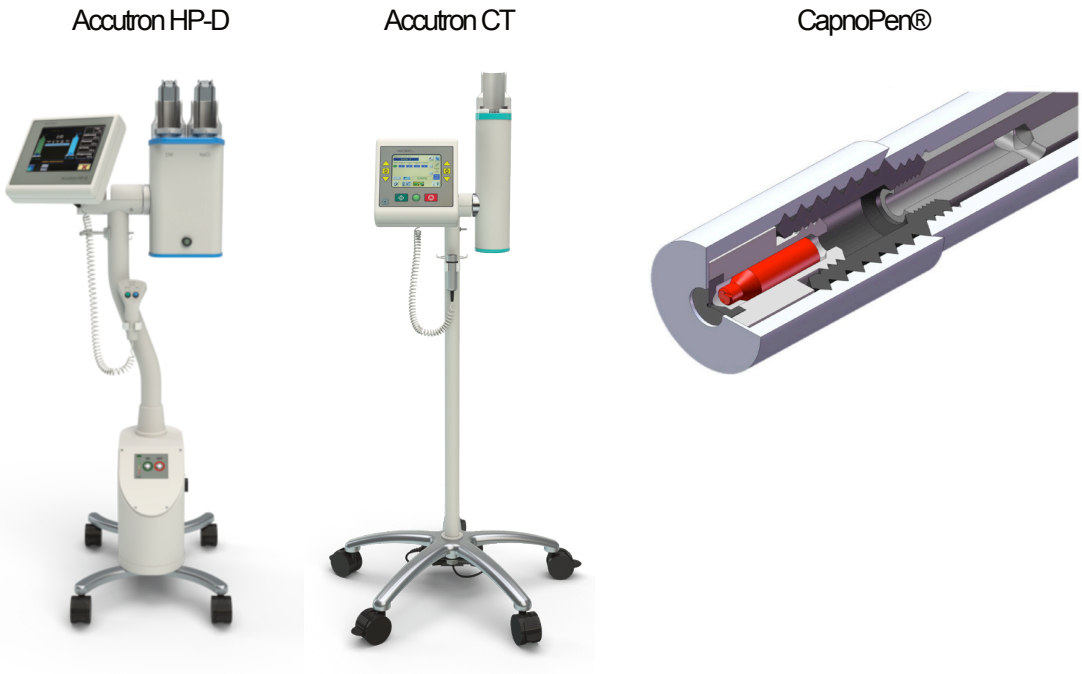

Figure 6.1: Devices used for PIPAC application.

Angioinjectors: Accutron HP-D and CT [303, 304]. CapnoPen®: schematic laparoscopic nebulizer for medical aerosols. Reprinted with permission [305]. Copyright © 2016, Springer Science Business Media New York.

biopsy slides by fluorescence microscopy were executed by Stefanie Spriewald, Laura Toussaint and others, and blinded measuring of penetration depth and statistical analysis were accomplished by Arianna Castagna. Results of the penetration experiments are already published in Castagna *et al.* [231].

6.2 Methods

6.2.1 *In vitro* nebulization of polymeric NP

Depending on the angioinjector provided by MedTron AG (Saarbrücken, Germany), Accutron HP-D or CT were used for the subsequent experiments. Nebulizers (CapnoPens®) were supplied by Capnomed (Zimmern ob Rottweil, Germany).

6.2.1.1 Stability of nebulized PLGA NP

For examination of stability and sprayability of PLGA NP, plain PLGA NP were prepared (section 2.2.2.1), and after purification the dispersion was diluted to a concentration of 0.75 % (84 ml) and filled in a 200 ml angioinjector capsule. At a flow rate of 0.5 ml/s, adjusted by the angioinjector Accutron HP-D, the dispersion was nebulized against silica wafers located at distances of 2, 5 and 10 cm positioned on the lid of plastic mini Petri dishes. In addition, the samples were collected in 3 ml MilliQ® water. During the spraying process, surfaces were changed and the height of the Capnopen® attached to a tripod was shifted to maintain the different distances to the surfaces. The

NP samples were characterized by DLS and SEM before spraying, visualized again by SEM after spraying, and evaluated for integrity with respect to their morphology.

Additionally, it was investigated whether heating of the formulation prior application is possible without changes in particle appearance (deformation), size and PDI. For this purpose, plain PLGA NP were prepared as triplicates and diluted to concentrations of 0.5, 0.75 and 1 % (w/v). Subsequently, individual particle dispersions of 30 ml each (minimally sprayable volume of the angioinjector) were applied to mini Petri dishes filled with 3 ml MilliQ® water at a distance of 5 cm using a flow rate of 0.5 ml/s. Temperatures of 22 (RT), 30, and 38 °C were investigated. For each temperature new samples of plain PLGA NP were prepared. Before and after aerosolization, the particle properties were examined by DLS and SEM. In addition, a 5 ml batch of 1 % (w/v) PLGA NP was slowly heated from 22 °C (RT) to 40 °C within 1 h to evaluate the stability of the particles upon heating (without the influence of nebulization). Starting at 30 °C, samples were collected at 2 °C intervals and evaluated by DLS and SEM.

6.2.1.2 Performance and pressure conditions of the angioinjector-nebulizer system

To evaluate the pressure conditions during the nebulization process within the angioinjector-nebulizer system, new nebulizers were tested on their pressure conditions at flow rates of 0.5 and 0.6 ml/s using 200 ml MilliQ® water as well as fresh, plain PLGA NP. For these trials, the angioinjector Accutron CT was used.

Furthermore, 200 ml of freeze-dried plain PLGA NP redispersed with 5 % (w/v) Glc, were nebulized in concentrations of 0.33 - 5 % (w/v) to evaluate pressure and feasibility of nebulization regarding NP concentrations and volumes. A 5 % (w/v) dispersion was determined as the highest tested concentration due to high manufacturing efforts. To determine the influence of 5 % (w/v) Glc, 200 ml solution without NP was nebulized. For cost reasons, the same nebulizer was reused, rinsed with hot MilliQ® water and ACE between NP samples, and tested with pure MilliQ® water before each sample. Spraying was performed at flow rates of 0.5 ml/s. Then, a rarely used nebulizer was compared to the frequently used nebulizer of previous experiment using both, fresh and freeze-dried plain PLGA NP of 5 % (w/v) concentration. Feasibility of nebulization of fresh, plain EC 4 NP (section 2.2.2.4) with concentrations of 0.33 - 5 % (w/v) and volumes of 200 ml were investigated using a rarely used nebulizer at flow rates of 0.5 ml/s.

6.2.2 *Ex vivo* penetration of fluorescently labelled PLGA NP

6.2.2.1 Sample preparation

For determination of the PLGA NP penetration in the eIBUB model, initial 1 % (w/v) CUR-loaded PLGA and CS-PLGA NP were prepared (sections 2.2.2.2 and 2.2.3.1). Colloidal properties, morphologies, and loadings were investigated, and NP were dispersed in 150 ml 0.9 % (w/v) NaCl solution with a concentration of 1.33 mg/ml. For later application, the dispersions were filled into

ELS 200 ml angioinjector capsules.

6.2.2.2 Application in eIBUB using PIPAC and ePIPAC procedures

Experiments on fresh bovine urinary bladders, stored on ice, and delivered in the early morning to the laboratory were performed within hours after removal (slaughterhouse). First, through the bladder neck a 12 mm double-balloon trocar was introduced and tightened with a Mersilene® suture. Then, a silicone tube was sewed on the bottom of the bladder to collect liquid dropping down along the peritoneal surface. The NP dispersions were applied to eIBUB using PIPAC and ePIPAC techniques. For PIPAC, a capnoperitoneum was established under standard laparoscopic pressure of 12 mmHg. Using new CapnoPen® nebulizers connected to a high-pressure angioinjector, the NP dispersions were aerosolized at RT. The closed system was maintained in steady state for 30 min. At the end of the procedure, the aerosol was discarded using a closed aerosol waste system. For application of NP dispersions by the ePIPAC technique, an Ionwand® brush electrode was additionally introduced through the bladder wall, and a return electrode was fixed on the external bladder surface. Both electrodes were connected to a generator with a voltage of 7,500 - 9,500 V. At the beginning of the aerosolization phase, the electrostatic system was started and maintained for 30 min. Figure 6.2 displays the setups of PIPAC and ePIPAC application in the eIBUB model. Subsequently, bladders were opened, placed on a colored inorganic substrate for proper orientation, and three biopsies with a diameter of 8 mm at three levels (top, middle, bottom) were taken perpendicularly through the bladder wall for tissue concentration measurements of CUR. At each location four additional biopsies were taken for histology examination of penetration depth. Biopsies were immediately frozen at -80 °C.

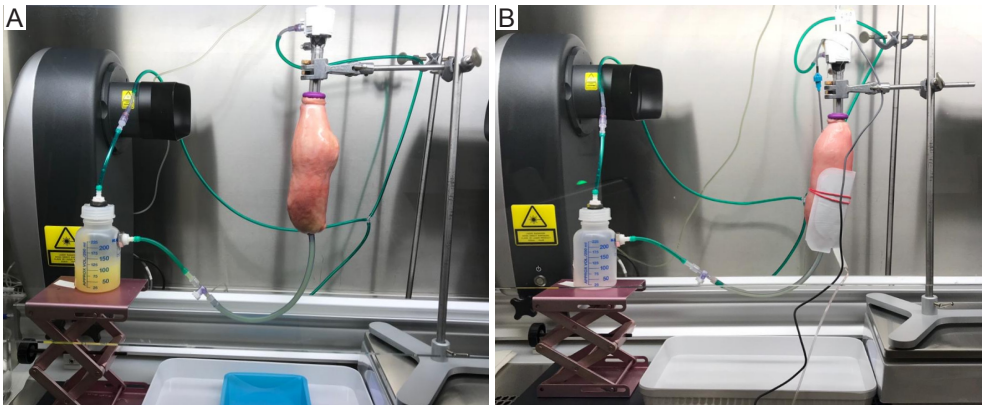

Figure 6.2: Setup of application in eIBUB for penetration studies.

A: PIPAC. B: ePIPAC. Photographs were provided by Dr. Ranjita Sahoo.

6.2.2.3 Histological examination of penetration depth

For cryo-sectioning, frozen biopsies were embedded in TissueTek® O.C.T.™ Compound on a cutting holder (vertical orientation to inorganic substrate), frozen at -22 °C, and cut in 10 µm thick

tissue slices using a Leica cryostat CM3050S. Tissue slices were placed on glass slides and were allowed to dry at RT. Then, biopsies were fixed with Cytoseal™ XYL and analyzed by fluorescence microscopy (10x magnitude). Three sections of each biopsy were examined. Each section was measured at three different positions regarding penetration depth with Leica Qwin 2002 software, and each measurement was repeated as triplicates. The analysis was blinded to the origin of tissue samples.

6.2.2.4 Determination of CUR concentration in bladder tissue

The frozen biopsies were lyophilized over-night using a BA-VC-300H vacuum concentrator (1,000 rpm; 100 mbar, RT), and rehydrated in a solvent mixture composed of 200 µl sterile Ampuwa® water and 1300 µl ACN over-night. Then, the biopsies were transferred into 2 ml PowerBead Tubes and milled in a TissueLyser LT. The samples were stored at -80 °C until shipping. For CUR quantification, samples were centrifuged (24,000 RCF, 30 min, 20 °C), and 200 µl supernatant was extracted and analyzed by fluorescence spectroscopy using an Infinite® M200 plate reader. A wavelength of 415 nm was used for excitation. Samples were detected at an emission wavelength of 533 nm. A calibration curve of CUR, dissolved in a solvent mixture of ACN and MilliQ® water (ratio 13:2), was created to calculate CUR concentrations. Using non-parametric tests, comparative statistics were carried out. SPSS software was used for statistical analysis.

6.3 Results and Discussion

6.3.1 *In vitro* nebulization of polymeric NP

Nebulization of nanoparticulate formulations was primarily tested using unloaded PLGA NP. Properties in terms of colloidal and morphological properties prior nebulization were already described in section 2.3.1.1.

6.3.1.1 Stability of nebulized PLGA NP

To approximate the scenario in the capnoperitoneum in terms of distances from the nozzle of the pen to the peritoneal tissue and its surface texture, different distances and surfaces were chosen for stability experiments. Due to the pressure prevailing in the capnoperitoneum, it was difficult to estimate the surface characteristics on which the particles would impact, and therefore two extremes were tested as a worst-case scenarios: a water surface and the surface of a silica wafer. SEM images of sprayed PLGA NP are shown in Figure 6.3. Particle sizes and distribution displayed no visually noticeable difference compared to unsprayed samples (Figure 2.1). In addition, the colloidal properties measured by Zetasizer did not change when spraying different concentrations of PLGA NP (Figure 6.4 B, samples sprayed at RT). Therefore, it can be assumed that no instabilities occur when spraying the formulation of polymeric PLGA NP, although high pressures

occured during the process. To date, there is little data published on the stability of nebulized NP applied by PIPAC procedure. Just recently in 2020, Van de Sande *et al*. reported unchanged colloidal properties of Carboxylate-modified FluoSpheres® (polystyrene) with diameters of 100 and 200 nm after spraying [52]. Thus, stability of polymeric particles seems to be sufficient for spraying procedures in PIPAC.

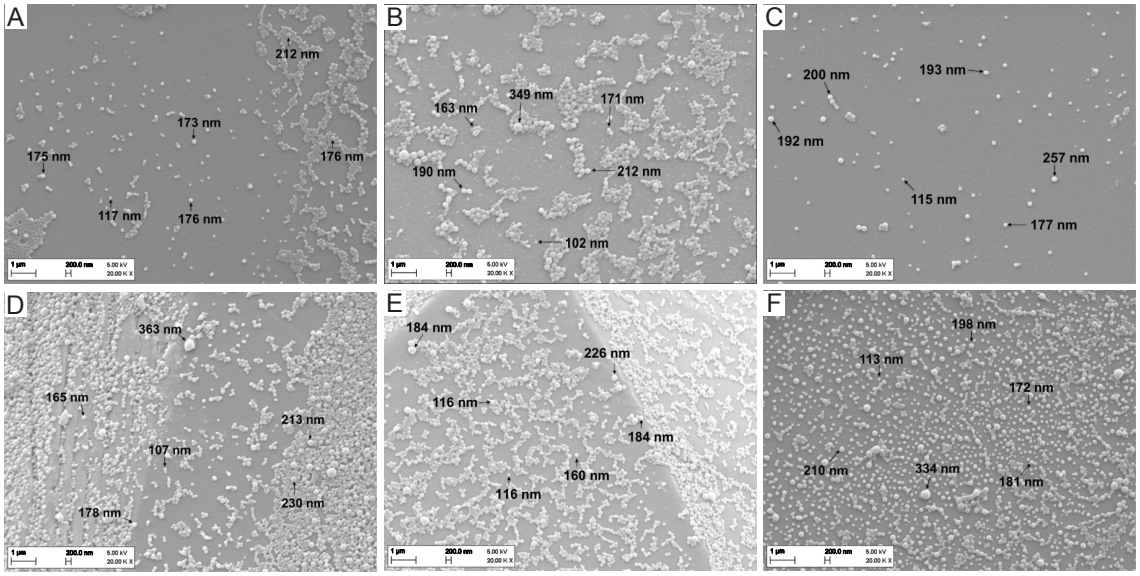

Figure 6.3: SEM images of 0.75 % (w/v) PLGA NP dispersion sprayed with different distances on water surface (A-C) or silica wafer (D-F).

A and D: 2 cm distance. B and E: 5 cm distance. C and F: 10 cm distance. Selected particle diameters were measured with Fiji 1.0.

Since pre-warmed samples might improve tissue penetration, such as in HIPEC, where intraperitoneal chemoperfusion is usually performed under hyperthermic conditions, temperature dependency of the particle application process is of special interest. The angioinjector allows pre-warming of samples until application [120], which enables measuring the impact of temperature on spraying. Properties of warmed PLGA NP were investigated to ensure stability. Slow heating of the NP dispersion up to temperatures of 40 °C did not noticeably affect the NP neither visually (SEM images not shown) nor in terms of their colloidal properties (Figure 6.4 A). No coalescence of the particles in the sense of agglomeration or particle growth was detected. The irreversible structural change described by Mdzinarashvili *et al*. due to phase transition of PLGA measured by differential scanning calorimetry, was not confirmed by morphological (SEM) and colloidal analysis [309]. However, the payload and the use of other stabilizers might contribute to these findings. Even after spraying NP, which were previously heated to 30 and 38 °C, no noticeable changes became apparent (Figure 6.4 B; SEM images not shown). Accordingly, the additional pressure applied to the heated particles during the spraying process also did not cause any change in particle properties.

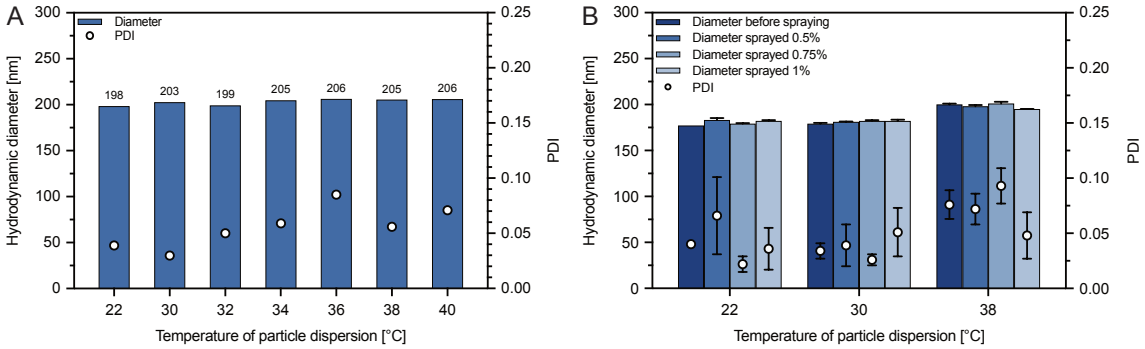

Figure 6.4: Changes in colloidal properties when heating PLGA NP dispersions during PIPAC application.

A: Influence of heat on colloidal properties of PLGA NP. B: Influence of nebulization colloidal properties of heated PLGA NP dispersions of different concentration.

6.3.1.2 Pressure conditions in the angioinjector-nebulizer system

Due to the high cost of the nebulizers, a cleaning procedure was established to remove formulation residues, and thus, to maintain reproducible pressure conditions within the injector-nebulizer system when using multiple times. Therefore, immediately after spraying of a sample, cleaning of the Capnopen® including the tubing system was performed flushing 200 ml hot MilliQ® water (80 °C) through the system from both sides using the angioinjector flow. In addition, the nebulizer pen was cleaned with ACE using a syringe. To confirm adequate spraying conditions in the angioinjector nebulizer device, water samples were tested at the flow rates given in literature [302]. Figure 6.5 A and B display the records of the pressure in the application device at 0.5 ml/s (A) and 0.6 ml/s (B) using the reused, cleaned pen.

After multiple use average pressures of 8 and 17 bar were achieved at the end of nebulization runs, respectively. Also remarkable was the delay of approx. 30 and 10 s, respectively, in the buildup of the spray cone and the pressure rise in the system. Using a new nebulizer at 0.5 ml/s and 0.6 ml/s, lower pressures of max. 5 and 9 bar were detected. The buildup of the spray cone and the pressure rise in the system was delayed by approx. 15 s and 5 - 10 s, respectively. A different unused pen showed no efficient pressure built-up in the system after three times of use and an incomplete spray cone (Figure 6.5 C). Accordingly, a slight decline in pressure conditions up to unserviceability of the pen can occur when reusing despite extensive cleaning after each sample.

Since initial trials of spraying a fresh 0.75 % (w/v) PLGA NP dispersion in the reused nebulizer was stopped at a flow rate of 0.6 ml/s after approx. 20 s by reaching the pressure limit of 21 bar, the flow rate for subsequent trials was set at 0.5 ml/s, which is the most commonly used flow rate reported in literature [302]. Usually, a constant pressure increase was observed during spraying of both fluids and NP dispersions. On occasion, pressure suddenly rose extremely accompanying with aborts of the spraying process. This was suspected to be due to clogging of the pen or its nozzle, e.g., by particle agglomerates. With sufficient pressure on the free-moving pin inside the CapnoPen® (Figure 6.1, red colored), it is forced onto the orifice of the pen tip and the liquid released from the nebulizer is aerosolized [305]. It is assumed that particle agglomerates can

obstruct the pin or directly clog the opening, and thus, might lead to an inefficient buildup of spray cone or an increase in pressure. Slightly pronounced increase in pressure due to presumed particle clogging of the pen are shown in Figure 6.5 D (red arrows).

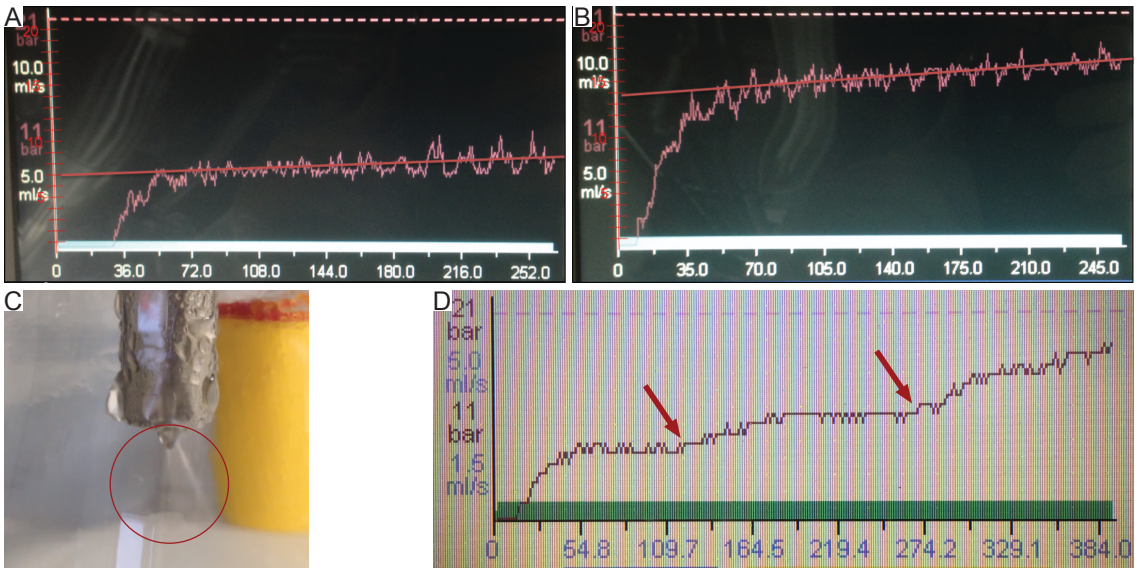

Figure 6.5: Pressure conditions in the angioinjector-nebulizer system.

A: Pressure plot of nebulization of water at a flow rate of 0.5 ml/s (reused pen). B: Pressure plot of nebulization of water at a flow rate of 0.6 ml/s (reused pen). C: Altered asymmetric spray cone after clogging of pen. D: Pressure plot of nebulization of 200 ml of 5 % (w/v) fresh PLGA NP. Red arrows display pressure increase due to clogging of the pen.

Furthermore, the assumptions that sprayability of PLGA NP dispersions relies on their concentration were confirmed (Figure 6.6 A). While the highest tested concentration of 5 % (w/v) could only be sprayed in volumes of approx. 30 ml, concentrations of 0.33 % (w/v) were sprayed in volumes of 200 ml without restrictions, with a substantial drop in volume between 0.5 and 0.33 % (w/v). The higher the number of particles per time was forced through the nebulizer the higher was the chance for clogging. However, data of this experiment represent a worst-case scenario using a frequently reused nebulizer pen with freeze-dried NP and additional 5 % (w/v) Glc. The nebulization of pure 5 % (w/v) Glc solution resulted in pressure conditions in the application system of max. 13 bar (5 bar higher than the max. pressure of the water sample). Using fresh, non-freeze-dried 5 % (w/v) PLGA NP dispersions (incl. 5 % (w/v) Glc) with the same nebulizer, the applicable volume was about twice as high than with freeze-dried NP (Figure 6.6 B). The sprayable volume was markedly increased applying a rarely used nebulizer. 5-fold increase in volume and even sprayability of complete volumes of the angioinjector capsules (200 ml) were possible with freeze-dried and non-freeze-dried NP, respectively.

Moreover, the concentration-dependent sprayability of fresh EC 4 NP was investigated to determine a sprayable concentration range for future formulations. At concentrations of 0.5 - 5 % (w/v), sometimes not even 20 ml volumes could be sprayed, although a rarely used pen was installed. At the lowest tested concentration of 0.33 % (w/v), however, the entire capsule volume was sprayable without encountering any problems. Accordingly, EC 4 NP appeared to be markedly more chal-

lenging to spray. However, since the PTX loading reached considerably higher values (section 2.2.2.4), less particles are required for adequate dosing, and thus, sprayable particle concentrations can be reached for application. However, release experiments (section 4.3.2) revealed that a delayed release of PTX was most pronounced with high particle concentrations and low DL. Therefore, it is uncertain whether the application of small amounts of EC 4 NP with high loading is useful to achieve the aimed pharmacokinetics. Overall, the experiments demonstrated that the reuse of the nebulizer for research purposes is possible and economically feasible but cannot be transferred to the *in vivo* scenario where a new pen is used for each application. By using constantly new pens, a significantly better sprayability is expected, and thus, the application of larger particle amounts, e.g., 5 % (w/v) PLGA NP indeed seems to be possible.

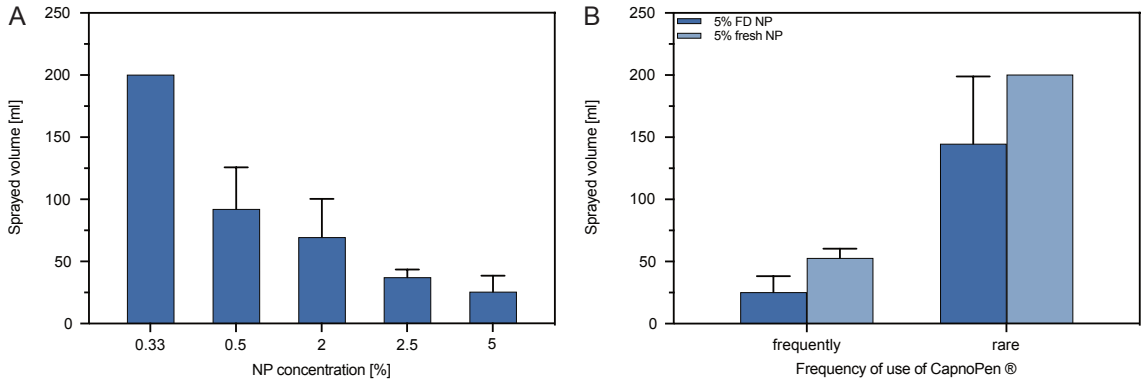

Figure 6.6: Sprayability of PLGA NP.

A: Concentration-dependent sprayability of freeze-dried PLGA NP in a frequently reused pen. B: Influence of reusing CapnoPens® on sprayability of PLGA NP.

Another crucial consideration is the fact that only unloaded, unmodified particles were tested in these trials. Thus, the influence of PTX and various substances, which are used for surface modification, on both sprayability and particle stability during nebulization is not predictable. Nevertheless, preliminary tests spraying initial 1 % (w/w) CUR-loaded CS-PLGA NP confirmed the feasibility of further penetration trials. The complete tested volume (100 ml) of the NP stock dispersion (2.4 % (w/v)) was successfully nebulized. Although CS is a rather sticky substance in processing, sprayability was feasible even using high particle concentrations. Accordingly, also other modifying substances may not significantly affect sprayability; however, this assumption needs to be confirmed by further experiments in the future.

6.3.2 *Ex vivo* penetration of fluorescently labelled PLGA NP

Properties in terms of colloidal and morphological character of CUR-loaded PLGA and CS-PLGA NP have already been described in section 2.3.2.1. Reproducible nebulization of NP was feasible in both PIPAC and ePIPAC procedure using an eIBUB model. After slicing the investigated bladders, yellow staining of the peritoneal lining can be observed being more intensely after ePIPAC (Figure 6.7 A II/IV), and thus, indicating superior amounts of penetrated NP. In addition, the intensity and depth of the fluorescence of the ePIPAC biopsies was more

pronounced for positively charged CS-PLGA NP (Figure 6.7 B II). The measurement of fluorescence depths in biopsies resulted in significantly higher values for ePIPAC samples (mean 156 µm, CI 5 - 95 %, 149 - 163 µm) compared to PIPAC samples (mean 119 µm, CI 5 - 95 %, 113 - 123 µm), $p < 0.001$). As shown in Figure 6.7 C, the largest depth of fluorescence, and thus, of tissue penetration, was achieved combining positively charged CS-PLGA NP with ePIPAC procedure (mean 208 µm, CI 5 - 95 %, 199 - 217 µm). Quantification of CUR tissue concentration did not significantly reveal deviations between positively and negatively charged CUR-loaded PLGA NP with mean values of 12.6 ng/ml (CI 5 - 95 %, 7.2 - 18.0 ng/ml) and 7.0 ng/ml (CI 5 - 95 %, 6.1 - 7.9 ng/ml), respectively ($p = 0.36$) (Figure 6.7 D). Applying NP by ePIPAC, no improve in tissue concentration (mean 9.1 ng/ml, CI 5 - 95 %, 5.3 - 13.0 ng/ml) was detected compared to PIPAC application (mean 10.5 ng/ml, CI 5 - 95 %, 6.1 - 14.9 ng/ml) ($p = 0.69$). According to this, the NP in ePIPAC seemed to reach deeper tissues, but not in larger amounts. Thus, particles are apparently not only accumulated in superficial tissue layers but are more effectively distributed into the deep.

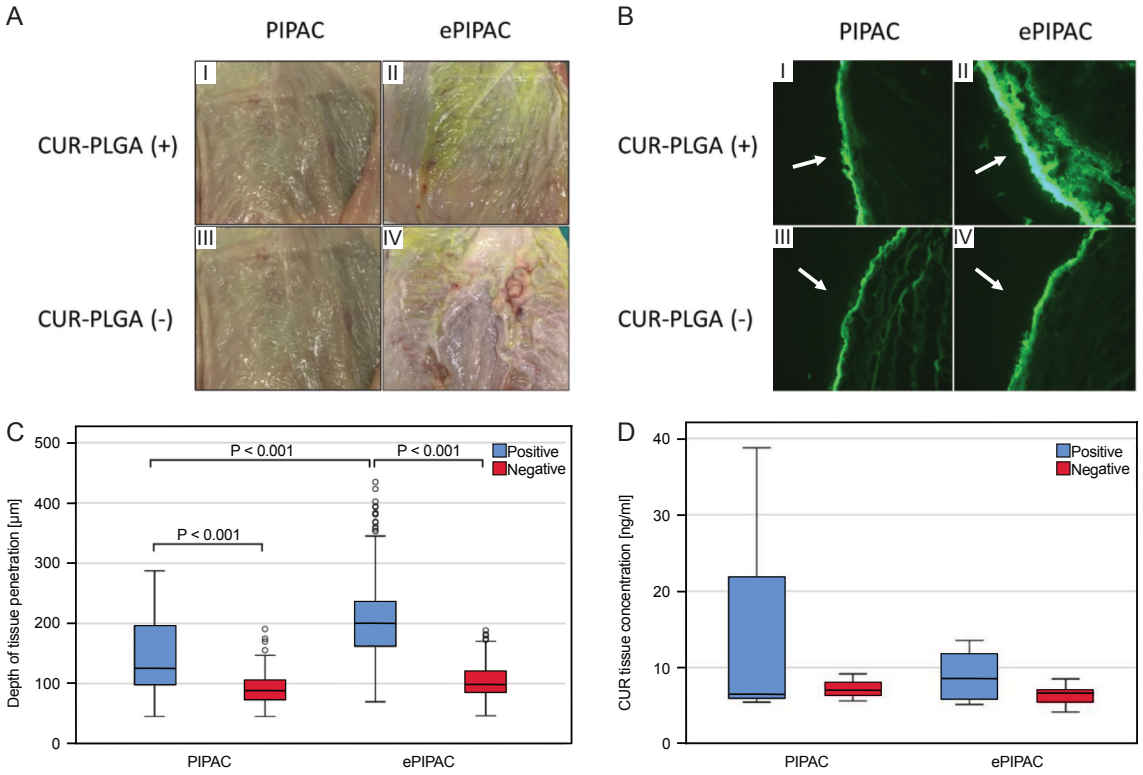

Figure 6.7: Penetration of positively and negatively charged fluorescent CUR-loaded PLGA NP in eIBUB model using PIPAC and ePIPAC technique.

A: Photographs of bovine urinary bladders after spraying and slicing. B: Visualization of penetration depths by fluorescence microscopy. C: Evaluation of penetration depths. D: Evaluation of CUR tissue concentration. Adapted from Nanomedicine (2021) 16(2), 109-120 with permission of Future Medicine Ltd. [231].

After recent developments in the intraperitoneal application of chemotherapeutic agents for improving tissue concentrations in terms of drug penetration by PIPAC and ePIPAC techniques, nebulization of nanoparticulate drug delivery systems promise further advancements for therapy of peritoneal metastasis [5, 120]. Recently, Shariati *et al.* proved the efficacy of this combined

approach in a rat model of disseminated peritoneal ovarian tumors [308]. Negatively charged, fluorescently labelled, cisplatin-loaded polyarginine-hyaluronic acid NP applied by PIPAC procedure enhanced intratumorally deposition and more efficiently eradicated peritoneal metastasis compared to free cisplatin. In 2020, Van de Sande *et al.* also reported application of NP in a rat model. Hereby, ePIPAC provided a more homogeneous delivery and significantly enhanced tissue penetration of Abraxane® (slightly negatively charged; section 5.3.2) in peritoneal tissue [52]. In the present thesis the possibility of changing the electric charge (positive vs. negative) of NP to increase tissue uptake was investigated. Additionally, the efficacy of ePIPAC vs. PIPAC for delivering the two types of NP was evaluated. Overall, this study showed that the combination of positively charged NP and the electrostatic precipitation increases the depth of tissue penetration of CUR-loaded PLGA NP, and thus, the results are consistent with the current literature [52, 308].

In the context of tissue penetration depth in ePIPAC, using positively charged CUR-loaded CS-PLGA NP doubled depths compared to negatively charged NP were achieved, reaching values of around 200 µm. The observed penetration pattern can be explained by the interaction of differently charged particles with the tissue. Without the application of electrostatic forces, the tissue is slightly negatively charged due to hydroxy groups of glycoproteins on the cellular surface and can therefore absorb positively charged particles more effectively than negatively charged particles. Sadzuka *et al.* reported similar effects in intraperitoneal administration of differently charged liposomes [310]. Using ePIPAC, the peritoneal tissue is slightly positively charged. The use of the brush electrode should not affect negatively charged particles, whereas positively charged particles presumably aim a stronger attraction to the tissue due to the transfer of a highly negative charge, and consequently reach deeper penetration. Nevertheless, both particle systems and application methods resulted in therapeutically relevant penetration depths of 100 - 200 µm to overcome peritoneal tissue (thickness of approx. 100 µm), and thus, to reach the hypervascularized invasion front of peritoneal metastasis [110, 311]. Comparing ePIPAC of positively charged NP with intraperitoneal liquid delivery, a multiple deeper tissue penetration is reached with ePIPAC. For example, doxorubicin permeates only 4 - 6 cell layers, which corresponds to a depth of 20 - 30 µm [312]. In addition, longer retention times of positively charged nanoparticulate delivery systems compared to negatively charged ones are reported in literature, thus, favorably contributing to the results of the present thesis [313]. Consequently, these findings might improve future therapy of peritoneal metastasis.

6.4 Conclusion

The nebulization and penetration trials of the present study confirmed both stability and sprayability of PLGA NP. Since the sprayability of the tested polymeric NP depends on their concentration, the future determination of PTX dosage will reveal whether the sprayable concentrations are sufficient. The use of disposable pens may possibly lead to an increase in concentration with regard to sprayability. Further spraying trials with PTX-loaded modified formulations should be performed. Here, the safety aspect of the aerosolization of formulations containing cytostatic drugs should,

however, require appropriate facilities. Nevertheless, initially successful spraying experiments provide a promising base for future nanoparticulate formulations.

Since the enhanced depth of tissue penetration of positively charged NP delivered by ePIPAC might be clinically relevant, further investigation will be required for the evaluation of the clinical significance. Nevertheless, it could be contemporarily evidently proven that IP drug delivery can be improved by combining application devices, formulation of the active ingredient, and control of the peritoneal environment.

7. Conclusion and outlook

The present work deals with the formulation development of a nanoparticulate drug delivery system for intraperitoneal application in the context of PIPAC in peritoneal malignancies. The main objective was to prolong the local duration of action of the cytostatic drug in tumor tissue to provide a more effective and efficient treatment option for cancer patients. First, PTX-loaded polymeric NP based on different polymers (PLGA, EC 4) and polymer compositions (CS-PLGA, CS-EC 4) were successfully prepared and coated with BSA and PEC in the case of CS-PLGA NP. The developed types of NP ranged in the size of 200 - 300 nm, which presumably allow cellular uptake to occur mainly via the macropinocytotic pathway (200 - 500 nm) and preferably bypass phagocytotic processes (> 500 nm). In addition, NP that did not penetrate the tissue after PIPAC application, and consequently reside in the peritoneal cavity, might be taken up by the lymphatic route (via LS) and reach well-vascularized tumor regions through the EPR effect.

Among all prepared formulations, CS-PLGA NP, which exhibited positive surface charges, showed the most promising data. The additive of CS resulted in improved DL and EE, as well as prolonged release of PTX. Moreover, the highest penetration depths were obtained with positively charged NP in combination with ePIPAC in the eIBUB model. These findings further favor the increased speed and extent of cellular particle uptake of positively charged NP. By surface coating with PEC, a further delay of PTX release could be achieved. However, this effect is substantially attenuated in physiological fluids (e.g., peritoneal fluid), which contain divalent cations such as Ca^{2+}, and thus, PEC coating does not provide the aimed benefit in pharmacokinetics. Nevertheless, hydrophilic, gelled PEC coatings might reduce the release of lipophilic active ingredients outside of divalent cationic fluid, e.g., during storage in liquid or after redispersion of NP before application and might improve stability of NP due to high negative repulsion. Further investigations based on this approach may reveal attractive potential for future development of NP formulations. Depending on the polymer and the selected manufacturing parameters, different loading rates were obtained, clearly indicating advantageous values for EC 4 NP. In addition, EC 4 NP demonstrated to be non-toxic regarding cell viability of HeLa cells. However, due to worse sprayability and increased PTX release rates at higher DL and lower particle quantities (constant dosage) of EC 4 NP, these particles are less suitable for this purpose. Different release setups were evaluated, and suitable release conditions were elaborated with respect to sink conditions and PTX stability. It has been demonstrated that an acidic pH is beneficial for the stability of PTX, and thus, the cytotoxic effect of PTX is expected particularly in poorly supplied, acidic tumor regions and after lysosomal uptake. Further investigations to determine an approximate *in vitro-in vivo* correlation should be pursued.

Due to the lack of manufacturing methods regarding large-scale production of polymeric NP, an evaporation-triggered NPr method was successfully developed. This offers the potential to produce PLGA NP in a larger size range compared to the common laboratory scale batch NPr. Additionally, SDS allows production of highly concentrated PLGA NP dispersions. The loading properties of the investigated (model) drugs CUR and PTX were markedly improved at comparable particle

sizes. By continuous administration of the pre-mixed polymer-drug solution and removal of the resulting NP dispersion, large-scale production of PLGA NP might be possible without suffering from batch-to-batch variations of laboratory manufacturing methods in the future. For this purpose, however, further research is required for introducing a non-volume-limited pump system and a rotating disc adapted to a polymer concentration, which maximizes yields even at high particle concentrations. In addition, CS-PLGA composition should be investigated in SDS to extend the previously described beneficial findings of continuous NP production.

Investigations on the existing approved PTX-loaded polymeric formulation Abraxane® confirmed and extended properties found in the literature. Due to the low particle stability and thus, fast disintegration, a "rapid release" occurs directly after transfer into the release medium. Accordingly, Abraxane® is unsuitable for the desired purpose of sustained release of PTX and prolonged cytostatic effects in tumor tissue.

At the beginning of the studies, it was uncertain whether NP could be aerosolized at all with medical devices used for drug application in PIPAC. The experiments revealed that PLGA and EC 4 NP can be successfully sprayed using the Capnopen®-angioinjector-system. However, since no therapeutic dosages of PTX and PTX-loaded nanoparticulate drug delivery systems are known and aerosolization of the investigated NP is concentration-dependent, the sprayability of required NP amounts in still uncertain. Concerning the currently used Capnopen®, which was originally developed as a medical product for the nebulization of liquids, a modification, for example an enlargement of the nozzle opening, for the application of nanoparticulate systems might enable the sprayability of higher concentrations or larger particles. Despite the sufficiently deep penetration of the tested NP formulations in the eIBUB model, results need to be verified *in vivo* (animal/human) and with PTX-loaded NP to obtain clinical relevance in the future. Moreover, a comparison between the approved solvent-based and NP-based PTX containing drugs (Taxol®, Abraxane®, and generics) should be considered to estimate penetration performance of the developed NP.

The formulations developed in this thesis and the promising results presented regarding a prolonged duration of action of the cytostatic drug in the target tissue encourage further research towards a commercially marketable, clinically significant product. Thus, the innovative combination of NP and PIPAC or ePIPAC, so called “nanoPIPAC”, might further improve therapy of patients with peritoneal malignancies and increase their outcome in terms of quality of life and overall survival.

8. Materials and devices

8.1 Chemicals

Table 8.1: Chemicals

Substance	Comment	Supplier	Chapter
3-(4, 5-dimethythiazol-2-yl)-2, 5-diphenyl tetrazolium bromide	MTT reagent	Sigma-Aldrich Laborchemikalien GmbH, Seelze, Germany	2
Abraxane®	provided by UKT	Celgene Corporation, Summit, USA	5
ACE	analytical reagent grade	Fisher Scientific UK Ltd, Loughborough, UK	2, 3
Acetic acid	ACS reagent, ± 99.7 %	Sigma-Aldrich Chemie GmbH, Steinheim, Germany	4, 5
ACN	HPLC gradient grade	Fisher Scientific UK Ltd, Loughborough, UK	2, 3, 4, 5
APF	Physioneal 40 Glc 2.27% (w/v)	Baxter, Unterschleißheim, Germany	4
BSA & FITC-BSA		Sigma-Aldrich Chemie GmbH, Steinheim, Germany	2, 4
Calcium chloride dihydrate		Arcos organics, New Jersey, USA	2, 4
CS	Chitoscience chitosan-HCl	Heppe Medical Chitosan GmbH, Halle, Germany	2, 4
CUR		Sigma Aldrich, Steinheim, Germany	2, 3
D-Glucose anhydrous		Fisher Scientific UK Ltd, Loughborough, UK	2, 4
EC	Ethocel™ Standard Premium type 4 and 10	Colorcon GmbH, Kent, Idstein, Germany	2, 4
Embedding medium	Tissue-Tek® O.C.T™ Compound	Sakura Finetek Germany GmbH, Staufen, Germany	6
EtOH	HPLC grade	Fisher Scientific UK Ltd, Loughborough, UK	2, 3
Fixing agent	Thermo Scientific™ Richard-Allan Scientific™ Cytoseal™ XYL	Fisher Scientific GmbH, Schwerte, Germany	6
Formaldehyde	ACS reagent, ± 36.5 %	Sigma-Aldrich Chemie GmbH, Steinheim, Germany	2, 4
HBSS buffer		Sigma-Aldrich Laborchemikalien GmbH, Seelze, Germany	2

Substance	Comment	Supplier	Chapter
iPrOH	HPLC grade	VWR International, Darmstadt, Germany	3
Magnesium chloride hexahydrate		VWR International, Darmstadt, Germany	4
MeOH	HPLC grade	VWR International, Darmstadt, Germany	3
MilliQ® water	Millipore Q-Grad 2	Merck Millipore, Billerica, USA	1 - 6
PEC	GENU® pectin type LM-5 CS	CP Kelco Germany GmbH, Großenbrode, Germany	2, 4
PLGA	Resomers® RG 502H, 503H, 504H, 653H, 753H	Evonik Industries AG, Essen, Germany	2, 3, 4
PS 80		Caesar & Loretz GmbH, Hilden, Germany	4, 5
PTX	semi-synthetic; provided by Capnomed GmbH	Hefei TNJ Chemical Industry Co.,Ltd., Hefei City, China	2, 3, 4
PVA	Mowiol® 4-88	Kuraray Europe, Hattersheim, Germany	2, 3, 4
SLS		Carl Roth GmbH + Co. KG, Karlsruhe, Germany	4
Sodium bicarbonate	CELLPURE®, $\pm$ 99.5 %	Carl Roth GmbH + Co. KG, Karlsruhe, Germany	4
Sodium chloride		Carl Roth GmbH + Co. KG, Karlsruhe, Germany	4
Sodium chloride solution	sterile, 0.9 % (w/v)	B. Braun Melsungen AG, Melsungen, Germany	5
Sodium lactate		Sigma-Aldrich, Steinheim, Germany	4
THF	analytical grade	Fisher Scientific UK Ltd, Loughborough, UK	2, 3
Triton X-100 2 %		Sigma-Aldrich Laborchemikalien GmbH, Seelze, Germany	2
Water for the purpose of injection (WFI)	Ampuwa®	Fresenius KABI Deutschland GmbH, Bad Homburg, Germany	6.2.2

8.2 Cell culture and *ex vivo* material

Table 8.2: Cell culture and *ex vivo* material

Material	Comment	Supplier	Chapter
Acites fluids	Human source	UKT, Prof. Marc Reymond	4
Bovine urinary bladders	Animals used in food chain	Slaughterhouse	6
Cell culture medium	DMEM, high glucose	Thermo Fisher Scientific GmbH, Dreieich, Germany	2
Fetal bovine serum	Gibco® Qualified FBS	Thermo Fisher Scientific GmbH, Dreieich, Germany	2
HeLa cells	ATCC® CCL-2	LGC Standards GmbH, Wesel, Germany	2
PenStrep	Gibco™ Penicillin-Streptomycin (10,000 U/ml)	Fisher Scientific GmbH, Schwerte, Germany	2

8.3 Equipment

Table 8.3: Equipment

Devices	Type / Comment	Company	Chapter
Brush electrode	Ionwand®	Alesi Surgical, Cardiff, UK	6
Carbon disk		Plano, Wetzlar, Germany	2, 3
Cetrifuges	Heraeus Multifuge X1R	Thermo Fisher Scientific GmbH, Osterode am Harz, Germany	2
	3-30 KS	Sigma Laborzentrifugen GmbH, Osterode am Harz, Germany	2, 3
CLSM	LSM710	Carl Zeiss AG, Oberkochen, Germany	2
Compact bead mill	TissueLyser LT	QIAGEN N.V., Hilden, Germany	6
Compressed air gun	LBP-1/4	Festo Vertrieb GmbH & Co. KG, Esslingen, Germany	5
Computer fan	12x12 cm	AVC, Taipei, Taiwan	3
Cryostat	Leica CM3050S	Leica Mikrosysteme Vertrieb GmbH, Wetzlar, Germany	6
Fluorescence microscope	AX10	Carl Zeiss AG, Oberkochen, Germany	2
	Type unknown (UKT)	Leica Mikrosysteme Vertrieb GmbH, Wetzlar, Germany	6

Devices	Type / Comment	Company	Chapter
Freeze-dryer	Alpha 2-4 LSC / Alpha 3-4 LSCbasic	Martin Christ Gefriertrocknungsanlagen GmbH, Osterode am Harz, Germany	2, 3
Generator	Ultravision®	Alesi Surgical Cardiff, UK	6
High-pressure angioinjectors	Accutron HP-D, Accutron CT	Medtron AG, Saarbrücken, Germany	6
HPLC column	LiChrospher® 100 RP-18 (5 µm) LiChroCART® 125-4	Merck KGaA, Darmstadt, Germany	2, 3
HPLC system	UltiMate 3000	Dionex Corporation, Sunnyvale, USA	2, 3
Incubation shaker	3031	GFL Gesellschaft für Labortechnik mgH, Burgwedel, Germany	4
Laboratory power supply unit	EA-PS 2323A	EA Elektro-Automatik GmbH & Co.KG, Viersen, Germany	3
Laminar flow bench	ENVAIReco® safe basic plus	ENVAIR Deutschland GmbH, Emmendingen, Germany	2, 3
Micro-Ubbelohde viscosimeter	0.01 K, calibrated, 0.4-6 mm^2/s	SI Analytics GmbH, Mainz, Germany	5
Nebulizer	CapnoPen®	Capnomed, Zimmern ob Rottweil, Germany	6
Osmometer	Osmomat 010	Gonotec GmbH, Berlin, Germany	5
Petri dishes	Steriplan: 15 x 100 mm, 15 x 80 mm	Brand GmbH Co KG, Wertheim, Germany	3
pH meter	SevenCompact pH S210 / EL 20	Mettler-Toledo GmbH, Schwerzenbach, Switzerland	2, 5
Pin stubs		Plano, Wetzlar, Germany	2, 3
Plate reader	Infinite M200	Tecan Trading AG, Männedorf, Switzerland	2, 3
Rotary-pumped sputter coater	Q150R	Quorum Technologies Ltd., Lewes, UK	2, 3
SEM (HIPS)	EVO HD15 / EVO 15	Carl Zeiss AG, Oberkochen, Germany	2, 3, 5
SEM (INM)	Quanta FEG 400	FEI Deutschland GmbH, Dreieich, Germany	2, 3
Silica wafer		Plano, Wetzlar, Germany	2, 3
Syringe Pumpe	PHD 2000 programmable	Harvard Apparatus Inc., Holliston, USA	2, 3
Tachometer	Voltcraft® DT-10L	Conrad Electronic AG, Wollerau, Switzerland	3

Devices	Type / Comment	Company	Chapter
Ultrasonic homogenizer	Generator: Sonoplus mini20, Converter: UW3100, Probe: MS73	Bandelin electronic GmbH & Co. KG, Berlin, Germany	2
Ultrasound bath	Elmasonic P	Elma Schmidbauer GmbH, Singen, Germany	2
UV/Vis spectrometer	Lambda 35	PerkinElmer LAS (Germany) GmbH, Rodgau, Germany	2
Vacuum concentrator	BA-VC-300H	H. Saur Laborbedarf, Reutlingen, Germany	6
Zetasizer®	Nano ZS/ Ultra	Malvern Panalytical GmbH, Malvern, UK, and Almelo, the Netherlands	2, 3

8.4 Consumables

Table 8.4: Consumables

Consumables	Comment	Supplier	Chapter
Angioinjector capsules	ELS 200 ml syringe, QFT	Medtron AG, Saarbrücken, Germany	6
Bead tubes	PowerBead Tubes, Metal 2.38 mm	Qiagen N.V., Hilden, Germany	6
Cannulas	Sterican® Gr. 17, G 24 x 1""/ 0,55 x 25 mm	B. Braun Melsungen AG, Melsungen, Germany	2, 3
Dialysis tubings	Fisherbrand® regenerated cellulose, MWCO 12-14k, 45 mm flat width	Fisher Scientific GmbH, Schwerte, Germany	4
Disposable biopsy punchs	BP-80F, 8 mm	kai Europe GmbH, Solingen, Germany	6
Disposable folded capillary cells	DTS 1070	Malvern Panalytical GmbH, Malvern, UK, and Almelo, the Netherlands	2, 3
Double-balloon trocars	Kii®, 12 mm	Applied Medial, Düsseldorf, Germany	6
Membrane filters	Target 2 (0.2 µm), Titan 3 (0.45 µm); regenerated cellulose	Thermo Fisher Scientific GmbH, Dreieich, Germany	2, 3, 4
Syringes	Injekt®; 1-20 ml	B. Braun Melsungen AG, Melsungen, Germany	2, 3, 4

Bibliography

[1] L. A. Lambert. Looking up: Recent advances in understanding and treating peritoneal carcinomatosis. *CA: A Cancer Journal for Clinicians*, 65(4):283–298, 2015.

[2] J. S. Spratt, R. A. Adcock, M. Muskovin, W. Sherrill, and J. McKeown. Clinical delivery system for intraperitoneal hyperthermic chemotherapy. *Cancer Research*, 40(2):256, 1980.

[3] P. H. Sugarbaker. Peritonectomy procedures. *Annals of surgery*, 221(1):29–42, 1995.

[4] W. Solass, R. Kerb, T. Murdter, U. Giger-Pabst, D. Strumberg, C. Tempfer, J. Zieren, M. Schwab, and M. A. Reymond. Intraperitoneal chemotherapy of peritoneal carcinomatosis using pressurized aerosol as an alternative to liquid solution: first evidence for efficacy. *Ann Surg Oncol*, 21(2):553–559, 2014.

[5] M. Nowacki, M. Peterson, T. Kloskowski, E. McCabe, D. C. Guiral, K. Polom, K. Pietkun, B. Zegarska, M. Pokrywczynska, T. Drewa, F. Roviello, E. A. Medina, S. L. Habib, and W. Zegarski. Nanoparticle as a novel tool in hyperthermic intraperitoneal and pressurized intraperitoneal aerosol chemotheprapy to treat patients with peritoneal carcinomatosis. *Oncotarget*, 8(44):78208–78224, 2017.

[6] E. Van Vugt, E. A. Van Rijthoven, E. W. Kamperdijk, and R. H. Beelen. Omental milky spots in the local immune response in the peritoneal cavity of rats. *Anat Rec*, 244(2):235–245, 1996.

[7] P. Sandoval, J. A. Jimenez-Heffernan, A. Rynne-Vidal, M. L. Perez-Lozano, A. Gilsanz, V. Ruiz-Carpio, R. Reyes, J. Garcia-Bordas, K. Stamatakis, J. Dotor, P. L. Majano, M. Fresno, C. Cabanas, and M. Lopez-Cabrera. Carcinoma-associated fibroblasts derive from mesothelial cells via mesothelial-to-mesenchymal transition in peritoneal metastasis. *J Pathol*, 231(4):517–531, 2013.

[8] L. März, R. Hofheinz, and P. Piso. Peritonealkarzinose bei gastrointestinalen malignomen. *Der Onkologe*, 22:351–362, 2016.

[9] International Agency for Research on Cancer (WHO). Cancer today, 2020. https://gco.iarc.fr/today/home, visited 2021-01-21.

[10] D. Z. J. Chu, N. P. Lang, C. Thompson, P. K. Osteen, and K. C. Westbrook. Peritioneal carcinomatosis in nongynecologic malignancy. a prospective study of prognostic factors. *Cancer*, 63(2):364–367, 1989.

[11] I. Königsrainer, S. Beckert, T. Lehmann, R. Ladurner, B. Brücher, and A. Königsrainer. Peritonealkarzinose. *Der Chirurg*, 82(4):375, 2011.

[12] H. Leebmann and P. Piso. [pipac and hipec-competing or supplementary therapeutic procedures for peritoneal metastases]. *Chirurg*, 89(9):693–698, 2018.

[13] E. P. Armour, D. McEachern, Z. Wang, P. M. Corry, and A. Martinez. Sensitivity of human cells to mild hyperthermia. *Cancer Research*, 53(12):2740, 1993.

[14] S. González-Moreno, L. A. González-Bayón, and G. Ortega-Pérez. Hyperthermic intraperitoneal chemotherapy: Rationale and technique. *World journal of gastrointestinal oncology*, 2(2):68–75, 2010.

[15] P. H. Sugarbaker. Laboratory and clinical basis for hyperthermia as a component of intracavitary chemotherapy. *International Journal of Hyperthermia*, 23(5):431–442, 2007.

[16] L.e Lemoine, P. Sugarbaker, and K. Van der Speeten. Drugs, doses, and durations of intraperitoneal chemotherapy: standardising hipec and epic for colorectal, appendiceal, gastric, ovarian peritoneal surface malignancies and peritoneal mesothelioma. *International Journal of Hyperthermia*, 33(5):582–592, 2017.

[17] M. Deraco, D. Baratti, S. Kusamura, B. Laterza, and M. R. Balestra. Surgical technique of parietal and visceral peritonectomy for peritoneal surface malignancies. *Journal of Surgical Oncology*, 100(4):321–328, 2009.

[18] P. Piso, H. Leebmann, L. März, and M. Mayr. Zytoreduktive chirurgie für maligne tumoren des peritoneums. *Der Chirurg*, 86(1):38–46, 2015.

[19] B. Rau, P. Piso, and A. Königsrainer. *Peritoneale Tumoren und Metastasen*. Springer-Verlag GmbH Deutschland, 2018. ISBN 978-3-662-54499-0.

[20] P. Jacquet and P. H. Sugarbaker. Clinical research methodologies in diagnosis and staging of patients with peritoneal carcinomatosis. *Cancer Treat Res*, 82:359–374, 1996.

[21] German Guideline Program in Oncology (AMWF). *S3-Guideline Colorectal Cancer*. AWMF, 2019.

[22] D. Elias, A. Mariani, A. S. Cloutier, F. Blot, D. Goéré, F. Dumont, C. Honoré, V. Billard, P. Dartigues, and M. Ducreux. Modified selection criteria for complete cytoreductive surgery plus hipec based on peritoneal cancer index and small bowel involvement for peritoneal carcinomatosis of colorectal origin. *Eur J Surg Oncol*, 40(11):1467–73, 2014.

[23] German Guideline Program in Oncology (AMWF). *S3-Leitlinie Magenkarzinom*. AWMF, 2019.

[24] German Guideline Program in Oncology (AMWF). *S3-Leitlinie Diagnostik, Therapie und Nachsorge maligner Ovarialtumoren*. AWMF, 2020.

[25] J. Esquivel, P. Piso, V. Verwaal, T. Bachleitner-Hofmann, O. Glehen, S. González-Moreno, M. Deraco, J. Pelz, R. Alexander, and G. Glockzin. American society of peritoneal surface malignancies opinion statement on defining expectations from cytoreductive surgery and hyperthermic intraperitoneal chemotherapy in patients with colorectal cancer. *Journal of Surgical Oncology*, 110(7):777–778, 2014.

[26] O. Glehen, F. N. Gilly, F. Boutitie, J. M. Bereder, F. Quenet, L. Sideris, B. Mansvelt, G. Lorimier, S. Msika, and D. Elias. Toward curative treatment of peritoneal carcinomatosis from nonovarian origin by cytoreductive surgery combined with perioperative intraperitoneal chemotherapy: a multi-institutional study of 1,290 patients. *Cancer*, 116(24): 5608–5618, 2010.

[27] P. H. Sugarbaker. New standard of care for appendiceal epithelial neoplasms and pseudomyxoma peritonei syndrome? *The Lancet Oncology*, 7(1):69–76, 2006.

[28] B. Furlow. No os benefit from hipec in colorectal cancer. *ASCO Annual Meeting: Colorectal Cancer*, 2018.

[29] I. Vergote, P. Harter, and L. Chiva. Hyperthermic intraperitoneal chemotherapy does not improve survival in advanced ovarian cancer. *Cancer*, 125(S24):4594–4597, 2019.

[30] B. Brücher and A. Königsrainer. Die peritonealkarzinose. *Chirurgische Allgemeine Zeitung*, 11:17–31, 2010.

[31] M. A. Reymond, W. Solass, G. Nadiradze, P. Horvath, and A. Königsrainer. *Pressurized Intraperitoneal Aerosol Chemotherapy (PIPAC)*, pages 235–243. Springer International Publishing, Cham, 2020. ISBN 978-3-030-28891-4.

[32] R. L. Dedrick and M. F. Flessner. Pharmacokinetic problems in peritoneal drug administration: Tissue penetration and surface exposure. *JNCI: Journal of the National Cancer Institute*, 89(7):480–487, 1997.

[33] W. Solass, A. Herbette, T. Schwarz, A. Hetzel, J. S. Sun, M. Dutreix, and M. A. Reymond. Therapeutic approach of human peritoneal carcinomatosis with dbait in combination with capnoperitoneum: proof of concept. *Surg Endosc*, 26(3):847–852, 2012.

[34] W. Solass, A. Hetzel, G. Nadiradze, E. Sagynaliev, and M. A. Reymond. Description of a novel approach for intraperitoneal drug delivery and the related device. *Surg Endosc*, 26 (7):1849–1855, 2012.

[35] A. Blanco, U. Giger-Pabst, W. Solass, J. Zieren, and M. A. Reymond. Renal and hepatic toxicities after pressurized intraperitoneal aerosol chemotherapy (pipac). *Ann Surg Oncol*, 20(7):2311–2316, 2013.

[36] H. Teixeira Farinha, F. Grass, A. Kefleyesus, C. Achtari, B. Romain, M. Montemurro, N. Demartines, and M. Hubner. Impact of pressurized intraperitoneal aerosol chemotherapy on quality of life and symptoms in patients with peritoneal carcinomatosis: A retrospective cohort study. *Gastroenterol Res Pract*, 2017:4596176, 2017.

[37] V. Khomyakov, A. Ryabov, A. Ivanov, L. Bolotina, A. Utkina, N. Volchenko, and A. Kaprin. Bidirectional chemotherapy in gastric cancer with peritoneal metastasis combining intravenous xelox with intraperitoneal chemotherapy with low-dose cisplatin and doxorubicin

administered as a pressurized aerosol: an open-label, phase-2 study (pipac-ga2). *Pleura Peritoneum*, 1(3):159–166, 2016.

[38] F. Struller, P. Horvath, W. Solass, F. J. Weinreich, D. Strumberg, M. K. Kokkalis, I. Fischer, C. Meisner, A. Konigsrainer, and M. A. Reymond. Pressurized intraperitoneal aerosol chemotherapy with low-dose cisplatin and doxorubicin (pipac c/d) in patients with gastric cancer and peritoneal metastasis: a phase ii study. *Ther Adv Med Oncol*, 11: 1758835919846402, 2019.

[39] C. B. Tempfer, U. Giger-Pabst, V. Seebacher, M. Petersen, A. Dogan, and G. A. Rezniczek. A phase i, single-arm, open-label, dose escalation study of intraperitoneal cisplatin and doxorubicin in patients with recurrent ovarian cancer and peritoneal carcinomatosis. *Gynecol Oncol*, 150(1):23–30, 2018.

[40] C. B. Tempfer, G. Winnekendonk, W. Solass, R. Horvat, U. Giger-Pabst, J. Zieren, G. A. Rezniczek, and M. A. Reymond. Pressurized intraperitoneal aerosol chemotherapy in women with recurrent ovarian cancer: A phase 2 study. *Gynecol Oncol*, 137(2):223–228, 2015.

[41] N. Bakrin, C. Tempfer, G. Scambia, M. De Simone, B. Gabriel, E. M. Grischke, and B. Rau. Pipac-ov3: A multicenter, open-label, randomized, two-arm phase iii trial of the effect on progression-free survival of cisplatin and doxorubicin as pressurized intra-peritoneal aerosol chemotherapy (pipac) vs. chemotherapy alone in patients with platinum-resistant recurrent epithelial ovarian, fallopian tube or primary peritoneal cancer. *Pleura Peritoneum*, 3(3):20180114, 2018.

[42] T. Oliver Goetze, S.-E. Al-Batran, U. Pabst, M. Reymond, C. Tempfer, W. O. Bechstein, U. Bankstahl, I. Gockel, A. Königsrainer, T. Kraus, S. P. Mönig, B. Rau, M. Schwarzbach, and P. Piso. Pressurized intraperitoneal aerosol chemotherapy (pipac) in combination with standard of care chemotherapy in primarily untreated chemo naïve upper gi-adenocarcinomas with peritoneal seeding – a phase ii/iii trial of the aio/caogi/aco. *Pleura and Peritoneum*, 3(2):20180113, 2018.

[43] C. Demtroder, W. Solass, J. Zieren, D. Strumberg, U. Giger-Pabst, and M. A. Reymond. Pressurized intraperitoneal aerosol chemotherapy with oxaliplatin in colorectal peritoneal metastasis. *Colorectal Dis*, 18(4):364–371, 2016.

[44] M. Graversen, S. Detlefsen, J. K. Bjerregaard, P. Pfeiffer, and M. B. Mortensen. Peritoneal metastasis from pancreatic cancer treated with pressurized intraperitoneal aerosol chemotherapy (pipac). *Clin Exp Metastasis*, 34(5):309–314, 2017.

[45] G. Nadiradze, U. Giger-Pabst, J. Zieren, D. Strumberg, W. Solass, and M. A. Reymond. Pressurized intraperitoneal aerosol chemotherapy (pipac) with low-dose cisplatin and doxorubicin in gastric peritoneal metastasis. *J Gastrointest Surg*, 20(2):367–73, 2016.

[46] C. B. Tempfer, G. A. Rezniczek, P. Ende, W. Solass, and M. A. Reymond. Pressurized intraperitoneal aerosol chemotherapy with cisplatin and doxorubicin in women with peritoneal carcinomatosis: A cohort study. *Anticancer Res*, 35(12):6723–6729, 2015.

[47] M. Alyami, F. Mercier, M. Siebert, P. E. Bonnot, N. Laplace, L. Villeneuve, G. Passot, O. Glehen, N. Bakrin, and V. Kepenekian. Unresectable peritoneal metastasis treated by pressurized intraperitoneal aerosol chemotherapy (pipac) leading to cytoreductive surgery and hyperthermic intraperitoneal chemotherapy. *Eur J Surg Oncol*, 47(1):128–133, 2021.

[48] M. Alyami, P. E. Bonnot, L. Villeneuve, N. Bakrin, and O. Glehen. Pressurized intraperitoneal aerosol chemotherapy (pipac) for nonresectable peritoneal carcinomatosis from gastric cancer. *Journal of Clinical Oncology*, 36:149–149, 2018.

[49] R. Girshally, C. Demtroder, N. Albayrak, J. Zieren, C. Tempfer, and M. A. Reymond. Pressurized intraperitoneal aerosol chemotherapy (pipac) as a neoadjuvant therapy before cytoreductive surgery and hyperthermic intraperitoneal chemotherapy. *World J Surg Oncol*, 14(1):253, 2016.

[50] S. J. Tate and J. Torkington. Pressurized intraperitoneal aerosol chemotherapy: a review of the introduction of a new surgical technology using the ideal framework. *BJS Open*, 4(2): 206–215, 2020.

[51] W.P. Ceelen and E. Levine. *Intraperitoneal Cancer Therapy: Principles and Practice*. CRC Press, 2015. ISBN 9781482261196.

[52] L. Van de Sande, M. Rahimi-Gorji, S. Giordano, E. Davoli, C. Matteo, S. Detlefsen, K. D'Herde, H. Braet, M. Shariati, K. Remaut, F. Xie, C. Debbaut, G. Ghorbaniasl, S. Cosyns, W. Willaert, and W. Ceelen. Electrostatic intraperitoneal aerosol delivery of nanoparticles: Proof of concept and preclinical validation. *Advanced Healthcare Materials*, 9(16):2000655, 2020.

[53] T. Kakchekeeva, C. Demtroder, N. I. Herath, D. Griffiths, J. Torkington, W. Solass, M. Dutreix, and M. A. Reymond. In vivo feasibility of electrostatic precipitation as an adjunct to pressurized intraperitoneal aerosol chemotherapy (epipac). *Ann Surg Oncol*, 23: 592–598, 2016.

[54] M. Reymond, C. Demtroeder, W. Solass, G. Winnekendonk, and C. Tempfer. Electrostatic precipitation pressurized intraperitoneal aerosol chemotherapy (epipac): first in-human application. *Pleura and Peritoneum*, 1(2):109–116, 2016.

[55] A. Taibi, H. Teixeira Farinha, S. Durand Fontanier, Z. Sayedalamin, M. Hubner, and O. Sgarbura. Pressurized intraperitoneal aerosol chemotherapy enhanced by electrostatic precipitation (epipac) for patients with peritoneal metastases. *Ann Surg Oncol*, 28: 3852–3860, 2020.

[56] W. Willaert, L. Van de Sande, E. Van Daele, D. Van De Putte, Y. Van Nieuwenhove, P. Pattyn, and W. Ceelen. Safety and preliminary efficacy of electrostatic precipitation during

pressurized intraperitoneal aerosol chemotherapy (pipac) for unresectable carcinomatosis. *Eur J Surg Oncol*, 45(12):2302–2309, 2019.

[57] O. Trédan, C. M. Galmarini, K. Patel, and I. F. Tannock. Drug resistance and the solid tumor microenvironment. *J Natl Cancer Inst*, 99(19):1441–1454, 2007.

[58] R. B. Wilson. Hypoxia, cytokines and stromal recruitment: parallels between pathophysiology of encapsulating peritoneal sclerosis, endometriosis and peritoneal metastasis. *Pleura and Peritoneum*, 3(1), 2018.

[59] S. Aznavoorian, M. L. Stracke, H. Krutzsch, E. Schiffmann, and L. A. Liotta. Signal transduction for chemotaxis and haptotaxis by matrix molecules in tumor cells. *J Cell Biol*, 110 (4):1427–1438, 1990.

[60] A. J. Leu, D. A. Berk, A. Lymboussaki, K. Alitalo, and R. K. Jain. Absence of functional lymphatics within a murine sarcoma: a molecular and functional evaluation. *Cancer Res*, 60(16):4324–4327, 2000.

[61] J. A. Nagy, D. Feng, E. Vasile, W. H. Wong, S.-C. Shih, A. M. Dvorak, and H. F. Dvorak. Permeability properties of tumor surrogate blood vessels induced by vegf-a. *Laboratory Investigation*, 86(8):767–780, 2006.

[62] R. K. Jain. Determinants of tumor blood flow: a review. *Cancer Res*, 48(10):2641–2658, 1988.

[63] P. Vaupel. Tumor microenvironmental physiology and its implications for radiation oncology. *Seminars in Radiation Oncology*, 14(3):198–206, 2004.

[64] C. V. Dang and G. L. Semenza. Oncogenic alterations of metabolism. *Trends in Biochemical Sciences*, 24(2):68–72, 1999.

[65] A. S. E. Ljungkvist, J. Bussink, P. F. J. W. Rijken, J. H. A. M. Kaanders, A. J. van der Kogel, and J. Denekamp. Vascular architecture, hypoxia, and proliferation in first-generation xenografts of human head-and-neck squamous cell carcinomas. *International Journal of Radiation Oncology*Biology*Physics*, 54(1):215–228, 2002.

[66] M. Janiszewska, M. C. Primi, and T. Izard. Cell adhesion in cancer: Beyond the migration of single cells. *The Journal of biological chemistry*, 295(8):2495–2505, 2020.

[67] C. H. Heldin, K. Rubin, K. Pietras, and A. Ostman. High interstitial fluid pressure - an obstacle in cancer therapy. *Nat Rev Cancer*, 4(10):806–813, 2004.

[68] T. Stylianopoulos. Epr-effect: utilizing size-dependent nanoparticle delivery to solid tumors. *Therapeutic Delivery*, 4(4):421–423, 2013.

[69] E. Blanco, H. Shen, and M. Ferrari. Principles of nanoparticle design for overcoming biological barriers to drug delivery. *Nature biotechnology*, 33(9):941–951, 2015.

[70] X. F. Li, S. Carlin, M. Urano, J. Russell, C. C. Ling, and J. A. O'Donoghue. Visualization of hypoxia in microscopic tumors by immunofluorescent microscopy. *Cancer Res*, 67(16): 7646–7653, 2007.

[71] R. K. Jain. Barriers to drug delivery in solid tumors. *Scientific American*, 271(1):58–65, 1994.

[72] P. Esquis, D. Consolo, G. Magnin, P. Pointaire, P. Moretto, M. D. Ynsa, J.-L. Beltramo, C. Drogoul, M. Simonet, L. Benoit, P. Rat, and B. Chauffert. High intra-abdominal pressure enhances the penetration and antitumor effect of intraperitoneal cisplatin on experimental peritoneal carcinomatosis. *Annals of Surgery*, 244(1):106–112, 2006.

[73] G. Griffon-Etienne, Y. Boucher, C. Brekken, H. D. Suit, and R. K. Jain. Taxane-induced apoptosis decompresses blood vessels and lowers interstitial fluid pressure in solid tumors: clinical implications. *Cancer Res*, 59(15):3776–3782, 1999.

[74] S. H. Jang, M. G. Wientjes, and J. L. Au. Enhancement of paclitaxel delivery to solid tumors by apoptosis-inducing pretreatment: effect of treatment schedule. *J Pharmacol Exp Ther*, 296(3):1035–1042, 2001.

[75] P. Kristjansen, Y. Boucher, and R. Jain. Dexamethasone reduces the interstitial fluid pressure in a human colon adenocarcinoma xenograft. *Cancer research*, 53:4764–4766, 1993.

[76] M. A. Islam, S. Barua, and D. Barua. A multiscale modeling study of particle size effects on the tissue penetration efficacy of drug-delivery nanoparticles. *BMC Systems Biology*, 11 (1):113, 2017.

[77] L. Tang, N. P. Gabrielson, F. M. Uckun, T. M. Fan, and J. Cheng. Size-dependent tumor penetration and in vivo efficacy of monodisperse drug–silica nanoconjugates. *Molecular Pharmaceutics*, 10(3):883–892, 2013.

[78] P. Wardman. Electron transfer and oxidative stress as key factors in the design of drugs selectively active in hypoxia. *Curr Med Chem*, 8(7):739–761, 2001.

[79] K. A. Kennedy, S. Rockwell, and A. C. Sartorelli. Preferential activation of mitomycin c to cytotoxic metabolites by hypoxic tumor cells. *Cancer Research*, 40(7):2356, 1980.

[80] M. D. Gray, M. Mann, J. L. Nitiss, and L. M. Hendershot. Activation of the unfolded protein response is necessary and sufficient for reducing topoisomerase iialpha protein levels and decreasing sensitivity to topoisomerase-targeted drugs. *Mol Pharmacol*, 68(6):1699–1707, 2005.

[81] B. P. Mahoney, N. Raghunand, B. Baggett, and R. J. Gillies. Tumor acidity, ion trapping and chemotherapeutics: I. acid ph affects the distribution of chemotherapeutic agents in vitro. *Biochemical Pharmacology*, 66(7):1207–1218, 2003.

[82] M. Geiser, B. Rothen-Rutishauser, N. Kapp, S. Schürch, W. Kreyling, H. Schulz, M. Semmler, V. Im Hof, J. Heyder, and P. Gehr. Ultrafine particles cross cellular membranes by nonphagocytic mechanisms in lungs and in cultured cells. *Environmental health perspectives*, 113(11):1555–1560, 2005.

[83] A. Aderem and D. M. Underhill. Mechanisms of phagocytosis in macrophages. *Annual Review of Immunology*, 17(1):593–623, 1999.

[84] R. Ard, K. Mulatz, J. L. Pomoransky, R. J. Parks, L. Trinkle-Mulcahy, J. C. Bell, and S. H. Gee. Regulation of macropinocytosis by diacylglycerol kinase ζ. *PLOS ONE*, 10(12): e0144942, 2015.

[85] C. M. Brown and N. O. Petersen. Free clathrin triskelions are required for the stability of clathrin-associated adaptor protein (ap-2) coated pit nucleation sites. *Biochemistry and Cell Biology*, 77(5):439–448, 1999.

[86] M. Ehrlich, W. Boll, A. van Oijen, R. Hariharan, K. Chandran, M. L. Nibert, and T. Kirchhausen. Endocytosis by random initiation and stabilization of clathrin-coated pits. *Cell*, 118(5):591–605, 2004.

[87] S. Behzadi, V. Serpooshan, W. Tao, M. A. Hamaly, M. Y. Alkawareek, E. C. Dreaden, D. Brown, A. M. Alkilany, O. C. Farokhzad, and M. Mahmoudi. Cellular uptake of nanoparticles: journey inside the cell. *Chemical Society reviews*, 46(14):4218–4244, 2017.

[88] G. Gabella and D. Blundell. Effect of stretch and contraction on caveolae of smooth muscle cells. *Cell Tissue Res*, 190(2):255–271, 1978.

[89] R. V. Stan. Structure of caveolae. *Biochimica et Biophysica Acta (BBA) - Molecular Cell Research*, 1746(3):334–348, 2005.

[90] S. Mayor and R. E. Pagano. Pathways of clathrin-independent endocytosis. *Nature Reviews Molecular Cell Biology*, 8(8):603–612, 2007.

[91] M. P. Desai, V. Labhasetwar, E. Walter, R. J. Levy, and G. L. Amidon. The mechanism of uptake of biodegradable microparticles in caco-2 cells is size dependent. *Pharm Res*, 14 (11):1568–1573, 1997.

[92] C. Brandenberger, C. Mühlfeld, Z. Ali, A.-G. Lenz, O. Schmid, W. J. Parak, P. Gehr, and B. Rothen-Rutishauser. Quantitative evaluation of cellular uptake and trafficking of plain and polyethylene glycol-coated gold nanoparticles. *Small*, 6(15):1669–1678, 2010.

[93] J. Dausend, A. Musyanovych, M. Dass, P. Walther, H. Schrezenmeier, K. Landfester, and V. Mailänder. Uptake mechanism of oppositely charged fluorescent nanoparticles in hela cells. *Macromolecular Bioscience*, 8(12):1135–1143, 2008.

[94] O. Harush-Frenkel, N. Debotton, S. Benita, and Y. Altschuler. Targeting of nanoparticles to the clathrin-mediated endocytic pathway. *Biochemical and Biophysical Research Communications*, 353(1):26–32, 2007.

[95] C. D. Walkey and W. Chan. Understanding and controlling the interaction of nanomaterials with proteins in a physiological environment. *Chemical Society Reviews*, 41(7):2780–2799, 2012.

[96] A. Banerjee, J. Qi, R. Gogoi, J. Wong, and S. Mitragotri. Role of nanoparticle size, shape and surface chemistry in oral drug delivery. *Journal of Controlled Release*, 238:176–185, 2016.

[97] B. D. Chithrani, A. Ghazani, and W. Chan. Determining the size and shape dependence of gold nanoparticle uptake into mammalian cells. *Nano letters*, 6(4):662–668, 2006.

[98] B. D. Chithrani and W. Chan. Elucidating the mechanism of cellular uptake and removal of protein-coated gold nanoparticles of different sizes and shapes. *Nano Letters*, 7(6):1542–1550, 2007.

[99] S. E. A. Gratton, P. A. Ropp, P. D. Pohlhaus, J. C. Luft, V. J. Madden, M. E. Napier, and J. M. DeSimone. The effect of particle design on cellular internalization pathways. *Proceedings of the National Academy of Sciences*, 105(33):11613–11618, 2008.

[100] Y.-B. Hu, E. B. Dammer, R.-J. Ren, and G. Wang. The endosomal-lysosomal system: from acidification and cargo sorting to neurodegeneration. *Translational neurodegeneration*, 4: 18, 2015.

[101] J. Hraběta, M. Belhajová, H. Šubrtová, M. A. Merlos Rodrigo, Z. Heger, and T. Eckschlager. Drug sequestration in lysosomes as one of the mechanisms of chemoresistance of cancer cells and the possibilities of its inhibition. *International journal of molecular sciences*, 21 (12):4392, 2020.

[102] B. Zhitomirsky and Y. G. Assaraf. Lysosomal accumulation of anticancer drugs triggers lysosomal exocytosis. *Oncotarget*, 8(28):45117–45132, 2017.

[103] M. Karimi, A. Ghasemi, P. Sahandi Zangabad, R. Rahighi, S. M. Moosavi Basri, H. Mirshekari, M. Amiri, Z. Shafaei Pishabad, A. Aslani, M. Bozorgomid, D. Ghosh, A. Beyzavi, A. Vaseghi, A. R. Aref, L. Haghani, S. Bahrami, and M. R. Hamblin. Smart micro/nanoparticles in stimulus-responsive drug/gene delivery systems. *Chemical Society reviews*, 45(5):1457–1501, 2016.

[104] G. Sahay, J. O. Kim, A. V. Kabanov, and T. K. Bronich. The exploitation of differential endocytic pathways in normal and tumor cells in the selective targeting of nanoparticulate chemotherapeutic agents. *Biomaterials*, 31(5):923–933, 2010.

[105] R. N. Baiti, H. Ardhyananta, and K. El Kirat. Effect of acidic and basic environment to the degradation behavior of plga nanocapsules for biomedical application. *Advanced Materials Research*, 1123:213–216, 2015.

[106] D. Li, L. Zhou, J. Huang, and X. Xiao. Effect of multidrug resistance 1/p-glycoprotein on the hypoxia-induced multidrug resistance of human laryngeal cancer cells. *Oncol Lett*, 12 (2):1569–1574, 2016.

[107] F. J. Sharom. The p-glycoprotein multidrug transporter. *Essays in Biochemistry*, 50:161–178, 2011.

[108] G. C. Rice, C. Hoy, and R. T. Schimke. Transient hypoxia enhances the frequency of dihydrofolate reductase gene amplification in chinese hamster ovary cells. *Proc Natl Acad Sci U S A*, 83(16):5978–5982, 1986.

[109] Z. Lu, J. Wang, M. G. Wientjes, and Jessie L. S. Au. Intraperitoneal therapy for peritoneal cancer. *Future oncology (London, England)*, 6(10):1625–1641, 2010.

[110] A. C. Abrahams, A. Dendooven, J. W. van der Veer, R. Wientjes, R. J. Toorop, Rlaw Bleys, A. P. A. Hendrickx, M. S. van Leeuwen, Q. G. de Lussanet, M. C. Verhaar, G. Stapper, and T. Q. Nguyen. Direct comparison of the thickness of the parietal peritoneum using peritoneal biopsy and ultrasonography of the abdominal wall in patients treated with peritoneal dialysis. *Perit Dial Int*, 39(5):455–464, 2019.

[111] M. F. Flessner, J. D. Fenstermacher, R. G. Blasberg, and R. L. Dedrick. Peritoneal absorption of macromolecules studied by quantitative autoradiography. *American Journal of Physiology-Heart and Circulatory Physiology*, 248(1):H26–H32, 1985.

[112] nanoComposix. Molecular weight to size calculator, 2021. https://nanocomposix.com/pages/molecular-weight-to-size-calculator#target, visited 2021-08-03.

[113] S. Togano, M. Yashiro, Y. Miki, Y. Yamamoto, T. Sera, Y. Kushitani, A. Sugimoto, S. Kushiyama, S. Nishimura, K. Kuroda, T. Okuno, M. Yoshii, T. Tamura, T. Toyokawa, H. Tanaka, K. Muguruma, S. Tanaka, and M. Ohira. Microscopic distance from tumor invasion front to serosa might be a useful predictive factor for peritoneal recurrence after curative resection of t3-gastric cancer. *PLoS One*, 15(1):e0225958, 2020.

[114] M. F. Flessner. The transport barrier in intraperitoneal therapy. *American Journal of Physiology-Renal Physiology*, 288(3):F433–F442, 2005.

[115] B. Rippe, D. Venturoli, O. Simonsen, and J. De Arteaga. Fluid and electrolyte transport across the peritoneal membrane during capd according to the three-pore model. *Peritoneal Dialysis International*, 24(1):10–27, 2004.

[116] C. B. S. Henry and B. R. Duling. Permeation of the luminal capillary glycocalyx is determined by hyaluronan. *American Journal of Physiology-Heart and Circulatory Physiology*, 277(2):H508–H514, 1999.

[117] H. Vink and B. R. Duling. Capillary endothelial surface layer selectively reduces plasma solute distribution volume. *Am J Physiol Heart Circ Physiol*, 278(1):H285–H289, 2000.

[118] R. A. Mactier and R. Khanna. *Peritoneal lymphatics*, pages 173–192. Springer Netherlands, Dordrecht, 2000. ISBN 978-94-017-3225-3.

[119] H. Shinohara, R. Kominami, Y. Taniguchi, and S. Yasutaka. The distribution and morphology of lymphatic vessels on the peritoneal surface of the adult human diaphragm, as revealed by an ink-absorption method. *Okajimas Folia Anatomica Japonica*, 79(6):175–183, 2003.

[120] G. R. Dakwar, M. Shariati, W. Willaert, W. Ceelen, S. C. De Smedt, and K. Remaut. Nanomedicine-based intraperitoneal therapy for the treatment of peritoneal carcinomatosis - mission possible? *Adv Drug Deliv Rev*, 108:13–24, 2017.

[121] K. Hirano and C. A. Hunt. Lymphatic transport of liposome-encapsulated agents: Effects of liposome size following intraperitoneal administration. *Journal of Pharmaceutical Sciences*, 74(9):915–921, 1985.

[122] P. Maincent, P. Thouvenot, C. Amicabile, M. Hoffman, J. Kreuter, P. Couvreur, and J. P. Devissaguet. Lymphatic targeting of polymeric nanoparticles after intraperitoneal administration in rats. *Pharmaceutical Research*, 9(12):1534–1539, 1992.

[123] L. Simón-Gracia, H. Hunt, P. D. Scodeller, J. Gaitzsch, G. B. Braun, A. M. Willmore, E. Ruoslahti, G. Battaglia, and T. Teesalu. Paclitaxel-loaded polymersomes for enhanced intraperitoneal chemotherapy. *Mol Cancer Ther*, 15(4):670–679, 2016.

[124] D. Reichel, M. Tripathi, and J. M. Perez. Biological effects of nanoparticles on macrophage polarization in the tumor microenvironment. *Nanotheranostics*, 3(1):66–88, 2019.

[125] D. Docter, D. Westmeier, M. Markiewicz, S. Stolte, S. K. Knauer, and R. H. Stauber. The nanoparticle biomolecule corona: lessons learned - challenge accepted? *Chem Soc Rev*, 44 (17):6094–6121, 2015.

[126] N. Backmann, N. Kappeler, T. Braun, F. Huber, H. Lang, C. Gerber, and R. Y. H. Lim. Sensing surface pegylation with microcantilevers. *Beilstein Journal of Nanotechnology*, 1: 3–13, 2010.

[127] S. Schöttler, G. Becker, S. Winzen, T. Steinbach, K. Mohr, K. Landfester, V. Mailänder, and F. R. Wurm. Protein adsorption is required for stealth effect of poly(ethylene glycol)- and poly(phosphoester)-coated nanocarriers. *Nature Nanotechnology*, 11(4):372–377, 2016.

[128] A. S. Abu Lila, H. Kiwada, and T. Ishida. The accelerated blood clearance (abc) phenomenon: Clinical challenge and approaches to manage. *Journal of Controlled Release*, 172(1):38–47, 2013.

[129] G. Bendas, U. Rothe, G. L. Scherphof, and J. A. A. M. Kamps. The influence of repeated injections on pharmacokinetics and biodistribution of different types of sterically stabilized immunoliposomes. *Biochimica et Biophysica Acta (BBA) - Biomembranes*, 1609(1):63–70, 2003.

[130] R. P. Garay, R. El-Gewely, J. K. Armstrong, G. Garratty, and P. Richette. Antibodies against polyethylene glycol in healthy subjects and in patients treated with peg-conjugated agents. *Expert Opinion on Drug Delivery*, 9(11):1319–1323, 2012.

[131] J. Szebeni, F. Muggia, A. Gabizon, and Y. Barenholz. Activation of complement by therapeutic liposomes and other lipid excipient-based therapeutic products: Prediction and prevention. *Advanced Drug Delivery Reviews*, 63(12):1020–1030, 2011.

[132] M. A. Miller, Y. R. Zheng, S. Gadde, C. Pfirschke, H. Zope, C. Engblom, R. H. Kohler, Y. Iwamoto, K. S. Yang, B. Askevold, N. Kolishetti, M. Pittet, S. J. Lippard, O. C. Farokhzad, and R. Weissleder. Tumour-associated macrophages act as a slow-release reservoir of nano-therapeutic pt(iv) pro-drug. *Nat Commun*, 6:8692, 2015.

[133] International Organisation for Standardisation. Iso/ts 80004-2: 2015 nanotechnologies - vocabulary - part 2: Nano-objects. 2015.

[134] K. K. Jain. *An Overview of Drug Delivery Systems*, pages 1–54. Springer New York, New York, NY, 2020. ISBN 978-1-4939-9798-5.

[135] B. Almería and A. Gomez. Electrospray synthesis of monodisperse polymer particles in a broad (60nm–2μm) diameter range: guiding principles and formulation recipes. *Journal of Colloid and Interface Science*, 417:121–130, 2014.

[136] J. P. Rao and K. E. Geckeler. Polymer nanoparticles: Preparation techniques and size-control parameters. *Progress in Polymer Science*, 36(7):887–913, 2011.

[137] H. Fessi, F. Puisieux, J. Ph Devissaguet, N. Ammoury, and S. Benita. Nanocapsule formation by interfacial polymer deposition following solvent displacement. *International Journal of Pharmaceutics*, 55(1):R1–R4, 1989.

[138] R. Rietscher, C. Thum, C. M. Lehr, and M. Schneider. Semi-automated nanoprecipitation-system–an option for operator independent, scalable and size adjustable nanoparticle synthesis. *Pharm Res*, 32(6):1859–1863, 2015.

[139] S. Schubert, Jr J. T. Delaney, and U. S. Schubert. Nanoprecipitation and nanoformulation of polymers: from history to powerful possibilities beyond poly(lactic acid). *Soft Matter*, 7 (5):1581–1588, 2011.

[140] E. Swider, O. Koshkina, J. Tel, L. J. Cruz, I. J. M. de Vries, and M. Srinivas. Customizing poly(lactic-co-glycolic acid) particles for biomedical applications. *Acta Biomater*, 73:38–51, 2018.

[141] T. Govender, S. Stolnik, M. C. Garnett, L. Illum, and S. S. Davis. Plga nanoparticles prepared by nanoprecipitation: drug loading and release studies of a water soluble drug. *Journal of Controlled Release*, 57(2):171–185, 1999.

[142] N. Lababidi, V. Sigal, A. Koenneke, K. Schwarzkopf, A. Manz, and M. Schneider. Microfluidics as tool to prepare size-tunable plga nanoparticles with high curcumin encapsulation for efficient mucus penetration. *Beilstein Journal of Nanotechnology*, 10:2280–2293, 2019.

[143] J. W. Vanderhoff, M. S. El-Aasser, and J. Ugelstad. Polymer emulsification process, U.S. Patent US4177177A, 1979.

[144] R. Dinarvand, N. Sepehri, S. Manoochehri, H. Rouhani, and F. Atyabi. Polylactide-co-glycolide nanoparticles for controlled delivery of anticancer agents. *International journal of nanomedicine*, 6:877–895, 2011.

[145] B. D. Ulery, L. S. Nair, and C. T. Laurencin. Biomedical applications of biodegradable polymers. *Journal of Polymer Science Part B: Polymer Physics*, 49(12):832–864, 2011.

[146] K. Wu and J. Li. Precipitation of a biodegradable polymer using compressed carbon dioxide as antisolvent. *The Journal of Supercritical Fluids*, 46(2):211–216, 2008.

[147] L. S. Nair and C. T. Laurencin. Biodegradable polymers as biomaterials. *Progress in Polymer Science*, 32(8):762–798, 2007.

[148] P.-L. Lai, D.-W. Hong, T.-H. Liu, Z.-T. Lai, M.-H. Cheng, L.-H. Chen, W.-J. Chen, and I. M. Chu. Validity of poly(1, 6-bis-(p-carboxyphenoxy hexane)-co-(sebacic anhydride)) copolymer in biomedical application. *Journal of Applied Polymer Science*, 128(6):3687–3695, 2013.

[149] A. Singh, N. R. Krogman, S. Sethuraman, L. S. Nair, J. L. Sturgeon, P. W. Brown, C. T. Laurencin, and H. R. Allcock. Effect of side group chemistry on the properties of biodegradable l-alanine cosubstituted polyphosphazenes. *Biomacromolecules*, 7(3):914–918, 2006.

[150] I. Vroman and L. Tighzert. Biodegradable polymers. *Materials*, 2(2):307–344, 2009.

[151] H.-B. Chen, B.-S. Chiou, Y.-Z. Wang, and D. A. Schiraldi. Biodegradable pectin/clay aerogels. *ACS Applied Materials & Interfaces*, 5(5):1715–1721, 2013.

[152] Bartosikova L. Necas J. Carrageenan: a review. *Veterinarni Medicina*, 58(4):187–205, 2013.

[153] K. K. Chereddy, C.-H. Her, M. Comune, C. Moia, A. Lopes, P. E. Porporato, J. Vanacker, M. C. Lam, L. Steinstraesser, P. Sonveaux, H. Zhu, L. S. Ferreira, G. Vandermeulen, and V. Préat. Plga nanoparticles loaded with host defense peptide ll37 promote wound healing. *Journal of Controlled Release*, 194:138–147, 2014.

[154] N. Günday Türeli, A. Torge, J. Juntke, B. C. Schwarz, N. Schneider-Daum, A. E. Türeli, C.-M. Lehr, and M. Schneider. Ciprofloxacin-loaded plga nanoparticles against cystic fibrosis p. aeruginosa lung infections. *European Journal of Pharmaceutics and Biopharmaceutics*, 117:363–371, 2017.

[155] N. Nafee, S. Taetz, M. Schneider, U. F. Schaefer, and C.-M. Lehr. Chitosan-coated plga nanoparticles for dna/rna delivery: effect of the formulation parameters on complexation and transfection of antisense oligonucleotides. *Nanomedicine: Nanotechnology, Biology and Medicine*, 3(3):173–183, 2007.

[156] D. Primavessy, N. Günday Türeli, and M. Schneider. Influence of different stabilizers on the encapsulation of desmopressin acetate into plga nanoparticles. *European Journal of Pharmaceutics and Biopharmaceutics*, 118:48–55, 2017.

[157] U.S. Food and Drug Administration. Inactive ingredients database, 2021. visited 2021-02-09.

[158] H. K. Makadia and S. J. Siegel. Poly lactic-co-glycolic acid (plga) as biodegradable controlled drug delivery carrier. *Polymers*, 3(3):1377–1397, 2011.

[159] Evonik. Setting the benchmark for biodegradable polymers for controlled release. https://healthcare.evonik.com/en/pharmaceuticals/parenteral-drug-delivery/parenteral-excipients/resomer-portfolio/standard-polymers, visited 2021-03-03.

[160] A. R. Rajabi-Siahboomi, R. Y. Mehta, V. Ambudkar, V. Dias, and S. Tiwari. *Ethylcellulose Applications in Multiparticulate Systems*, pages 267–299. Springer New York, New York, NY, 2017. ISBN 978-1-4939-7012-4.

[161] G. Murtaza. Ethylcellulose microparticles: a review. *Acta Pol Pharm*, 69(1):11–22, 2012.

[162] G. Morris, S. Kok, S. Harding, and G. Adams. Polysaccharide drug delivery systems based on pectin and chitosan. *Biotechnol Genet Eng Rev*, 27:257–284, 2010.

[163] A. Lončarević, M. Ivanković, and A. Rogina. Lysozyme-induced degradation of chitosan: the characterisation of degraded chitosan scaffolds. *Journal of Tissue Repair and Regeneration*, 1(1):12, 2017.

[164] U.S. Food and Drug Administration. Gras notice inventory - agency response letter, GRAS Notice No. GRN 000397. 2011. https://wayback.archive-it.org/7993/20171031010838/https://www.fda.gov/Food/IngredientsPackagingLabeling/GRAS/NoticeInventory/ucm287638.htm, visited 2021-02-10.

[165] U.S. Food and Drug Administration. Gras notice inventory - agency response letter, GRAS Notice No. GRN 000443. 2013. https://wayback.archive-it.org/7993/20171031005742/https://www.fda.gov/Food/IngredientsPackagingLabeling/GRAS/NoticeInventory/ucm347791.htm, visited 2021-02-10.

[166] U.S. Food and Drug Administration. Premarket notification - agency summary 510(k), No. K143124. 2015. https://www.accessdata.fda.gov/cdrh_docs/pdf14/K143124.pdf, visited 2021-02-10.

[167] U.S. Food and Drug Administration. Premarket notification - agency summary 510(k), No. K190246. 2019. https://www.accessdata.fda.gov/cdrh_docs/pdf19/K190246.pdf, visited 2021-02-10.

[168] D. Chuan, T. Jin, R. Fan, L. Zhou, and G. Guo. Chitosan for gene delivery: Methods for improvement and applications. *Advances in Colloid and Interface Science*, 268:25–38, 2019.

[169] M. A. Mohammed, J. T. M. Syeda, K. M. Wasan, and E. K. Wasan. An overview of chitosan nanoparticles and its application in non-parenteral drug delivery. *Pharmaceutics*, 9(4):53, 2017.

[170] G. Moku, V. R. Gopalsamuthiram, T. R. Hoye, and J. Panyam. *Surface Modification of Nanoparticles: Methods and Applications*, pages 317–346. William Andrew Publishing, 2019.

[171] F. Chen, K. Ma, B. Madajewski, L. Zhuang, L. Zhang, K. Rickert, M. Marelli, B. Yoo, M. Z. Turker, M. Overholtzer, T. P. Quinn, M. Gonen, P. Zanzonico, A. Tuesca, M. A. Bowen, L. Norton, J. A. Subramony, U. Wiesner, and M. S. Bradbury. Ultrasmall targeted nanoparticles with engineered antibody fragments for imaging detection of her2-overexpressing breast cancer. *Nature Communications*, 9(1):4141, 2018.

[172] S. Jain, G. Spandana, A. K. Agrawal, V. Kushwah, and K. Thanki. Enhanced antitumor efficacy and reduced toxicity of docetaxel loaded estradiol functionalized stealth polymeric nanoparticles. *Molecular Pharmaceutics*, 12(11):3871–3884, 2015.

[173] P. Naruphontjirakul and K. Viravaidya-Pasuwat. Development of anti-her2-targeted doxorubicin-core-shell chitosan nanoparticles for the treatment of human breast cancer. *International journal of nanomedicine*, 14:4105–4121, 2019.

[174] J. Sheng, L. Han, J. Qin, G. Ru, R. Li, L. Wu, D. Cui, P. Yang, Y. He, and J. Wang. N-trimethyl chitosan chloride-coated plga nanoparticles overcoming multiple barriers to oral insulin absorption. *ACS Applied Materials & Interfaces*, 7(28):15430–15441, 2015.

[175] H. Song, C. Su, W. Cui, B. Zhu, L. Liu, Z. Chen, and L. Zhao. Folic acid-chitosan conjugated nanoparticles for improving tumor-targeted drug delivery. *BioMed Research International*, 2013:723158, 2013.

[176] B. Xiao, M. K. Han, E. Viennois, L.n Wang, M. Zhang, X. Si, and D. Merlin. Hyaluronic acid-functionalized polymeric nanoparticles for colon cancer-targeted combination chemotherapy. *Nanoscale*, 7(42):17745–17755, 2015.

[177] N. H. Abd Ellah and S. A. Abouelmagd. Surface functionalization of polymeric nanoparticles for tumor drug delivery: approaches and challenges. *Expert Opinion on Drug Delivery*, 14(2):201–214, 2017.

[178] Z. Amoozgar, J. Park, Q. Lin, and Y. Yeo. Low molecular-weight chitosan as a ph-sensitive stealth coating for tumor-specific drug delivery. *Molecular pharmaceutics*, 9(5):1262–1270, 2012.

[179] J. S. Suk, Q. Xu, N. Kim, J. Hanes, and L. M. Ensign. Pegylation as a strategy for improving nanoparticle-based drug and gene delivery. *Advanced Drug Delivery Reviews*, 99:28–51, 2016.

[180] N. K. Al-Nemrawi, N. H. Alshraiedeh, A. L. Zayed, and B. M. Altaani. Low molecular weight chitosan-coated plga nanoparticles for pulmonary delivery of tobramycin for cystic fibrosis. *Pharmaceuticals (Basel)*, 11(1):28, 2018.

[181] F. Chai, L. Sun, X. He, J. Li, Y. Liu, F. Xiong, L. Ge, T. J. Webster, and C. Zheng. Doxorubicin-loaded poly (lactic-co-glycolic acid) nanoparticles coated with chitosan/alginate by layer by layer technology for antitumor applications. *Int J Nanomedicine*, 12:1791–1802, 2017.

[182] J. M. Chan, L. Zhang, K. P. Yuet, G. Liao, J. W. Rhee, R. Langer, and O. C. Farokhzad. Plga-lecithin-peg core-shell nanoparticles for controlled drug delivery. *Biomaterials*, 30(8): 1627–1634, 2009.

[183] Y. Jia, A. Omri, L. Krishnan, and M. J. McCluskie. Potential applications of nanoparticles in cancer immunotherapy. *Human vaccines & immunotherapeutics*, 13(1):63–74, 2017.

[184] P. H. Sugarbaker, J. T. Mora, P. Carmignani, O. A. Stuart, and D. Yoo. Update on chemotherapeutic agents utilized for perioperative intraperitoneal chemotherapy. *The Oncologist*, 10(2):112–122, 2005.

[185] P. H. Sugarbaker and K. Van der Speeten. Surgical technology and pharmacology of hyperthermic perioperative chemotherapy. *J Gastrointest Oncol*, 7(1):29–44, 2016.

[186] M. C. Wani, H. L. Taylor, M. E. Wall, P. Coggon, and A. T. McPhail. Plant antitumor agents. vi. the isolation and structure of taxol, a novel antileukemic and antitumor agent from taxus brevifolia. *J Am Chem Soc*, 93(9):2325–2327, 1971.

[187] J.-N. Denis, A.E. Greene, D. Guénard, F. Guéritte-Voegelein, L. Mangatal, and P. Potier. A highly efficient, practical approach to natural taxol. *Journal of American Chemical Society*, 110(17):5917–5919, 1988.

[188] S. B. Horwitz. Mechanism of action of taxol. *Trends Pharmacol Sci*, 13(4):134–136, 1992.

[189] A. K. Dash. The dark side of paclitaxel. *Oncology Reviews*, 4(2):71–72, 2010.

[190] R. T. Liggins, W. L. Hunter, and H. M. Burt. Solid-state characterization of paclitaxel. *J Pharm Sci*, 86(12):1458–1463, 1997.

[191] F. Mohamed and P. H. Sugarbaker. Intraperitoneal taxanes. *Surgical Oncology Clinics of North America*, 12(3):825–833, 2003.

[192] Fresenius Kabi Deutschland GmbH. Fachinformation paclitaxel kabi 6 mg/ml. 2020.

[193] Bristol-Myers Squibb Pharma EEIG. Fachinformation abraxane 5 mg/ml. 2021.

[194] J. Rubin, M. Clawson, A. Planch, and Q. Jones. Measurements of peritoneal surface area in man and rat. *The American Journal of the Medical Sciences*, 295(5):453–458, 1988.

[195] S. K. Williamson, G. A. Johnson, H. A. Maulhardt, K. M. Moore, D. S. McMeekin, T. K. Schulz, G. A. Reed, K. F. Roby, C. B. Mackay, H. J. Smith, S. J. Weir, J. A. Wick, M. Markman, G. S. diZerega, M. J. Baltezor, J. Espinosa, and C. J. Decedue. A phase i study of intraperitoneal nanoparticulate paclitaxel (nanotax) in patients with peritoneal malignancies. *Cancer Chemother Pharmacol*, 75(5):1075–1087, 2015.

[196] M. C. Cristea, P. Frankel, T. Synold, S. Rivkin, D. Lim, V. Chung, J. Chao, M. Wakabayashi, B. Paz, E. Han, P. Lin, L. Leong, A. Hakim, M. Carroll, N. Prakash, T. Dellinger, M. Park, and R. J. Morgan. A phase i trial of intraperitoneal nab-paclitaxel in the treatment of advanced malignancies primarily confined to the peritoneal cavity. *Cancer Chemother Pharmacol*, 83(3):589–598, 2019.

[197] L. Van De Sande, M. Graversen, M. Hubner, M. Pocard, M. Reymond, M. Vaira, S. Cosyns, W. Willaert, and W. Ceelen. Intraperitoneal aerosolization of albumin-stabilized paclitaxel nanoparticles (abraxane™) for peritoneal carcinomatosis – a phase i first-in-human study. *Pleura and Peritoneum*, 3(2):20180112, 2018.

[198] F. Farjadian, A. Ghasemi, O. Gohari, A. Roointan, M. Karimi, and M. R. Hamblin. Nanopharmaceuticals and nanomedicines currently on the market: challenges and opportunities. *Nanomedicine (London, England)*, 14(1):93–126, 2019.

[199] U.S. Food and Drug Administration. Hematology/oncology (cancer) approvals & safety notifications, 2021. https://www.fda.gov/drugs/resources-information-approved-drugs/hematologyoncology-cancer-approvals-safety-notifications, visited 2021-02-09.

[200] A. C. Anselmo and S. Mitragotri. Nanoparticles in the clinic: An update. *Bioengineering & Translational Medicine*, 4(3):e10143, 2019.

[201] O. J. Wouters, M. McKee, and J. Luyten. Estimated research and development investment needed to bring a new medicine to market, 2009-2018. *JAMA*, 323(9):844–853, 2020.

[202] R. Bosetti. Cost–effectiveness of nanomedicine: the path to a future successful and dominant market? *Nanomedicine*, 10(12):1851–1853, 2015.

[203] Globenewswire Inc. Nanobiotix announces first ever radioenhancer to receive european market approval, 2019. https://ml-eu.globenewswire.com/Resource/Download/63f3c5b2-c59b-4e44-abb9-168ef2a5df31, visited 2021-02-11.

[204] D. S. Kohane, J. Y. Tse, Y. Yeo, R. Padera, M. Shubina, and R. Langer. Biodegradable polymeric microspheres and nanospheres for drug delivery in the peritoneum. *J Biomed Mater Res A*, 77(2):351–361, 2006.

[205] E. Marin, J. Rojas, and Y. Ciro. A review of polyvinyl alcohol derivatives: Promising materials for pharmaceutical and biomedical applications. *African Journal of Pharmacy and Pharmacology*, 8:674–684, 2014.

[206] B. Friedrichs. Th. peters. jr.: All about albumin. biochemistry, genetics, and medical applications. xx and 432 pages, numerous figures and tables. academic press, inc., san diego, california, 1996. *Food / Nahrung*, 41(6):382–382, 1997.

[207] A. M. Merlot, D. S. Kalinowski, and D. R. Richardson. Unraveling the mysteries of serum albumin-more than just a serum protein. *Frontiers in physiology*, 5:299, 2014.

[208] C. Tiruppathi, W. Song, M. Bergenfeldt, P. Sass, and A. B. Malik. Gp60 activation mediates albumin transcytosis in endothelial cells by tyrosine kinase-dependent pathway. *J Biol Chem*, 272(41):25968–25975, 1997.

[209] G. Stehle, H. Sinn, A. Wunder, H. H. Schrenk, J. C. Stewart, G. Hartung, W. Maier-Borst, and D. L. Heene. Plasma protein (albumin) catabolism by the tumor itself–implications for tumor metabolism and the genesis of cachexia. *Crit Rev Oncol Hematol*, 26(2):77–100, 1997.

[210] L. Bo, L. Lili, H. Dingyu, P. Bo, L. Qin, X. Shengyuan, L. Yujuan, and D. Yulin. A study of cross-linkage of formaldehyde with human serum albumin. *3rd International Conference on Bioinformatics and Biomedical Engineering*, pages 1–6, 2009.

[211] H. Niknejad and R. Mahmoudzadeh. Comparison of different crosslinking methods for preparation of docetaxel-loaded albumin nanoparticles. *Iranian journal of pharmaceutical research : IJPR*, 14(2):385–394, 2015.

[212] A. Vogel and Pelletier. Examen chimique de la racine de curcuma. *Journal de Pharmacie*, 1815.

[213] W. Abdelwahed, G. Degobert, S. Stainmesse, and H. Fessi. Freeze-drying of nanoparticles: formulation, process and storage considerations. *Adv Drug Deliv Rev*, 58(15):1688–1713, 2006.

[214] Z. Urban-Morlan, S. Mendoza-Elvira, R. Hernandez-Ceron, S. Alcala, H. Ramirez-Mendoza, A. Ciprian-Carrasco, E. Pinon-Segundo, and D. Quintanar. Preparation of ethyl cellulose nanoparticles by solvent-displacement using the conventional method and a recirculation system. *Journal of the Mexican Chemical Society*, 59:173–180, 2015.

[215] N. Nafee, S. Taetz, M. Schneider, U. F. Schaefer, and C. M. Lehr. Chitosan-coated plga nanoparticles for dna/rna delivery: effect of the formulation parameters on complexation and transfection of antisense oligonucleotides. *Nanomedicine*, 3(3):173–183, 2007.

[216] C. Furman, R. Carpentier, A. Barczyk, P. Chavatte, D. Betbeder, and E. Lipka. Development and validation of a reversed-phase hplc method for the quantification of paclitaxel in different plga nanocarriers. *Electrophoresis*, 38(19):2536–2541, 2017.

[217] R. D. Deegan, O. Bakajin, T. F. Dupont, G. Huber, S. R. Nagel, and T. A. Witten. Contact line deposits in an evaporating drop. *Physical Review E*, 62(1):756–765, 2000.

[218] G. Dalwadi, H. A. Benson, and Y. Chen. Comparison of diafiltration and tangential flow filtration for purification of nanoparticle suspensions. *Pharm Res*, 22(12):2152–2162, 2005.

[219] S. S. Chakravarthi, S. De, D. W. Miller, and D. H. Robinson. Comparison of anti-tumor efficacy of paclitaxel delivered in nano- and microparticles. *Int J Pharm*, 383(1-2):37–44, 2010.

[220] M. D. Chavanpatil, Y. Patil, and J. Panyam. Susceptibility of nanoparticle-encapsulated paclitaxel to p-glycoprotein-mediated drug efflux. *Int J Pharm*, 320(1-2):150–156, 2006.

[221] Y. Dong and S. S. Feng. Poly(d,l-lactide-co-glycolide) (plga) nanoparticles prepared by high pressure homogenization for paclitaxel chemotherapy. *Int J Pharm*, 342(1-2):208–214, 2007.

[222] M. Esfandyari-Manesh, S. H. Mostafavi, R. F. Majidi, M. N. Koopaei, N. S. Ravari, M. Amini, B. Darvishi, S. N. Ostad, F. Atyabi, and R. Dinarvand. Improved anticancer delivery of paclitaxel by albumin surface modification of plga nanoparticles. *Daru*, 23:28, 2015.

[223] C. Fonseca, S. Simoes, and R. Gaspar. Paclitaxel-loaded plga nanoparticles: preparation, physicochemical characterization and in vitro anti-tumoral activity. *J Control Release*, 83 (2):273–286, 2002.

[224] P. N. Gupta, S. Jain, C. Nehate, N. Alam, V. Khare, R. D. Dubey, A. Saneja, S. Kour, and S. K. Singh. Development and evaluation of paclitaxel loaded plga: poloxamer blend nanoparticles for cancer chemotherapy. *Int J Biol Macromol*, 69:393–399, 2014.

[225] C. Jin, L. Bai, H. Wu, W. Song, G. Guo, and K. Dou. Cytotoxicity of paclitaxel incorporated in plga nanoparticles on hypoxic human tumor cells. *Pharm Res*, 26(7):1776–1784, 2009.

[226] M. Li, E. A. Czyszczon, and J. J. Reineke. Delineating intracellular pharmacokinetics of paclitaxel delivered by plga nanoparticles. *Drug Deliv Transl Res*, 3(6):551–561, 2013.

[227] Y. Liu, J. Pan, and S. S. Feng. Nanoparticles of lipid monolayer shell and biodegradable polymer core for controlled release of paclitaxel: effects of surfactants on particles size, characteristics and in vitro performance. *Int J Pharm*, 395(1-2):243–250, 2010.

[228] J. Ma, M. Shen, C. S. Xu, Y. Sun, Y. R. Duan, and L. F. Du. Biodegradable double-targeted ptx-mpeg-plga nanoparticles for ultrasound contrast enhanced imaging and antitumor therapy in vitro. *Oncotarget*, 7(48):80008–80018, 2016.

[229] L. Vicari, T. Musumeci, I. Giannone, L. Adamo, C. Conticello, R. De Maria, R. Pignatello, G. Puglisi, and M. Gulisano. Paclitaxel loading in plga nanospheres affected the in vitro drug cell accumulation and antiproliferative activity. *BMC Cancer*, 8:212, 2008.

[230] X. Wang, J. Gao, X. Ouyang, J. Wang, X. Sun, and Y. Lv. Mesenchymal stem cells loaded with paclitaxel-poly(lactic-co-glycolic acid) nanoparticles for glioma-targeting therapy. *Int J Nanomedicine*, 13:5231–5248, 2018.

[231] A. Castagna, A. J. Zander, I. Sautkin, M. Schneider, R. Shegokar, A. Königsrainer, and M. A. Reymond. Enhanced intraperitoneal delivery of charged, aerosolized curcumin nanoparticles by electrostatic precipitation. *Nanomedicine*, 16(2):109–120, 2021.

[232] F. M. Goycoolea and V. Milkova. Electrokinetic behavoir of chitosan adsorbed on o/w nanoemulsion droplets. *Colloids and Surfaces A: Physicochemical and Engineering Aspects*, 519:205–211, 2017.

[233] Y. Li, H. Zhao, L.-R. Duan, H. Li, Q. Yang, H.-H. Tu, W. Cao, and S.-W. Wang. Preparation, characterization and evaluation of bufalin liposomes coated with citrus pectin. *Colloids and Surfaces A: Physicochemical and Engineering Aspects*, 444:54–62, 2014.

[234] K. Paál, J. Müller, and L. Hegedûs. High affinity binding of paclitaxel to human serum albumin. *European Journal of Biochemistry*, 268(7):2187–2191, 2001.

[235] M. Purcell, J. F. Neault, and H. A. Tajmir-Riahi. Interaction of taxol with human serum albumin. *Biochim Biophys Acta*, 1478(1):61–68, 2000.

[236] L. Trynda-Lemiesz. Paclitaxel-hsa interaction. binding sites on hsa molecule. *Bioorg Med Chem*, 12(12):3269–3275, 2004.

[237] N. K. Ibrahim, N. Desai, S. Legha, P. Soon-Shiong, R. L. Theriault, E. Rivera, B. Esmaeli, S. E. Ring, A. Bedikian, G. N. Hortobagyi, and J. A. Ellerhorst. Phase i and pharmacokinetic study of abi-007, a cremophor-free, protein-stabilized, nanoparticle formulation of paclitaxel. *Clinical Cancer Research*, 8(5):1038, 2002.

[238] M. Celus, C. Kyomugasho, A. M. Van Loey, T. Grauwet, and M. E. Hendrickx. Influence of pectin structural properties on interactions with divalent cations and its associated functionalities. *Comprehensive Reviews in Food Science and Food Safety*, 17(6):1576–1594, 2018.

[239] A. S. Fulcher, S. G. O'Sullivan, E. M. Segreti, and B. D. Kavanagh. Recurrent cervical carcinoma: Typical and atypical manifestations. *RadioGraphics*, 19:S103–S116, 1999.

[240] S. Singhal, S. Kumar, D. Sharma, and S. Mathur. Peritoneal metastasis in stage ib1 adenocarcinoma cervix: A rare entity. *Journal of Cancer Research and Therapeutics*, 15(6): 1415–1417, 2019.

[241] J. López-García, M. Lehocký, P. Humpolíček, and P. Sáha. Hacat keratinocytes response on antimicrobial atelocollagen substrates: Extent of cytotoxicity, cell viability and proliferation. *Journal of functional biomaterials*, 5(2):43–57, 2014.

[242] N. M. Lopes, E. G. Adams, T. W. Pitts, and B. K. Bhuyan. Cell kill kinetics and cell cycle effects of taxol on human and hamster ovarian cell lines. *Cancer Chemother Pharmacol*, 32(3):235–242, 1993.

[243] J. E. Liebmann, J. A. Cook, C. Lipschultz, D. Teague, J. Fisher, and J. B. Mitchell. Cytotoxic studies of paclitaxel (taxol) in human tumour cell lines. *British journal of cancer*, 68 (6):1104–1109, 1993.

[244] E. Raymond, A. Hanauske, S. Faivre, E. Izbicka, G. Clark, E. K. Rowinsky, and D. D. Von Hoff. Effects of prolonged versus short-term exposure paclitaxel (taxol) on human tumor colony-forming units. *Anticancer Drugs*, 8(4):379–385, 1997.

[245] O. Müller-Plathe. *Osmolalität*, pages 1793–1795. Springer Berlin Heidelberg, Berlin, Heidelberg, 2019. ISBN 978-3-662-48986-4.

[246] B. Braun Melsungen AG. Fachinformation isotone natriumchloridlösung 0.9 infusionslösung. 2014.

[247] Baxter Deutschland GmbH. Fachinformation glucose baxter 50 mg/ml (5 %) infusionslösung. 2015.

[248] J. Xu, S. Strandman, J. X. Zhu, J. Barralet, and M. Cerruti. Genipin-crosslinked catechol-chitosan mucoadhesive hydrogels for buccal drug delivery. *Biomaterials*, 37:395–404, 2015.

[249] K. Park, S. Skidmore, J. Hadar, J. Garner, H. Park, A. Otte, B. K. Soh, G. Yoon, D. Yu, Y. Yun, B. K. Lee, X. Jiang, and Y. Wang. Injectable, long-acting plga formulations: Analyzing plga and understanding microparticle formation. *Journal of Controlled Release*, 304: 125–134, 2019.

[250] J. Hiemer, A. Clausing, T. Schwarz, and K. Stöwe. Microjet reactor technology: An automated, continuous approach for nanoparticle syntheses. *Chemical Engineering & Technology*, 42(10):2018–2027, 2019.

[251] S. Schiller, A. Hanefeld, M. Schneider, and C. M. Lehr. Focused ultrasound as a scalable and contact-free method to manufacture protein-loaded plga nanoparticles. *Pharm Res*, 32 (9):2995–3006, 2015.

[252] S. Ding, N. Anton, T. F. Vandamme, and C. A. Serra. Microfluidic nanoprecipitation systems for preparing pure drug or polymeric drug loaded nanoparticles: an overview. *Expert Opinion on Drug Delivery*, 13(10):1447–1460, 2016.

[253] P. M. Valencia, O. C. Farokhzad, R. Karnik, and R. Langer. Microfluidic technologies for accelerating the clinical translation of nanoparticles. *Nature nanotechnology*, 7(10):623–629, 2012.

[254] K. V. K. Boodhoo and R. J. Jachuck. Process intensification: spinning disk reactor for styrene polymerisation. *Applied Thermal Engineering*, 20(12):1127–1146, 2000.

[255] D. Ghiasy, M. T. Tham, and K. V. K. Boodhoo. Control of a spinning disc reactor: An experimental study. *Industrial & Engineering Chemistry Research*, 52(47):16832–16841, 2013.

[256] P. Oxley, C. Brechtelsbauer, F. Ricard, N. Lewis, and C. Ramshaw. Evaluation of spinning disk reactor technology for the manufacture of pharmaceuticals. *Industrial & Engineering Chemistry Research*, 39(7):2175–2182, 2000.

[257] B. de Caprariis, M. Di Rita, M. Stoller, N. Verdone, and A. Chianese. Reaction-precipitation by a spinning disc reactor: Influence of hydrodynamics on nanoparticles production. *Chemical Engineering Science*, 76:73–80, 2012.

[258] S. Mohammadi, A. Harvey, and K. V. K. Boodhoo. Synthesis of tio2 nanoparticles in a spinning disc reactor. *Chemical Engineering Journal*, 258:171–184, 2014.

[259] K. J. Hartlieb, C. L. Raston, and Martin S. Controlled scalable synthesis of zno nanoparticles. *Chemistry of Materials*, 19(23):5453–5459, 2007.

[260] S. F. Chin, K. S. Iyer, C. L. Raston, and M. Saunders. Size selective synthesis of superparamagnetic nanoparticles in thin fluids under continuous flow conditions. *Advanced Functional Materials*, 18(6):922–927, 2008.

[261] N. Smith, C. Raston, M. Saunders, and R. Woodward. Synthesis of magnetic nanoparticles using spinning disc processing. *NSTI Nanotech*, 2006.

[262] J. W. Loh, J. Schneider, M. Carter, M. Saunders, and L.-Y. Lim. Spinning disc processing technology: Potential for large-scale manufacture of chitosan nanoparticles. *Journal of Pharmaceutical Sciences*, 99(10):4326–4336, 2010.

[263] N. Anantachoke, M. Makha, C. L. Raston, V. Reutrakul, N. C. Smith, and M. Saunders. Fine tuning the production of nanosized β-carotene particles using spinning disk processing. *Journal of the American Chemical Society*, 128(42):13847–13853, 2006.

[264] S. Sana, K. Boodhoo, and V. Zivkovic. Production of starch nanoparticles through solvent-antisolvent precipitation in a spinning disc reactor. *Green Processing and Synthesis*, 8(1): 507–515, 2019.

[265] W. H. Khan and V. K. Rathod. Process intensification approach for preparation of curcumin nanoparticles via solvent–nonsolvent nanoprecipitation using spinning disc reactor. *Chemical Engineering and Processing: Process Intensification*, 80:1–10, 2014.

[266] K. V. K. Boodhoo and S. R. Al-Hengari. Micromixing characteristics in a small-scale spinning disk reactor. *Chemical Engineering & Technology*, 35(7):1229–1237, 2012.

[267] A. Aoune and C. Ramshaw. Process intensification: heat and mass transfer characteristics of liquid films on rotating discs. *International Journal of Heat and Mass Transfer*, 42(14): 2543–2556, 1999.

[268] M. Akhtar, P. Chan, N. Safriani, B. Murray, and G. Clayton. Concentration of apple juice using spinning disc reactor technology. *Journal of Food Processing & Technology*, 2, 2011.

[269] I. J. Joye and D. J. McClements. Production of nanoparticles by anti-solvent precipitation for use in food systems. *Trends in Food Science & Technology*, 34(2):109–123, 2013.

[270] W. Huang and C. Zhang. Tuning the size of poly(lactic-co-glycolic acid) (plga) nanoparticles fabricated by nanoprecipitation. *Biotechnology Journal*, 13(1):1700203, 2018.

[271] R. H. Müller and R. Schuhmann. *Teilchengrößenmessung der Laborpraxis*. Wissenschaftliche Verlagsgesellschaft mbH Stuttgart, 1996. ISBN 3-8047-1490-0.

[272] U. Bilati, E. Allémann, and E. Doelker. Development of a nanoprecipitation method intended for the entrapment of hydrophilic drugs into nanoparticles. *European Journal of Pharmaceutical Sciences*, 24(1):67–75, 2005.

[273] A. Budhian, S. J. Siegel, and K. I. Winey. Haloperidol-loaded plga nanoparticles: Systematic study of particle size and drug content. *International Journal of Pharmaceutics*, 336 (2):367–375, 2007.

[274] C. I. C. Crucho and M. T. Barros. Polymeric nanoparticles: A study on the preparation variables and characterization methods. *Materials Science and Engineering: C*, 80:771–784, 2017.

[275] DDBST GmbH. Dortmund data bank. 2020. http://www.ddbst.com/en/EED/PCP/PCPindex.php, visited 2020-04-12.

[276] C. M. Hansen. *Hansen Solubility Parameter: A User's Handbook*. CRC Press, Boca Raton, 2nd edition edition, 2007. ISBN 9780429127526 & 978-0-8493-7248-3 (Hardcover).

[277] C. G. Madsen, A. Skov, S. Baldursdottir, T. Rades, L. Jorgensen, and N. J. Medlicott. Simple measurements for prediction of drug release from polymer matrices – solubility parameters and intrinsic viscosity. *European Journal of Pharmaceutics and Biopharmaceutics*, 92:1–7, 2015.

[278] J. S. Choi, J. Cao, M. Naeem, J. Noh, N. Hasan, H. K. Choi, and J. W. Yoo. Size-controlled biodegradable nanoparticles: preparation and size-dependent cellular uptake and tumor cell growth inhibition. *Colloids Surf B Biointerfaces*, 122:545–551, 2014.

[279] European Pharmacopoeia Commission. European pharmacopoeia (ph. eur.). 10, 2020.

[280] United States Pharmacopeial Convention. United states pharmacopeia (usp). 43, 2020.

[281] J. Weng, H. H. Y. Tong, and S. F. Chow. In vitro release study of the polymeric drug nanoparticles: Development and validation of a novel method. *Pharmaceutics*, 12(8), 2020.

[282] X. Wang, L. Yang, H. Zhang, B. Tian, R. Li, X. Hou, and F. Wei. Fluorescent magnetic peiplga nanoparticles loaded with paclitaxel for concurrent cell imaging, enhanced apoptosis and autophagy in human brain cancer. *Colloids Surf B Biointerfaces*, 172:708–717, 2018.

[283] N. Griese, G. Blaschke, J. Boos, and G. Hempel. Determination of free and liposome-associated daunorubicin and daunorubicinol in plasma by capillary electrophoresis. *Journal of Chromatography A*, 979(1):379–388, 2002.

[284] D. Juenemann, E. Jantratid, C. Wagner, C. Reppas, M. Vertzoni, and J. B. Dressman. Biorelevant in vitro dissolution testing of products containing micronized or nanosized fenofibrate with a view to predicting plasma profiles. *European Journal of Pharmaceutics and Biopharmaceutics*, 77(2):257–264, 2011.

[285] Baxter. *Product Information: Physioneal 40 Glucose Solution for Peritoneal Dialysis.* Baxter, 2014.

[286] S. Bhattacharjee. Understanding the burst release phenomenon: toward designing effective nanoparticulate drug-delivery systems. *Therapeutic Delivery*, 12(1):21–36, 2020.

[287] S. S. Chakravarthi and D. H. Robinson. Enhanced cellular association of paclitaxel delivered in chitosan-plga particles. *Int J Pharm*, 409(1-2):111–120, 2011.

[288] B. Lu, X. Lv, and Y. Le. Chitosan-modified plga nanoparticles for control-released drug delivery. *Polymers*, 11(2):304, 2019.

[289] M. Yu, W. Yuan, D. Li, A. Schwendeman, and S. P. Schwendeman. Predicting drug release kinetics from nanocarriers inside dialysis bags. *Journal of Controlled Release*, 315:23–30, 2019.

[290] S. D'Souza, J. A. Faraj, S. Giovagnoli, and P. P. DeLuca. In vitro–in vivo correlation from lactide-co-glycolide polymeric dosage forms. *Progress in Biomaterials*, 3(2):131–142, 2014.

[291] M Neubeck. Paclitaxel, paclitaxelum. *Kommentar zur Ph. Eur. 6.1*, 31. Lfg, 2009.

[292] J. Tian and V. J. Stella. Degradation of paclitaxel and related compounds in aqueous solutions iii: Degradation under acidic ph conditions and overall kinetics. *J Pharm Sci*, 99(3): 1288–1298, 2010.

[293] A. Seshadri and E. Rangel. *Chapter 24: Peritoneal Cavity*. McGraw Hill, 15 edition, 2020. ISBN 978-1-260-12221-3.

[294] M. G. Wacker and C. Janas. Dialysis cell for an in-vitro release test apparatus, use of the dialysis cell and in vitro release test apparatus, Patent No. DE102013015522 A1. 2013.

[295] P. Soon-Shiong. *Abraxane™ for Injectable Suspension (paclitaxel protein-bound particles for injectable suspension) (albumin-bound), for intravenous use*. Abraxis BioScience Inc: United States, 2005.

[296] V. Bartsch. *Das Taxol-Buch*. Thieme, 2nd edition, 2004. ISBN 978-3-13-105462-3.

[297] Albert J. ten Tije, Jaap Verweij, Walter J. Loos, and Alex Sparreboom. Pharmacological effects of formulation vehicles. *Clinical Pharmacokinetics*, 42(7):665–685, 2003.

[298] L. van Zuylen, M. O. Karlsson, J. Verweij, E. Brouwer, P. de Bruijn, K. Nooter, G. Stoter, and A. Sparreboom. Pharmacokinetic modeling of paclitaxel encapsulation in cremophor el micelles. *Cancer Chemotherapy and Pharmacology*, 47(4):309–318, 2001.

[299] N. Desai. *Nanoparticle Albumin-Bound Paclitaxel (Abraxane®)*, pages 101–119. Springer Singapore, Singapore, 2016. ISBN 978-981-10-2116-9.

[300] Abraxis BioScience. Full prescribing information - abraxane® for injectable suspension (paclitaxel protein-bound particles for injectable suspension) (albumin-bound). *U.S. Food and Drug Administration*, Reference ID: 3656415. 2014.

[301] R. Radev. Druckmessung des angioinjektors. 2020. Global Partner Manager and Product Manager of MedTron AG.

[302] O. Sgarbura, L. Villeneuve, M. Alyami, N. Bakrin, J. J. Torrent, C. Eveno, and M. Hübner. Current practice of pressurized intraperitoneal aerosol chemotherapy (pipac): Still standardized or on the verge of diversification? *European Journal of Surgical Oncology*, 47(1): 149–156, 2020.

[303] Medtron AG. Produktfoto accutron ct, 2021. https://www.medtron.com/fileadmin/produkte/CT/CT_871_Netz_shadow_0000.png, visited 2021-05-04.

[304] Medtron AG. Produktfoto accutron hp-d, 2021. https://www.medtron.com/de/angiographie/accutron-hp-d/, visited 2021-05-04.

[305] D. Gohler, V. Khosrawipour, T. Khosrawipour, D. Diaz-Carballo, T. A. Falkenstein, J. Zieren, M. Stintz, and U. Giger-Pabst. Technical description of the microinjection pump (mip((r))) and granulometric characterization of the aerosol applied for pressurized intraperitoneal aerosol chemotherapy (pipac). *Surg Endosc*, 31(4):1778–1784, 2017.

[306] D. Schnelle, F.-J. Weinreich, J. Kibat, and M.A. Reymond. A new ex vivo model for optimizing distribution of therapeutic aerosols: the (inverted) bovine urinary bladder. *Pleura and Peritoneum*, 2(1):37–41, 2017.

[307] I. Sautkin, W. Solass, F.-J. Weinreich, A. Königsrainer, M. Schenk, K. Thiel, and M. A. Reymond. A real-time ex vivo model (eibub) for optimizing intraperitoneal drug delivery as an alternative to living animal models. *Pleura and Peritoneum*, 4(3), 2019.

[308] M. Shariati, G. Lollo, K. Matha, B. Descamps, C. Vanhove, L. Van de Sande, W. Willaert, L. Balcaen, F. Vanhaecke, J.-P. Benoit, W. Ceelen, S. C. De Smedt, and K. Remaut. Synergy between intraperitoneal aerosolization (pipac) and cancer nanomedicine: cisplatin-loaded polyarginine-hyaluronic acid nanocarriers efficiently eradicate peritoneal metastasis of advanced human ovarian cancer. *ACS Applied Materials & Interfaces*, 12(26):29024–29036, 2020.

[309] T. Mdzinarashvili, M. Khvedelidze, E. Shekiladze, A. Koenneke, and M. Schneider. Stability of various plga and lipid nanoparticles in temperature and in time and new technology for the preparation of liposomes for anticancer and antibiotic loading. *Journal of Thermal Analysis and Calorimetry*, 139(2):1131–1140, 2020.

[310] Y. Sadzuka, S. Hirota, and T. Sonobe. Intraperitoneal administration of doxorubicin encapsulating liposomes against peritoneal dissemination. *Toxicology Letters*, 116(1):51–59, 2000.

[311] S. Togano, M. Yashiro, Y. Miki, Y. Yamamato, T. Sera, Y. Kushitani, A. Sugimoto, S. Kushiyama, S. Nishimura, K. Kuroda, T. Okuno, M. Yoshii, T. Tamura, T. Toyokawa, H. Tanaka, K. Muguruma, S. Tanaka, and M. Ohira. Microscopic distance from tumor invasion front to serosa might be a useful predictive factor for peritoneal recurrence after curative resection of t3-gastric cancer. *PLOS ONE*, 15(1):e0225958, 2020.

[312] E. de Bree, D. Michelakis, D. Stamatiou, J. Romanos, and O. Zoras. Pharmacological principles of intraperitoneal and bidirectional chemotherapy. *Pleura Peritoneum*, 2(2):47–62, 2017.

[313] S. Dadashzadeh, N. Mirahmadi, M. H. Babaei, and A. M. Vali. Peritoneal retention of liposomes: Effects of lipid composition, peg coating and liposome charge. *Journal of Controlled Release*, 148(2):177–186, 2010.

Acknowledgements

Zuallererst möchte ich mich bei meinem Doktorvater Prof. Dr. Marc Schneider für das spannende und auch herausfordernde Thema meiner Promotion bedanken. Vielen Dank Marc, für die vielen Stunden an Diskussion, motivierender Gespräche und Deine regelmäßige Begleitung zu den Meetings mit unseren Projektpartnern nach Tübingen.

Prof. Dr. Claus-Michael Lehr möchte ich für die wissenschaftliche Betreuung meiner Promotion und für die Erstellung des Gutachtens danken. Des Weiteren gilt mein Dank den weiteren Mitgliedern der Prüfungskommission.

Zudem möchte ich mich bei meinen Projektpartnern am Universitätsklinikum Tübingen, Prof. Dr. Marc Reymond sowie seinen Mitarbeitern und Doktoranden, die an den Penetrationsversuchen mitgewirkt haben, für die gute Zusammenarbeit bedanken. Ich möchte mich bei der Capnomed GmbH, allen voran bei Herrn Groß, bedanken. Ohne die finanzielle Unterstützung des Projekts und die Bereitstellung der PIPAC-spezifischen, medizinischen Produkte wäre diese Arbeit nicht zustande gekommen. In diesem Zusammenhang gilt mein Dank auch deren Kooperationsfirma Medtron AG, insbesondere Herrn Romano, Herrn Glößner und Herrn Feber für die Lieferung der Geräte inkl. großzügigem Equipment an die Universität sowie Herrn Radev, der meinen technischen Fragen zu den Injektoren fachlich nachgegangen ist. Bei Dr. Ranjita Sahoo, die das Projekt seitens der Firma Capnomed betreut hat, danke ich für die gute Zusammenarbeit, den wissenschaftlichen Input und die Koordination zwischen den Projektpartnern.

Ein besonderer Dank gilt meinen Kollegen und Freunden des Arbeitskreises. Für die gemeinsame Zeit, die vielen fachlichen sowie auch privaten Gespräche im und abseits des Instituts einen großen Dank vor allem an Karola Lima-Engelmann, Johannes Büscher, Tomas Pioch und Thorben Fischer. Julia Metz und Johannes danke ich für die gute und oftmals unterhaltsame Zusammenarbeit bei der Betreuung und Planung der Studentenpraktika. Vielen Dank an Thorben, meinem direkten Bürokollegen, für die Unterstützung jeglicher Art und dass du immer ein offenes Ohr für mich hattest. Aljoscha Könneke danke ich vor allem für die Einweisung und Hilfe bei der Etablierung der HPLC-Methode und Marcel Pourasghar für seine Hilfe bei Computer-spezifischen Problemen. Salma AbdelHafez möchte ich für die vielen fachlichen Diskussionen im Labor und auch das leckere Humus Rezept danken! Vielen Dank an Dr. Agnes Weiß für die Erstkorrektur meiner schriftlichen Arbeit.

Ich möchte mich sehr herzlich bei Peter Meiers vor allem für seine Hilfe bei HPLC Problemen und Marijas Jurisic für die Durchführung und Unterstützung bei der Testung der Zytotoxizität meiner Formulierungen bedanken. Auch an Isabelle Conrad-Kehl herzlichen Dank für die gemeinsame Zeit und die vielen französische Leckereien.

Ebenfalls gebührt Dr. Chiara de Rossi ein großer Dank für die Unterstützung und Einarbeitung am REM des HIPS (DDEL). Und auch den Mitarbeitern und Doktoranden der DDEL- und BION-Gruppe des HIPS möchte ich für ihre Unterstützung und die gemeinsame Zeit danken. Dr. Marcus Koch am INM danke ich für seine REM-Aufnahmen und Dr. Josef Zapp (UdS) für die NMR-

Analytik zur Identifizierung des Paclitaxels. Für die UHPLC-MC Analytik und die fachlichen Diskussionen danke ich Dr. Stefan Böttcher (UdS) sehr. Des Weiteren bedanke ich mich bei Dr. Britta Diesel (UdS) für die Mitbenutzung der Räumlichkeiten der pharmazeutischen Biologie für die zur Vorbereitung des Zytostatikums. Der Glasbläserin der UdS-internen Werkstatt Britta Schreiber möchte ich für die engagierte Anfertigung des Glassammelbehältnisses meines Prototypen danken.

Auch bei meinem ehemaligen Studenten Alexander Baus möchte ich mich für das gesprächige Zuarbeiten und die Unterstützung bei meinen ersten Sprühversuchen bedanken. Meiner Masterandin Marie-Sophie Ehrlich bin ich sehr dankbar für die gute Zusammenarbeit beim Spinning-Disc Projekt und die schöne gemeinsame Zeit im Labor.

Ein großer Dank gilt meiner Familie und meinen Freunden, die immer offene Ohren, motivierende Worte und auch den ein oder anderen guten Ratschlag für mich hatten. Vielen Dank für eure bedingungslose Unterstützung und euer Verständnis für all die Feiern und Treffen, bei denen ich während meiner gesamten akademischen Ausbildung aufgrund von Laborversuchen und der räumlichen Distanz nicht dabei sein konnte.

Meinem Mann David danke ich für unseren ständigen wissenschaftlichen Austausch, welcher manche Zusammenhänge auch mal aus anderen Perspektiven dargestellt hat. Und von Herzen möchte ich mich für Deine immerwährende Geduld, Motivation und alles überdauernde Liebe bedanken, die mich positiv in unsere gemeinsame Zukunft blicken lässt.